Doctoral Dissertation
Doctoral Program in Electronics Engineering (XXXIIIrd cycle)

Novel Modeling and Simulation Concepts for Power Distribution Networks

A dissertation submitted to Politecnico di Torino and Xi'an Jiaotong University in partial fulfillment of the requirements for the degree of Doctor of Philosophy

Zain Anwer Memon
* * * * * *

Supervisors
Prof. Igor Simone Stievano, Supervisor
Prof. Xie Yanzhao, Supervisor
Prof. Flavio G. Canavero Co-supervisor

Doctoral Examination Committee:
Prof. Sami Barmada, Referee, Università di Pisa, Italy
Prof. Flavia Grassi, Politecnico di Milano, Italy
Prof. Antonino Laudani, Referee, Università degli Studi Roma Tre, Italy
Prof. Walter Zamboni, Università degli Studi di Salerno, Italy
Prof. Xu Yang, Referee, Xi'an Jiaotong University, China

Politecnico di Torino
August 16th, 2021

I hereby declare that, the contents and organisation of this dissertation constitute my own original work and does not compromise in any way the rights of third parties, including those relating to the security of personal data.

. . . . . .

Zain Anwer Memon

Turin, August 16th, 2021

This dissertation is submitted for a Double Degree Program to Politecnico di Torino, Italy, and Xi'an Jiaotong University, China. The official submission of the Thesis work required using the Theses templates of the two Universities. Hence, the content of this document is the same for both, with only format changed, matching the templates for the two universities.

Summary

Current and next generation power distribution networks (PDNs) are complex systems characterized by a large size, the interconnection of heterogeneous objects (e.g., distributed renewable sources or storages such as electric vehicles charging hubs, etc), and a stochastic behavior due to both unknown customer demand and other external conditions affecting power generation. All the above system features require the availability of innovative and general modeling solutions for the accurate prediction of the network state. This research focuses on theoretical investigation of model generation algorithms for complex systems and networks and their application to the problem at hand.

First in this dissertation, an alternate modeling technique for the power-flow analysis of PDNs is presented. The PDN is suitably interpreted as a decoupled circuit in the phasor domain, which is split into a linear and a non-linear sub-circuits, of which the large linear part represents the source and the interconnecting blocks including transmission lines, while the small non-linear part accounts for load characteristics and distributed generators (DGs). The circuital interpretation is directly solved in the frequency domain via a standard tool for circuit analysis in combination with a simple iterative scheme. At each iteration, the large linear part can be solved via either the modified nodal analysis (MNA) or any simulation program with integrated circuit emphasis (SPICE). The link of the proposed numerical scheme with the so-called waveform relaxation technique is also thoroughly discussed. The proposed approach has been proven to offer a general solution allowing to handle multiple DGs and other heterogeneous sources without requiring custom modifications for any arbitrary network. Additionally, it features fast convergence and very good accuracy.

While the first part deals with steady-state analysis of PDNs, the effect of stochastic behavior of distributed renewables and the changes in the physical medium (e.g., equivalent resistance, reactance, capacitance, etc.), due to external factors, on the network voltage profile is analyzed, in the second part of the Thesis, by performing the uncertainty quantification (UQ) of power networks. Several techniques are presented ranging from standard Monte Carlo (MC) simulation to the regression based accurate and fast-to-evaluate surrogate models such as the polynomial chaos expansion (PCE)

and machine learning (ML) based least square support vector machines (LS-SVM). A two-step scheme is proposed, that involves the compression of the training response set with principal component analysis (PCA) and the generation of surrogate models from a limited number of samples.

The above proposed techniques are assessed for their accuracy and effectiveness by considering multiple test networks in chapters 2 and 3. These are further analyzed to handle larger realistic networks by considering a three-phase benchmark network, the IEEE 8500-node test feeder, used by Institute of Electrical and Electronics Engineers (IEEE) power research community. Specifically, a power-flow solution is performed for the mentioned test network using the proposed circuital interpretation with the fixed-point iteration and two state-of-the-art methods, the *Z-bus* method and the benchmark open source distribution system simulator (openDSS) software. After that, the proposed compressed surrogate model of network nodal voltages is built with LS-SVM in conjuction with PCA, whose predictions are compared in terms of accuracy and simulation time with those of the sparse PCE and MC simulation, where the former is a polynomial regression technique while the latter is a simple traditional scheme.

The results collected in this research work demonstrate the benefits and strengths of the proposed modeling and simulation solutions for PDNs compared to currently available state-of-the-art techniques [1, 2, 3].

摘　要

当前和下一代配电网是大规模复杂系统，其中不同对象（例如分布式可再生能源、电动汽车充电中心等储能）之间互联，另外未知的用电需求和影响发电的外部条件等行为具有随机性。针对上述系统特征，为准确预测网络状态，需要提供创新的通用建模方案。本文主要研究复杂系统和网络的模型生成算法及其在实际问题中的应用。本文首先提出了一种用于配电网潮流分析的新型建模方法。配电网被建模为相量域中的解耦电路，分为线性子电路和非线性子电路，其中大型线性部分表征电源和含传输线的互连模块，而小型非线性部分表征负荷特性和分布式发电机。通过标准电路分析工具，并结合一个简单的迭代格式，在频域中对电路直接求解。在每次迭代中，大型线性部分可以通过修改节点分析 (MNA) 或任何具有集成电路重点的仿真程序 (SPICE) 来求解。还彻底讨论了所提出的数值方案与所谓的波形松弛技术之间的联系。。本文提出的方法为处理多个分布式发电机和其他电源提供了一种通用方案，而无需对任何网络进行特定修改。此外，该算法收敛速度快，精度高。在第一部分配电网稳态分析的基础上，本文第二部分通过开展电网的不确定度量化，分析了由外部因素引起的分布式可再生能源的随机行为以及物理介质（等值电阻、电感和电容等）的变化对网络电压分布的影响。对比分析了多种不确定度量化方法，从标准的蒙特卡洛模拟到基于回归的精确快速评估的代理模型，后者包括多项式混沌展开模型和基于机器学习的 小二乘支持向量机模型。提出了一种两步算法，先使用主成分分析压缩训练响应集，再从有限数量的样本生成代理模型。在第 2 章和第 3 章中，利用多个电网测试算例评估了上述方法的准确性和有效性。利用电气与电子工程师学会电力研究团体的 IEEE 8500 节点测试馈线，进一步分析了三相基准网络，以处理规模更大的实际电网。利用所提出的定点迭代电路算法对上述测试网络进行了潮流求解，并与其他两种 先进的 Z-bus 方法和开源配电系统模拟器（openDSS）软件进行了对比。然后，采用 小二乘支持向量机和主成分分析相结合的方法，建立了网络节点电压的压缩代理模型，并将其预测精度和仿真时间与稀疏多项式混沌展开和蒙特卡洛模拟方法相比较，前者是多项式回归方法，后者是简单的传统方法。本文研究结果表明了所提出的配电网建模和仿真方案相比现有方法的优点。

Acknowledgements

It gives me great pleasure in acknowledging the support of all the people who have helped me accomplishing this Thesis. First and foremost, I would like to thank my Politecnico di Torino supervisors, Prof. Igor Simone Stievano and Prof. Flavio Canavero, for their constant, irreplaceable support and presence in completion of this activity and guiding me in carrying out the joint research program with Xi'an Jiaotong University.

I would also like to thank my EMC group colleagues for their ideas and discussions, during these three fruitful years of my life. Special thanks to Riccardo Trinchero and Paolo Manfredi, who have always guided and helped uplift my confidence in undertaking this activity.

I am indebted to Prof. Xie Yan-zhao and Xi'an Jiaotong University research group who provided me all the necessary things to carry out joint research and offering me great opportunity to work with State Grid Simulation Center of China Electric Power Research Institute, which helped my deep dive research and cross-cultural life.

I also acknowledge my colleagues who made the work environment enjoyable, with coffee and lunch breaks, which will definitely be cherished all my life.

I owe my deepest gratitude to all the Pakistani community in Torino, who have always stood with me during my stay, and felt like home; For sure Torino would remain my second home.

Last but not the least, I would like to thank my family for their constant support, prayers and love which made me who I am.

Dedicate to prayers, love and smile of family; And To parents, who have always inspired me walk with the storms.

Contents

List of Tables

List of Figures

Chapter 1

Introduction

1.1 Research Background

Right from the begining, electrical power industry has faced many issues including generation demand gap, reliability, planning and operational back-offs and weather vulnerabilities. These factors affect the smooth operation of generation, transmission and distribution networks and might result in a total blackout. PDNs in particular, which are responsible for supplying power to the end nodes (consumers), are in a shift towards a smarter grid structure for more reliable and optimal performance. These advancements, with the involvement of multiple heterogeneous sources (renewables, electric vehicles, etc.) require the capability of handling power-flow in both ways (supply and consume) along with the synchronized information transfer among various equipment. In this framework, specific attention is given to the availability of modeling and simulation methods for both transient and steady-state assessment of the power networks. For the latter, several analyses have been proposed in the literature including, power-flow, three-phase power-flow, and harmonic analyses which have been proven to be mature tools successfully adopted in recent application problems [4, 5, 6, 7].

Without loss of generality, efficient and reliable power-flow solution techniques have been developed and widely used [8, 9, 10, 11, 12, 13, 14, 15]. Recently, different class of approaches have been proposed which offer a general solution with improved convergence for very large structures including weakly and heavily meshed PDNs. The first part of this work focuses class of approaches which propose a different interpretation of the PDNs in terms of a non-linear circuit in the *frequency*-domain. It allows decoupling the solution of the inherent non-linear problem in the harmonic domain into the solution of a large linear network followed by a subsequent non-linear computation related to some of the network components only (e.g., renewable sources). The resulting circuit is then solved by combining the MNA [16] with an iterative scheme based on the waveform

relaxation technique [17]. The approach is simple, general, and applies to any kind of network, including meshed structures [1]. The proposed contribution shares the idea of using a circuit-based approach, which has already been proven to be general and robust in terms of convergence [18], but it offers a more intuitive and graphical procedure, also highlighting the link between the waveform relaxation technique and the fixed point iteration. It is an alternative that can be readily applied to the number of applications, including the co-simulation of multi-energy networks, possibly including gas distribution systems [19]. An additional important feature of this relies on its flexibility allowing the application of alternative numerical schemes (such as Newton Raphson or fixed-point iteration, being latter considered in this work only). It is also verified that at each iteration of the method, the resulting circuit can be alternatively solved by any SPICE-based solver at a single frequency analysis.

The second part of this work focuses on the surrogate modeling of power networks for performing UQ. The modeling techniques for the analysis of power networks should account for the variations in some parameters that have inherent stochastic nature. Typical examples are represented by the pervasive spread of DGs for which the injected power depends on weather conditions; the impact of hubs of charging electrical vehicles, located in different points of the network; and the unpredictable user behavior, a scenario in which both users and buildings play an active role in the continuous monitoring of the fluid electricity fees, and modify their power consumption accordingly [20, 21, 22, 23]. Therefore, the inherent statistical nature of the problem makes the deterministic interpretation unsuitable, and demands for stochastic methodologies for the UQ [24, 25, 26].

MC simulation represents the most straightforward way of performing a statistical load-flow analysis of a power grid with uncertain loads [27, 28, 29, 30, 31, 32, 33, 34, 35, 36, 37, 38]. The underlying idea is to run a large set of deterministic simulations in which the power level of each uncertain node is drawn according to its probability density function (PDF). Despite its simplicity and accuracy, a naive MC simulation turns out to be extremely expensive in terms of simulation time because of its slow convergence rate. Indeed, it requires a huge number (typically, on the order of thousands) of samples, which makes its direct application to a *full-computational model* unfeasible for realistic scenarios.

This reason motivated the growing interest, expressed by the electrical and electronic engineering community during the last fifteen years, in the development of enhanced and efficient alternatives to MC simulation for both the worst-case and the statistical assessment of the stochastic responses of complex systems [39, 40, 41]. PCE can be considered for the UQ [42, 43], whose underlying idea is to represent the relationship between uncertain variables and outputs of interest in terms of an expansion of suitable

orthogonal polynomial basis functions [44]. While this method is proved well to work for many uncertain parameters, but similar to most parametric regression methods, the number of unknowns depends on the number of input parameters, as the number of basis functions, and thus of regression coefficients, grows exponentially, for example, a second-order PCE for 500 uncertain variables requires the estimation of 250k coefficients: this is the so called "curse of dimensionality", which thus led ML methods [45, 46], which have been effectively applied to build accurate surrogate models starting from a limited number of training samples. The resulting surrogate model is capable of predicting both the deterministic and stochastic behavior of the system output for any configuration of the uncertain parameters. As opposed to PCE-based methods, the above ML techniques allow constructing non-parametric surrogates in which the number of regression unknowns is independent from the dimensionality of the input space (i.e., the number of uncertain parameters) [47, 48]. Therefore, ML methods appear to be an attractive solution to mitigate the curse of dimensionality and provide a powerful alternative for tackling UQ problems with a huge number (e.g., thousands) of variables. In this work, sparse PCE and LS-SVM regression are employed in conjuction with PCA compression to build a compressed surrogate model of the nodal voltages of typical power transmission and distribution networks with a large number of uncertain parameters consisting of physical medium, power loads and renewable sources. The performance of the proposed modeling scheme, in terms of efficiency, accuracy and convergence, is thoroughly investigated by means of multiple test networks ranging from low number of nodes (118) to a comparatively very large node-network (8500).

1.2 Literature Review

1.2.1 State of the Art load-flow techniques

Since few decades, efficient and fast power-flow solution techniques have been developed and widely used for the assessment of power system operation [8, 9, 10, 11]. Low resistive/reactive ratio for transmission lines (i.e., the so-called R/X factor) results in the decoupled real and reactive powers and thus few assumptions can be made to linearize the power-flow solution in terms of simple DC power-flow as opposed to AC power-flow [12, 13, 14, 15]. This DC power-flow was improved in [49], which approximates complex parameters rather than only real parameters, applied to three-phase node feeder. Most of the methods available in the literature largely focus on Newton Raphson, Gauss Seidel or backward/forward sweep algorithms for radial distribution networks [50, 51, 52, 53, 54, 55, 56, 57, 58, 59, 60, 61, 62]. Zhang in [50] modified Newton Raphson in which the Jacobian matrix is formed by backward/forward sweep, however the solution of

Jacobian matrix might include negative reactances whose effects are studied by [51] and reveals that the negative reactances in the solution models have significant effect on the eigen values of the Jacobian matrix and affects the convergence rate. Furthermore, the limitation of Jacobian matrix in terms of singularities is eliminated in [52] for achieving maximum loading point operation. Teng [53] proposed a method based on mixing the so-called *Z-bus* & traditional Guass Siedal method to solve three-phase equations separately and obtains a closed-form solution, [54] implements backward/forward sweep for three-phase power-flow and extends the method to find optimal feeding points for the reactive power compensation. For radial feeders only, Teng in [55] proposed a solution by forming a relation between bus injections and bus voltages directly through matrices based on backward/forward sweep algorithm. Eminoglu and Hocaoglu in [56] used polynomial equations to solve for nodal voltages and backward propagation for branch currents. The above method however turns out to be slower compared to other sweep algorithms. A hybrid power system model is proposed in [57] to model both transmission and distribution single- and three-phase networks, which are connected by a virtual connector acting as a coupler between single- and three-phase models without altering the power levels. This power flow model comprises of constant and periodic functions for single- and three-phase connections respectively, and mainly highlights the coupling connections between different models present in a hybrid power system. In [58], algebraic recursive equations are used for power-flow solution, and Garces in [59] proposed linear approximation on the complex plane to solve unbalanced power-flow equations without taking into acount the power-voltage (PV) nodes for loads/DGs. A similar linear approximation is proposed by Wang in [61] based on backward/forward sweep propagation. Differential transformation, which is mostly used for transient analysis, is implemented in [62] to convert the non-linear power-flow problem into a linear set of equations in the time domain solved by a non-iterative algorithm. For DGs specific, a grid-connected photovoltaic array model is proposed in [63] for power-flow solution, which includes state variables of photovoltaic plant alongwith the nodal voltages of the network in the Jacobian matrix, while the reduction in the network nodal voltages caused by photovoltaic systems is analyzed in [64] with a proposed two-node distribution model, whose results are verified with power-voltage curves of a real network, however, the proposed model needs to be further verified for its effectiveness on comparatively large networks. Moreover, microgrids connected with the network are considered as a separate node by Gibran in [65] and solved by a two-step heriarchical control to stabilize the frequency and voltage levels of the microgrid units. Nikkhajoei [66] also proposed a two-step approach with a closed-form model, but this two-step control can be costly with comparatively large three-phase power networks. The droop controlled islanded microgrids, which differ

from the grid-connected microgrids in terms of frequency and reactive power, are solved for the power flow by Morad [67], in which the author analyzes the effect of reactive power limits of distributed generators.

Recently, Bazrafshan et al. [68] proposed a new approach for modeling three-phase distribution systems based on the *Z-bus* method, which however does not explicitly exploit the radial and weakly meshed network structure of distribution systems and it requires the solution of a set of equations whose size is proportional to the number of buses (and/or looping branches). As a result, it converges for weakly meshed configuration only under some specific assumptions, as pointed out in [69]. It important to point out that the solution of weakly meshed networks requires, in general, custom adjustments in which the network is first converted into an equivalent radial network by breaking the looping branches, with detrimental impacts on accuracy, efficiency and simplicity of the solution. Line-wise power flow is also used, as oppose to the bus-wise power flow, to identify the voltage sensitive nodes that could lead to a network voltage collapse [70].

A different formulation of the power-flow analysis for both power transmission and distribution networks by means of a circuital interpretation of the network and the application of classical tools for circuit analysis are instead presented in [18, 71, 72], offering a general solution with improved convergence for very large structures including weakly and heavily meshed structures. In particular, [18] proposes the three-phase solution of PDNs with modified augmented nodal analyses (MANA), [71] models the PDNs with equivalent circuit and uses circuit simulation techniques for steady-state analyses, and [72] discusses the implementation of step voltage regulators (SVRs) in solving power-flow with MANA and Newton's methods. Various Newton Raphson-based power-flow solvers are analyzed for their accuracy and effectiveness in [73]. Additionally, the existence of power-flow solution and boundary conditions critera are presented in [74, 75].

The strength and efficiency of the above methods are analyzed by solving various test networks, generally ranging from 4 to 8500 node points, provided by Institute of IEEE Power and Energy Society (PES) [76], where the large test network IEEE 8500-node [77] is considered as the benchmark.

1.2.2 State of the Art techniques for variability analysis of Power Networks

The classical approach for performing variability analyses of power systems is MC, which has been implemented by many authors [27, 28, 29, 30, 31, 32, 33, 34, 35, 36, 37, 38]. Specifically, [27, 28, 29] estimated probablistic power-flow (PPF) with DGs, through

MC simulation, [30] performs PPF based on frequency variation as a result of large distrubances, [31, 32] performed optimal power-flow and [33] proposed latin supercube sampling for efficiently sampling random variables for PPF. While, [34] assessed the reliability of PDNs with DGs operating in parallel to the distribution network with MC simulation on high core computing and concluded that solution of large networks is only possible when higher computing cores are available, [35] uses GPU-based open computing language to accelerate the execution of MC simulation for power-flow, and [36] uses method of moments, where probability of occurence is calculated with Taylor series, to analyze the uncertainty in the power networks, but it fails to fully characterize the exact distribution window for non-linear systems. Additionally, Interval Power Flow methods including Rectangular and Polar Interval are improved to propose Mix Interval Power flow in [37], for performing probabilistic power flow using affine arithmatics, whose results are again compared with the MC simulation. A reachable power-flow method is proposed in [38] in which the ordinary differential equations are used to solve PPF with uncertain microgrid parameters.

On the other hand, surrogate modeling for power systems is the most reliable approach for performing UQ fast and effective. In particular, PCE can be considered as the reference technique for UQ [42, 43, 78, 79]. The basic idea is to map inputs and outputs in terms of an expansion of orthogonal polynomial basis functions [44]. The expansion coefficients can be computed by means of least square regression, starting from a limited set of random "training samples" obtained from the full-computational model. The resulting surrogate model allows an expedite statistical assessment of the original system. However, similar to most parametric regression methods, in which the number of unknowns depends on the number of input parameters, the application of classical PCE becomes impractical for systems with a large number of uncertain parameters. Fortunately, owing to the *sparsity-of-effects* principle, most of the model coefficients are in practice negligible. This led to the development of sparse algorithms [80, 81, 82], which reduce the number of unknowns and allow dealing with hundreds of uncertain variables (e.g., see [83]).

Recently, advanced ML methods [45, 46] have also been employed for the UQ of several realistic problems in electrical engineering [84, 85]. Specifically, flexible and powerful ML regressions such as support vector machine (SVM) [86, 87], LS-SVM [47], and Gaussian processes [48], were effectively applied to build accurate surrogate models starting from a limited set of training samples [88, 89, 90, 91]. The resulting surrogate model is capable to predict both the deterministic and stochastic behavior of the system output for any configuration of the uncertain input parameters. As opposed to PCE-based methods, the above ML techniques allow constructing non-parametric surrogates in which the number of regression unknowns is independent from the dimensionality

of the input space (i.e., the number of uncertain parameters) [47, 48].

1.3 Organization of the thesis

As mentioned above, the main research object of this dissertation is to model PDNs . Specifically, a novel modeling of PDNs is performed by interpreting the network as a decoupled circuit in the phasor domain and solving it with simple iterative process. In addition, equivalent surrogate models are built by using ML techniques to accurately predict the network voltage profile.

The structure of this dissertation is arranged as follows:

Chapter 2 presents an alternate solution of the power-flow analysis of power distribution systems with distributed generators. The appraoch relies on a suitable interpretation of power networks by equivalent circuit in the phasor domain. The circuit is then split into a linear and a non-linear sub-circuits. The interpreted circuit is then solved by using MNA and a simple iterative solution. The results of the proposed technique are validated with state-of-the-art software OpenDSS, the *Z-bus* method and an industrial software used by China Electric Power Research Institute (CEPRI).

In Chapter 3, UQ of power networks is performed based on MC simulation and on surrogate models built via ML techniques. LS-SVM regression is combined with the PCA to build a compressed surrogate model capable of predicting all the nodal voltages of the network as a function of the uncertain electrical parameters of the transmission lines. The power-flow analysis of the IEEE118-bus system with 250 uncertain parameters is considered as a test case. The performance of the proposed modeling strategy in terms of accuracy, efficiency and convergence, are assessed and compared with those of alternative surrogate model based on sparse PCE.

In Chapter 4, the techniques proposed in previous chapters are further verified in terms of feasibility, strength and effectiveness on comparatively very large three-phase benchmark network, the IEEE 8500-node test feeder. The network contains both medium voltage (MV) and low voltage (LV) levels and most of the components available in a typical North American MV feeder. The results prove that the proposed techniques can handle large realistic networks very well.

Finally, Chapter 5 summarizes the work performed and achieved results and highlights the future work.

Chapter 2

Modeling of Power Distribution Networks based on Decoupled Circuit Equivalents

The existing methodologies for performing power-flow analyses for power transmission & distribution networks, stated in previous chapter, are very efficient and have been widely used. PDNs in particular, are modeled as radial or weakly meshed networks, but as systems move towards a more advanced smart grid, the networks may become heavily meshed along with the increasing day-by-day integration of distributed generators (e.g., renewable energy sources (RES)). This shift in network topology requires some modifications in these methods, which turn out to become inefficient. The above aspect is even more evident for the case of power-flow analysis of large distribution networks for which conventional modeling and simulation solutions are often based on the basic tools developed for radial network topologies, with custom adjustments accounting for the loops [50, 53, 54, 55, 56, 58, 59]. As a result, cumbersome mathematical formulations, slow convergence and possible limits to the applicability to weakly meshed structures are typical problems [68, 69]. As an alternative, solutions based on a more classical circuital interpretation of the network have been presented and proven to be effective [71, 18, 72, 1].

In this chapter, the latter approach is used to propose an alternative, simple and viable technique for the power-flow analysis of PDNs. The proposed contribution shares the idea of using a circuit-based approach, which has already been proven to be general and robust in terms of convergence [18], but it offers a more intuitive and graphical procedure. In particular, the proposed work has an inherent emphasis on circuital approach rather than the numerical scheme applied to the MNA in matrix form. This is specifically provided by the proven robust link (in terms of equivalence) between

the waveform relaxation technique (which has an inherent circuital interpretation) and the fixed point numerical scheme, which in the case of [18] is applied to matrices only. The idea lies in a suitable interpretation of the power network in terms of a non-linear circuit in the phasor domain. The above circuital interpretation can be solved directly in *frequency*-domain via the combination of standard tools for circuit analysis with an iterative numerical scheme, providing directly the steady-state solution of the network variables. At each iteration, the resulting circuit turns out to be composed of two decoupled networks, a large linear part and a set of smaller non-linear pieces accounting for load characteristics, with evident benefits in terms of computational time. Here, a custom Matlab implementation of the algorithm is presented, in which the solution of the large linear part is carried out by means of either the classical MNA tool or via any SPICE-based commercial software. The proposed approach has been proven to offer a general solution allowing to handle multiple distributed generators and other heterogeneous sources without requiring custom modifications for any arbitrary network. It is important to highlight that the proposed technique put emphasis on a circuital representation rather than only a matrix approach. Moreover, a strong link between waveform relaxation and fixed-point iteration, which is carried out in [18] is provided and proves that both are equivalent.

The chapter is organized as follows. Section 2.1 illustrates the circuital interpretation of a PDN in the phasor domain and its MNA description. Section 2.2 focuses on the proposed numerical scheme based on the fixed-point iteration. Section 2.3 introduces SPICE in the loop for the *frequency*-domain solution of the large linear network. Validation results based on multiple IEEE benchmark test cases are collected in Section 2.4. Conclusions and remarks are eventually drawn in Section 2.5.

2.1 Circuital Interpretation

This section presents the circuital interpretation of a generic PDN in the phasor domain with emphasis on the main constitutive blocks, including transmission lines, loads and renewable generators, which are usually described in terms of compact black boxes with target information about the complex power absorbed or supplied. In addition, the description of the network via the classical MNA formulation and its extension to handle three-phase networks are included as well.

2.1.1 Illustrative Example

The discussion starts by taking the simple 4-node radial PDN shown in Figure 2.1. For the sake of illustration, it represents the symbolic circuit in the phasor domain of a

single phase network where an ideal sinusoidal voltage source, that corresponds to the substation, is feeding the network with voltage $\hat{E}(\omega)$. The absorbing loads or the distributed renewables injecting complex power $S_3 = P_3 + jQ_3$ and $S_4 = P_4 + jQ_4$ are represented by the circuital elements connected to the nodes 3 and 4 respectively, whereas the two-terminal elements (Y_1,Y_2, & Y_3) correspond to the transmission lines described by lumped RL equivalents.

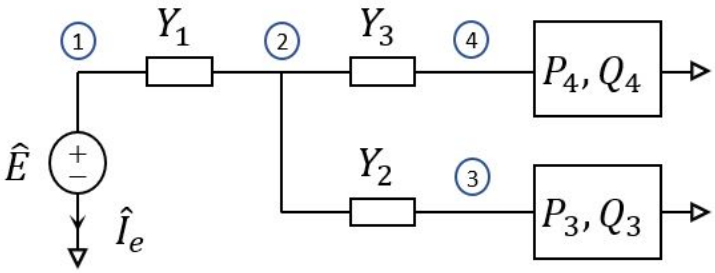

Figure 2.1: Interpretation of a generic radial PDN in the phasor domain. The loads/DGs connected at nodes 3 and 4 are here represented by black-boxes with information on the absorbed/injected complex power.

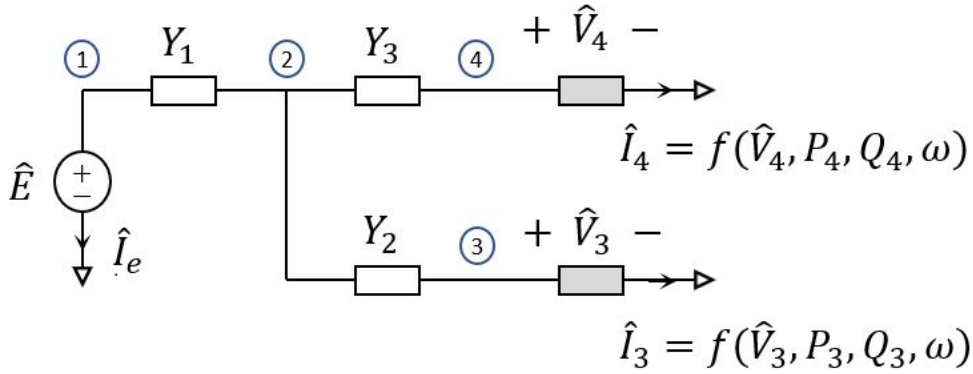

Figure 2.2: Alternate interpretation of the scheme of Figure 2.1 where the loads/DGs are described as non-linear voltage controlled elements.

The above PDN can be represented by the equivalent circuit in phasor domain shown in Figure 2.2. The connected load/DGs at the nodes 3 and 4, which can absorb/supply

complex power, can be interpreted by non-linear voltage controlled current sources $f(\hat{V}_k)$, as a function of complex power defined by:

$$S_k = P_k + jQ_k = \hat{V}_k \hat{I}_k^*, \tag{2.1}$$

where, P_k and Q_k are the real and reactive powers for the load/DG at node k (e.g., k = 3 and 4), this yields $f(\hat{V}_k)$ as,

$$\hat{I}_k = f(\hat{V}_k; P_k, Q_k, \omega) = \left(\frac{P_k + jQ_k}{\hat{V}_k} \right)^*, \tag{2.2}$$

In this framework, it is important to point out that the DGs are small generators (usually at most few MW) connected at different nodes for various reasons, such as, reducing generation demand gap, or improving voltage profile, for increased reliability and operation [92]. DGs can be connected in different configurations like power-factor controlled, voltage controlled, or current controlled modes depending on the need of operation. DGs can be traditional generators or RES, such as photovoltaic, wind, fuel cells, etc. For performing power-flow analysis, there are four parameters at each node, real power (P), reactive power (Q), voltage magnitude (V) and voltage phase angle (θ), out of which any two are known and two unknowns, and thus DGs are classified into the type of known variables as PQ, PQ(V), PV(or PI). In this work, our focus is to take into account the network behavior according to RES, thus DGs hereafter refer to RES only.

Any type of DG, can be readily converted to equivalent source (injection or consumption) as briefly done for the simple PQ case above via (2.2). For PQ(V) DG case, the current injection can be done via the same equation, with the only exception that the reactive power turns out to be the function of voltage magnitude. However for PV type, with rated real power and voltage magnitude given, the optimal reactive power needs to be calculated via an iterative process called reactive power compensation [93, 94]. After the required power values are obtained, for particular DG, the equivalent current injection is computed via (2.2) to obtain power-flow results.

Loads, on the other hand, are the power consumption units connected at each node. The type of loads can be characterized according to the static (constant) parameter, such as constant power (PQ type) or power as a function of voltage (constant current or constant impedance) [95]. For initial understanding and for simplicity, we use only constant PQ type of load, which is converted to equivalent current consumption unit via (2.2) to be used for the power-flow solution.

2.1.2 Modified Nodal Analysis

The MNA is one of the most established formulation for solving linear and non-linear circuits and is being used in many commercial circuit analysis softwares [18, 16]. It is a simple and effective method to describe the governing equations of a circuit in terms of the following compact matrix equation,

$$\mathbf{MW} = \mathbf{A} \tag{2.3}$$

where $\mathbf{W} = [\mathbf{V}^T, \mathbf{I}^T]^T$ collects the problem unknowns consisting of all the nodal voltages ($\mathbf{V}$) and currents ($\mathbf{I}$) flowing through current controlled elements such as the ideal voltage source in the scheme of Figure 2.2.

The above equation can be further expanded as follows,

$$\left[\begin{array}{c|c} Y_R & B \\ \hline C & D \end{array}\right] \left[\begin{array}{c} V \\ \hline I \end{array}\right] = \left[\begin{array}{c} J \\ \hline F \end{array}\right] \tag{2.4}$$

Where Y_R is the so-called reduced admittance matrix built from circuit topology and from the information about the characteristics of all the circuit elements but ideal voltage sources and other elements such as current controlled sources. Matrices $\mathbf{C}$ and $\mathbf{D}$ contain branch constitutive relations for current controlled elements. Matrix $\mathbf{B}$ takes into account the contribution of the currents flowing through current controlled elements. In most of the applications such as PDNs, $\mathbf{B} = \mathbf{C}^T$ and both $\mathbf{B}$ and $\mathbf{C}$ consist of entries which are $\{0, \pm 1\}$. $\mathbf{J}$ and $\mathbf{F}$, which define vector $\mathbf{A} = [\mathbf{J}^T, \mathbf{F}^T]^T$, collect the excitations of ideal current and voltage sources. Additional details can be found in [16].

For the case of PDNs, such as the illustrative example of Figure 2.1, the non-linear elements corresponding to the black-box loads/DGs connected at nodes 3 and 4 are represented as voltage controlled elements, e.g., see Figure 2.2, plugged into the $\mathbf{J}$ vector in the previous matrix form, allowing to recast the MNA equation as

$$\mathbf{MW} = \mathbf{A_0} + \mathbf{A_1}(\mathbf{W}), \tag{2.5}$$

$\mathbf{W} \in \mathbb{C}^5$, $\mathbf{W} = [\hat{V}_1, \hat{V}_2, \hat{V}_3, \hat{V}_4, \hat{I}_e]^T$ and $\mathbf{A_0} \in \mathbb{C}^5$, $\mathbf{A_0} = [0,0,0,0, \hat{E}]^T$ collects the excitation voltage (i.e., elements of sub-matrix $\mathbf{F}$), which is only one in the case of above PDN. $\mathbf{A_1}(\mathbf{W}) \in \mathbb{C}^5$ takes into account the non-linear I-V characteristics of loads/renewables (i.e., the current injections in (2.2)).

$$\mathbf{A_1}(\mathbf{W}) = \left[0,\ 0,\ -f(\hat{V}_3; P_3, Q_3, \omega),\ -f(\hat{V}_4; P_4, Q_4, \omega),\ 0\right]^T. \tag{2.6}$$

The expanded matrix form of (2.5) for the considered PDN network is written as

$$\left[\begin{array}{cccc|c} Y_1 & -Y_1 & 0 & 0 & 1 \\ -Y_1 & Y_1+Y_2+Y_3 & -Y_2 & -Y_3 & 0 \\ 0 & -Y_2 & Y_2 & 0 & 0 \\ 0 & -Y_3 & 0 & Y_3 & 0 \\ \hline 1 & 0 & 0 & 0 & 0 \end{array}\right]\left[\begin{array}{c} \hat{V}_1 \\ \hat{V}_2 \\ \hat{V}_3 \\ \hat{V}_4 \\ \hline \hat{I}_e \end{array}\right] = \left[\begin{array}{c} 0 \\ 0 \\ 0 \\ 0 \\ \hline \hat{E} \end{array}\right] + \left[\begin{array}{c} 0 \\ 0 \\ -f(\hat{V}_3; P_3, Q_3, \omega) \\ -f(\hat{V}_4; P_4, Q_4, \omega) \\ \hline 0 \end{array}\right] \tag{2.7}$$

where the admittance elements are defined as $Y_i = 1/(R_i + j\omega L_i)$ for $i = 1,2$ and 3, while the angular frequency dependency is omitted for compactness.

At this stage, we have formulated the problem for the given equivalent PDN. However, the solution to the transcendental equation (2.5) is rather complex, and it can be solved by either the traditional Newton Raphson or alternative simple and effective numerical scheme, which has been proven to work well for weakly non-linear large realistic networks [1].

It is important to point out that the proposed approach for modeling a generic PDN is done for single phase equivalent circuit only, by approximating the balanced power among the phase lines. However, realistic PDNs are mostly unbalanced, due to various components (e.g., induction motors, synchronous motors, etc.) operating in either leading or lagging power factor. Thus, a three-phase modeling has to be carried out to account for all the phase unbalances.

This three-phase modeling yields an unavoidable increase in the size of the involved matrices with a factor of three. Both the magnitude and angle of the nodal voltages associated with the three phases, hereafter referred to as phases a, b, and c, are thus considered. The three-phase operation also includes three phases of transformers, voltage regulators, loads and current injections at all the node points. Hence, for particular network shown in Figure 2.2, the parameters in (2.5) would include three phases and mutual admittances, and thus the order of new matrix for the above mentioned three-phase network would be $\hat{\mathbf{M}} \in \mathbb{C}^{15x15}$ and consequently the matrices $\hat{\mathbf{W}} \in \mathbb{C}^{15}$, $\hat{\mathbf{A}}_0 \in \mathbb{C}^{15}$ and $\hat{\mathbf{A}}(\hat{\mathbf{W}}) \in \mathbb{C}^{15}$. Thus, the method does not change ([68, 71] presented detailed three-phase power-flow solution).

2.2 Fixed-Point Iteration

In the proposed numerical scheme, the first step towards the solution of (2.5) requires the interpretation of the circuit in Figure 2.2 in terms of the circuit shown in Figure 2.3, in which, without loss of generality, the circuit is split in two sub-circuits, i.e., a usually large linear (the left part) and small non-linear (the right part) portions of the network, coupled through current and voltage controlled sources.

The next step in solving the non-linear circuit in the phasor domain involves replacing the voltage controlled current sources with independent current sources of values $\hat{I}_3$ and $\hat{I}_4$, as shown in Figure 2.4, which means the linear circuit is decoupled from the non-linear circuit.

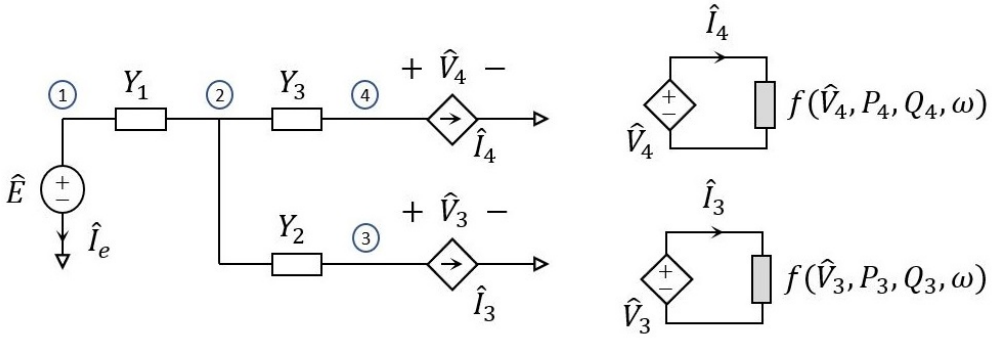

Figure 2.3: Arbitrary PDN with two renewables connected at nodes 3 and 4 - circuit equivalent with controlled circuits, splitting the original network into two parts, a large linear portion and a non-linear portion defined by the non-linear elements only.

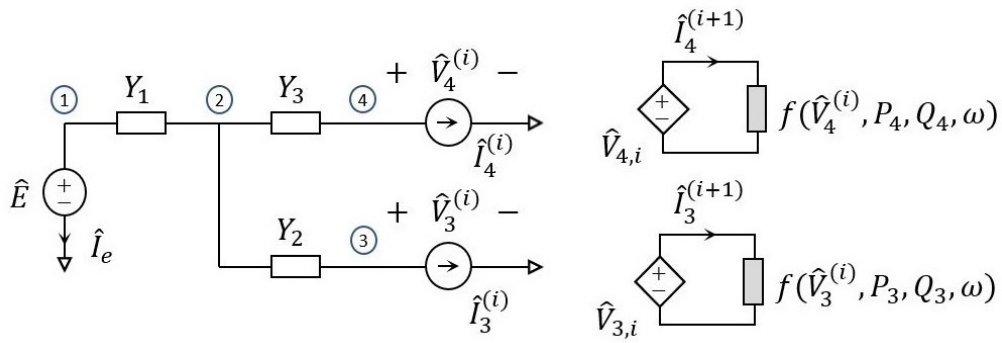

Figure 2.4: Arbitrary PDN with two renewables connected at nodes 3 and 4 - circuital interpretation of the proposed iterative solution scheme.

Now, according to the so-called waveform relaxation idea [17], the non-linear MNA

equation (2.5), for the above network, can be approximated by the following iteration scheme:

$$\begin{cases} \mathbf{M}\mathbf{W}^{(i)} = \mathbf{A}_0 + \mathbf{A_1}^{(i)} \\ \mathbf{A_1}^{(i+1)} = \mathbf{A_1}(\mathbf{W}^{(i)}), \end{cases} \tag{2.8}$$

where, complex vector $\mathbf{A_1}^{(i)} = [0,0,-\hat{I}_3^{(i)},-\hat{I}_4^{(i)},0]^T$ collects the amplitude at i-th iteration of the independent current sources connected to the linear portion of the network (left part of the circuit in Figure 2.4) and $\mathbf{A_1}^{(i+1)}$ is a complex vector that collects the currents flowing though the voltage controlled sources in the non-linear portion (right part of the circuit in Figure 2.4), as function of voltages $\mathbf{W}$, defined by (2.6), as:

$$\mathbf{A_1}^{(i+1)} = [0\ ,0\ , f(\hat{V}_3^{(i)}; P_3, Q_3, \omega),\ \ f(\hat{V}_4^{(i)}; P_4, Q_4, \omega),\ \ 0] \tag{2.9}$$

The above equation can be solved iteratively via the update rule:

$$\mathbf{W}^{(i+1)} = \mathbf{M}^{-1}(\mathbf{A}_0 + \mathbf{A_1}(\mathbf{W}^{(i)})). \tag{2.10}$$

An error convergence criterion can be used for the above iteration technique. L-2 norm is commonly used to converge the error between values of unknown vector $\mathbf{W}$, subsequent with a given threshold (ε) as:

$$\|\mathbf{W}^{(i+1)} - \mathbf{W}^{(i)}\|_{L_\infty} \leq \varepsilon. \tag{2.11}$$

Conveniently, the above scheme can be derived via an alternate and thorough mathematical formulation in terms of a fixed-point equation by recasting the MNA equation (2.5) in terms of the following non-linear,

$$\mathbf{F}(\mathbf{W}) = 0 \tag{2.12}$$

where, $\mathbf{F}$ is a continuous vector-valued map,

$$\mathbf{F}(\mathbf{W}) = \mathbf{W} - \mathbf{M}^{-1}(\mathbf{A}_0 + \mathbf{A_1}(\mathbf{W})) \tag{2.13}$$

Solving the above equation is equivalent to solving the fixed-point equation as:

$$\mathbf{W} = \boldsymbol{\Phi}(\mathbf{W}), \tag{2.14}$$

where:

$$\boldsymbol{\Phi}(\mathbf{W}) = \mathbf{W} - \mathbf{F}(\mathbf{W}) \tag{2.15}$$

Here, the vector $\mathbf{W}$ is the fixed-point which solves the equation. This means the equation is solved iteratively by starting from the initial guess value $\mathbf{W}^{(0)}$, with the following scheme,

$$\mathbf{W}^{(i+1)} = \boldsymbol{\Phi}(\mathbf{W}^{(i)}). \tag{2.16}$$

If we assume the starting value is sufficiently close to the actual fixed-point, the above iteration scheme converges after few iterations. Substituting the equations (2.13) and (2.15) in (2.16), the above equation is equivalent to the one derived by the circuital approach in (2.10).

It is important to highlight that the main advantage of the above proposed formulation is that the linear portion, which is generally large for a typical PDN, is solved only once during the iterative process, (i.e., the inverse Matrix $\boldsymbol{M}^{-1}$ must be calculated once since all the entries are known according to the topology and do not vary). Also, the MNA equation does not contain any differential operator, which means it is static non-linear, as we are working in the complex domain, and unlike Newton Raphson, it does not require to compute jacobian matrix of the network. Thus it leads to much simpler and fast solution.

The above scheme works well for weakly non-linear problems, and it has been verified to be effective for the class of problem at hand. However, it is important to remark that this fixed-point iteration can be rearranged, if needed, to cope up with Newton Raphson based procedure, again with a similar interpretation of the circuit arising from the splitting between a linear and a non-linear part. Moreover, the above circuital interpretation of PDNs enables the implementation in any SPICE-based circuit solver (e.g., HSPICE, PSPICE, LTSpice, etc) in the solution, explained in the next section.

2.3 SPICE in the loop

Considering the PDN equivalent circuit in Figure 2.4, the decoupled linear and non-linear portion of the circuits are solved separately as discussed above, where the linear part is usually very large which involves the inversion of topology matrix **M**. Alternatively, this linear portion can be solved by using SPICE-based solver for computing the network unknowns (**W**). It can be done by drawing the circuit in LTSpice integrated developement environment (IDE) or equivalently a netlist text file written through MATLAB and then solved by performing AC analysis at a single frequency.

This means that a generic PDN circuit is solved by first decoupling the linear and non-linear portions, and then fixed-point iteration is used to solve the circuit, which involves SPICE for solving the linear portion (instead of MNA (2.10)), while the non-linear portion is still solved by the same iterative scheme (see Figure 2.5).

For the SPICE solution, the netlist of linear portion of the network is automatically generated by MATLAB based on the topology. The equivalent current injections for the loads/renewables calculated by (2.2) are fed to LTSpice, which then produces the phasor responses of the nodal voltages. These phasor responses are used for the fixed-point iteration to update the netlist at each iteration until a given threshold is achieved for the load-flow solution.

Please note that the LTSpice netlist is run through MATLAB using the matlab function *LTspice2matlab.m* which is available online [96].

The LTSpice netlist for the above discussed circuit is available in Appendix A, while the detailed netlist syntax and SPICE tutorial can be found in [97]. Section 2.4 further validates the above approach for solving test distribution networks.

It is pertinent to point out that the non-linear portion of the equivalent PDN can also be solved with SPICE, but for that a particular iterative scheme (e.g., fixed-point iteration) is still required.

2.4 Validation of the Circuital Approach - Numerical Results

The feasibility and effectiveness of the proposed circuital approach for power-flow solution is investigated by considering multipe single phase and three-phase test networks. The first two single phase networks include 33-node and 90-node radial networks, where the latter network is then modified as a weakly-meshed to further analyze the convergence of the proposed approach. Three-phase test networks involve 37-, 123-, and 906-bus feeders provided by IEEE PES. The above mentioned test networks are solved

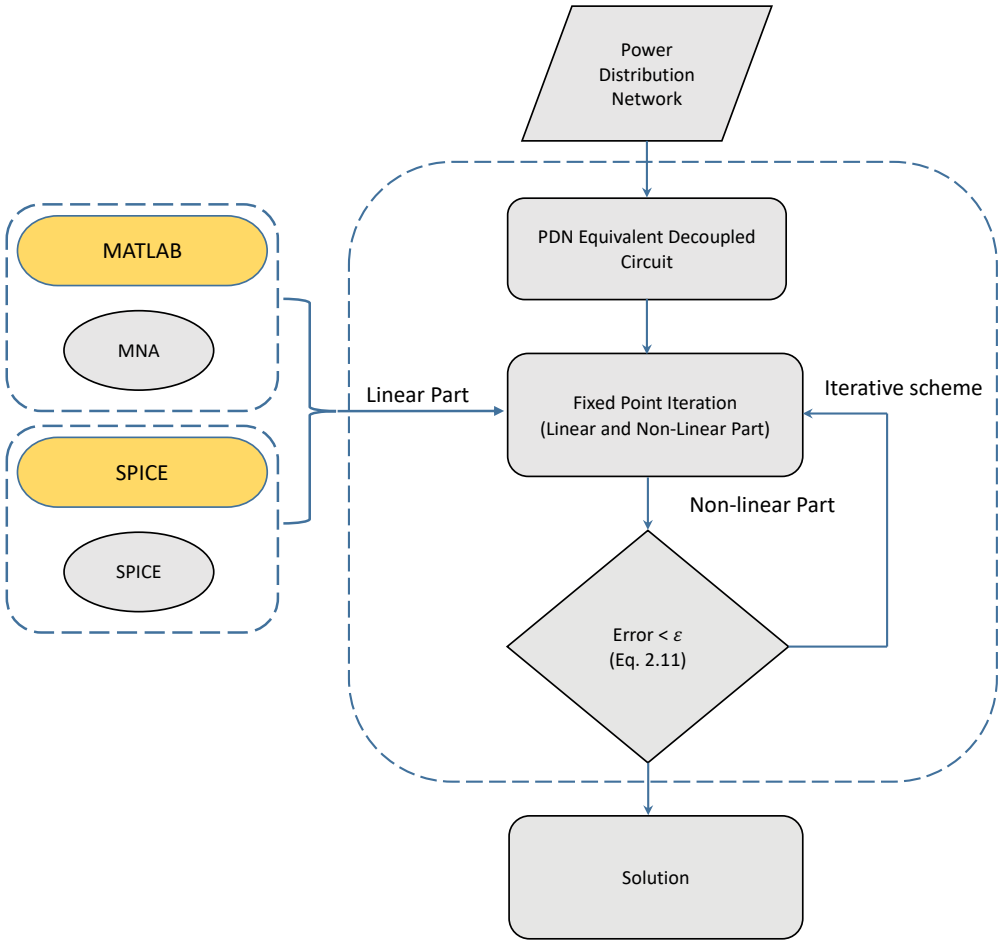

Figure 2.5: Solution scheme of a generic PDN

via the proposed iterative scheme via MATLAB and via the SPICE integration and the obtained power-flow results for both cases are validated via OpenDSS [98], a reference tool released by the Electric Power Research Institute (EPRI) and the *Z-bus* method [68]. Additionally, the solutions are validated with the industrial tool Power System Analysis Software Package (PSASP) [99], which was carried out during research fellowship at the State Grid Simulation Center of CEPRI. For all the validation tests, the tolerance ε in (2.11) is set to 10^{-4}. The simulation and plots are generated running the scripts on a PC equipped with a CPU Intel Core i7 (seventh generation) with 3.6 GHz and 32 GB ram.

2.4.1 33-Node Single Phase Network

This is a single phase radial network with 33 nodes and 32 branch connections, hereafter referred to as Test33, with no transformer or regulators, and has a total load of 3.7 MW operating at voltage 12.66 kV [100]. The topological configuration of this network is shown in the Figure 2.6. The network branch connections with equivalent resistance and reactance are given in Table 2.1 while the load power ratings are listed in Table 2.2.

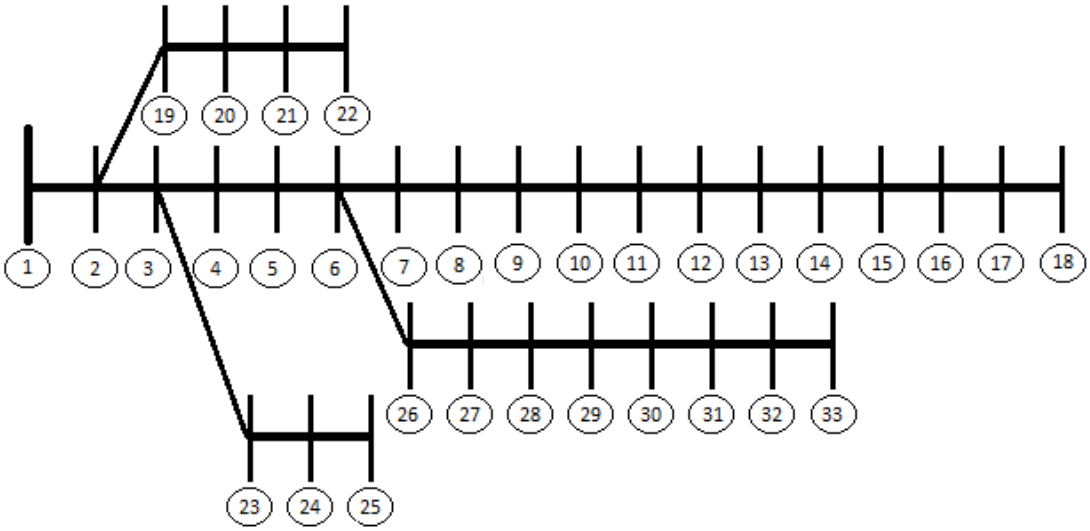

Figure 2.6: Topological structure considered for the Test33 network.

Table 2.1: Branch Parameters for the Test33 PDN

Node i	Node j	Branch r (ohms)	branch x (ohms)
1	2	0.0922	0.047
2	3	0.4930	0.2511
3	4	0.3660	0.1864
4	5	0.3811	0.1941
5	6	0.819	0.707
6	7	0.1872	0.6188
7	8	1.7114	1.2351
8	9	1.03	0.74
9	10	1.04	0.74

10	11	0.1966	0.065
11	12	0.3744	0.1238
12	13	1.468	1.155
13	14	0.5416	0.7129
14	15	0.591	0.526
15	16	0.7463	0.545
16	17	1.289	1.721
17	18	0.732	0.574
2	19	0.164	0.1565
19	20	1.5042	1.3554
20	21	0.4095	0.4784
21	22	0.7089	0.9373
3	23	0.4512	0.3083
23	24	0.898	0.7091
24	25	0.896	0.7011
6	26	0.203	0.1034
26	27	0.2842	0.1447
27	28	1.059	0.9337
28	29	0.8042	0.7006
29	30	0.5075	0.2585
30	31	0.9744	0.963
31	32	0.3105	0.3619
32	33	0.341	0.5302

Table 2.2: Load data for the Test33 PDN

Node i	**Load P (kW)**	**Load Q (kVAr)**
1	0	0
2	100	60
3	90	40
4	120	80

5	60	30
6	60	20
7	200	100
8	200	100
9	60	20
10	60	20
11	45	30
12	60	35
13	60	35
14	120	80
15	60	10
16	60	20
17	60	20
18	90	40
19	90	40
20	90	40
21	90	40
22	90	40
23	90	50
24	420	200
25	420	200
26	60	25
27	60	25
28	60	20
29	120	70
30	200	600
31	150	70
32	200	100
33	60	40

The network power-flow solution is performed with the above proposed circuital

approach, both with MNA (2.10) and LTSpice implementation (section 2.3). All loads are PQ type and their corresponding current injections are calculated using (2.2), with no DGs connected. Figure 2.7 collects the voltage profile, in per unit (p.u.), of the network calculated with, proposed circuital approach, the OpenDSS, PSASP and Direct Approach load flow solution [55]. It is important to point out that for very small networks there are some minor differences between OpenDSS and the curves obtained using all the other approaches, which provide overlapped curves. Also, both OpenDSS and PSASP are blind tools whose some parameters are hidden or automatically set and for which it is difficult to set up a completely coherent and consistent comparison. On the other hand, the proposed approach generates responses fully matching with the ones of PSASP, thus validating the method. What is more important, these differences disappeared for the larger networks considered in the next sections, highlighting that possible minor differences in the settings will produce negligible effects in real applications.

This is a small test network for analyzing the initial simulation of the proposed approach with MNA and LTspice solution. In the next section, a larger network is solved via the proposed circuital approach to further validate the effectiveness of the technique.

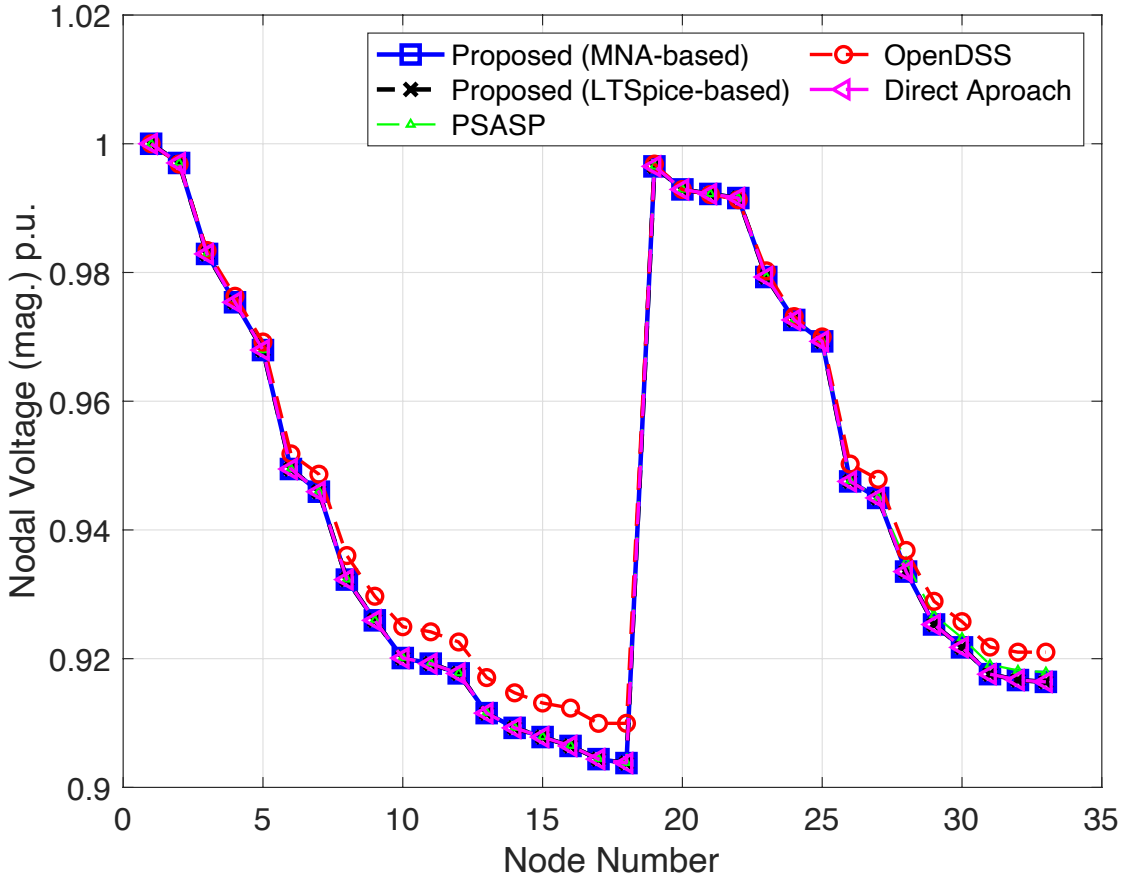

Figure 2.7: Validation of the Test33 network carried out with proposed method, OpenDSS, PSASP and Direct Approach.

2.4.2 90-Node Single Phase Network

This is a 10 kV single phase radial distribution network. It has 90 nodes and 89 branches with no transformer and regulators, hereafter referred as Test90 [101]. The topological configuration of this network is shown in Figure 2.8. The network branch connections with equivalent resistance and reactance for this 90-node network are given in Table 2.3 while the load power ratings are listed in Table 2.4.

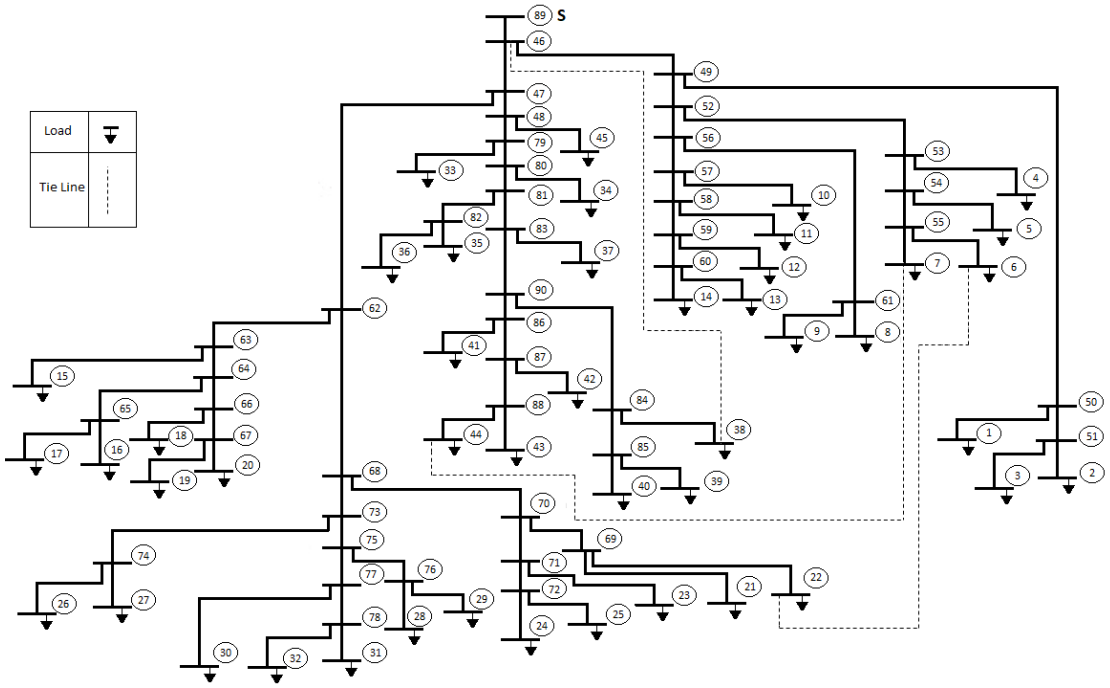

Figure 2.8: Topological structure considered for the Test90 network.

Table 2.3: Branch Parameters for the Test90 PDN

Node i	Node j	Branch r (ohms)	branch x (ohms)
89	46	0.002	0.015
47	46	0.004	0.019
48	47	0.003	0.02
48	45	0.001	0.012
49	46	0.005	0.021
49	50	0.01	0.05
50	1	0.001	0.07
50	51	0.015	0.075
51	2	0.016	0.08
51	3	0.017	0.082
49	52	0.003	0.01
53	52	0.0015	0.021
53	4	0.0012	0.003

53	54	0.012	0.076
54	5	0.02	0.09
54	55	0.012	0.095
55	6	0.025	0.087
55	7	0.128	0.425
52	56	0.09	0.31
56	61	0.085	0.125
66	67	0.0015	0.045
67	19	0.002	0.009
67	20	0.003	0.016
62	68	0.0001	0.0005
68	70	0.0004	0.0009
69	70	0.001	0.006
69	21	0.001	0.005
69	22	0.002	0.008
70	71	0.002	0.007
71	23	0.001	0.009
71	71	0.012	0.075
72	24	0.025	0.085
72	25	0.015	0.079
68	73	0.001	0.012
73	74	0.002	0.007
74	26	0.003	0.008
74	27	0.005	0.012
73	75	0.004	0.007
75	76	0.002	0.006
76	28	0.001	0.007
76	29	0.002	0.005
75	77	0.002	0.008
77	30	0.001	0.009

77	78	0.004	0.0071
78	31	0.005	0.009
61	8	0.012	0.075
61	9	0.015	0.161
56	57	0.002	0.015
57	10	0.003	0.025
58	57	0.001	0.005
58	11	0.002	0.006
58	59	0.015	0.025
59	12	0.003	0.015
59	60	0.009	0.021
60	13	0.001	0.004
60	14	0.006	0.01
47	62	0.001	0.009
62	63	0.0015	0.008
63	15	0.01	0.04
63	64	0.004	0.009
64	65	0.002	0.008
65	16	0.015	0.017
65	17	0.01	0.025
64	66	0.001	0.003
66	18	0.001	0.004
78	32	0.003	0.01
79	48	0.0002	0.0005
79	33	0.002	0.001
79	80	0.004	0.008
80	34	0.002	0.008
80	81	0.001	0.007
81	82	0.005	0.01
82	35	0.004	0.008

82	36	0.002	0.01
81	83	0.007	0.012
83	37	0.01	0.072
83	90	0.012	0.021
90	84	0.015	0.0025
84	38	0.001	0.07
84	85	0.0002	0.009
85	39	0.012	0.072
85	40	0.015	0.092
90	86	0.02	0.08
86	41	0.007	0.014
86	87	0.009	0.021
87	42	0.015	0.028
87	88	0.017	0.027
88	43	0.0013	0.023
88	44	0.017	0.025
6	22	0.005	0.01
7	44	0.018	0.022
46	38	0.02	0.07

Table 2.4: Load data for the Test90 PDN

Node	**Load P (kW)**	**Load Q (kVAr)**
1	120	60
2	670	230
3	870	450
4	1230	710
5	820	320
6	620	340
7	3400	1200
8	230	170

9	240	180
10	250	190
11	340	140
12	290	190
13	160	120
14	170	110
15	1810	670
16	2450	1230
17	140	110
18	130	110
19	280	170
20	1230	510
21	910	450
22	1230	670
23	890	340
24	450	190
25	130	90
26	350	120
27	320	140
28	240	j30
29	1240	570
30	980	670
31	880	540
32	770	520
33	660	230
34	760	340
35	2310	1230
36	780	350
37	2340	1150
38	2430	1240

39	670	240
40	880	330
41	1320	760
42	450	210
43	120	90
44	1230	540
45	1650	910

Voltage magnitude values calculated through the proposed MNA and LTspice, and OpenDSS, are shown in Figure 2.9. These overlapped curves for the above mentioned methods highlight the feasibility of the proposed approach and also proves the flexibility of the technique which allows a custom MATLAB implementation.

For further analyzing the proposed approach, the Test90 network is suitably modified as a weakly meshed network by closing the connections of three tie branches shown by dashed lines in Figure 2.8. The voltage profile of this modified network as compared to the original radial network is shown in Figure 2.10.

It is pertinent to highlight that the convergence for radial and weakly meshed networks are of the same order, with only few dozens of milliseconds of CPU execution time, which is 16.9 ms for radial versus 18.2 ms for weakly meshed. Most importantly, the branches with a loop (in weakly meshed) are treated in the same way, without any custom modification in the iterative technique, which stresses the generality of the proposed approach.

It is important to remark that for this example network, both the accuracy and efficiency are merely the same as those obtained via the alternate approaches. An additional validation is instead provided in chapter 4, where the proposed tool is applied to the large benchmark IEEE 8500-node test feeder.

2.4.3 IEEE 37-bus Feeder

This is a radial three-phase distribution network based on an actual feeder in California, USA. It has mix type of loads, all with delta configuration operating at 4.8 kV [76]. The topological connection is shown in Figure 2.11. The network is heavily unbalanced with the details given below,

1. 37 three-phase buses yielding to 111 node points operating at 4.8 kV

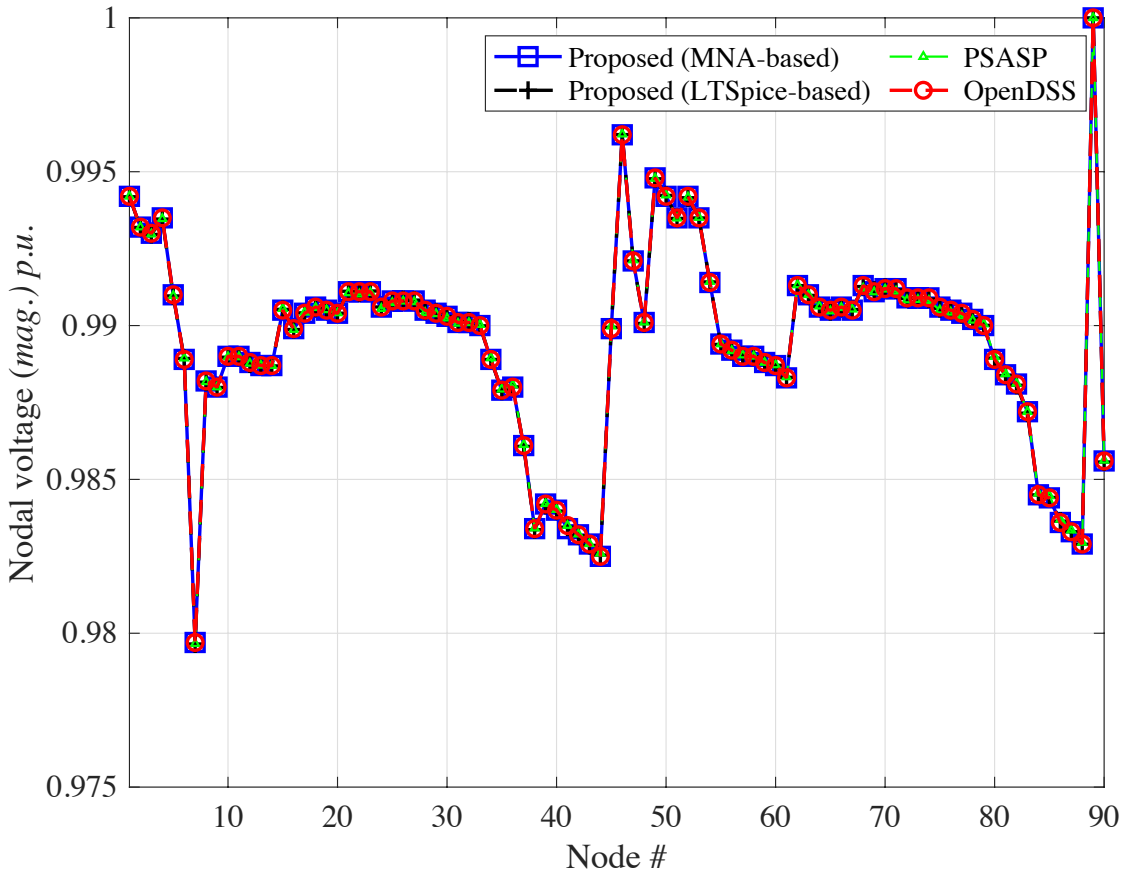

Figure 2.9: Validation of the Test90 network carried out with proposed method, OpenDSS and PSASP

2. a substation transformer connected in delta-delta, rated at 2500 kVA, 230kV/4.8 kV line-to-line, with transformer impedance of $(2 + j8)\%$

3. 1 transformer to serve LV node, connected in delta-delta, rated at 500 kVA, 4.8kV/0.48 kV line-to-line, with transformer impedance of $(0.09 + j1.81)\%$

4. 1 open-delta connected step SVRs whose tap positions are given in Table 2.5

5. 25 delta connected constant-power, constant-current and constant-impedance single-phase loads

6. 36 three-phase branch connections with three-,two-, and single-phase laterals

The network is solved with proposed MNA-based, *Z-bus* and the OpenDSS in which the transformers and voltage regulators are modeled as in [95, 68]. The voltage magnitude and phase angles for phases a, b, & c are shown in Figure 2.12, which show overlapped

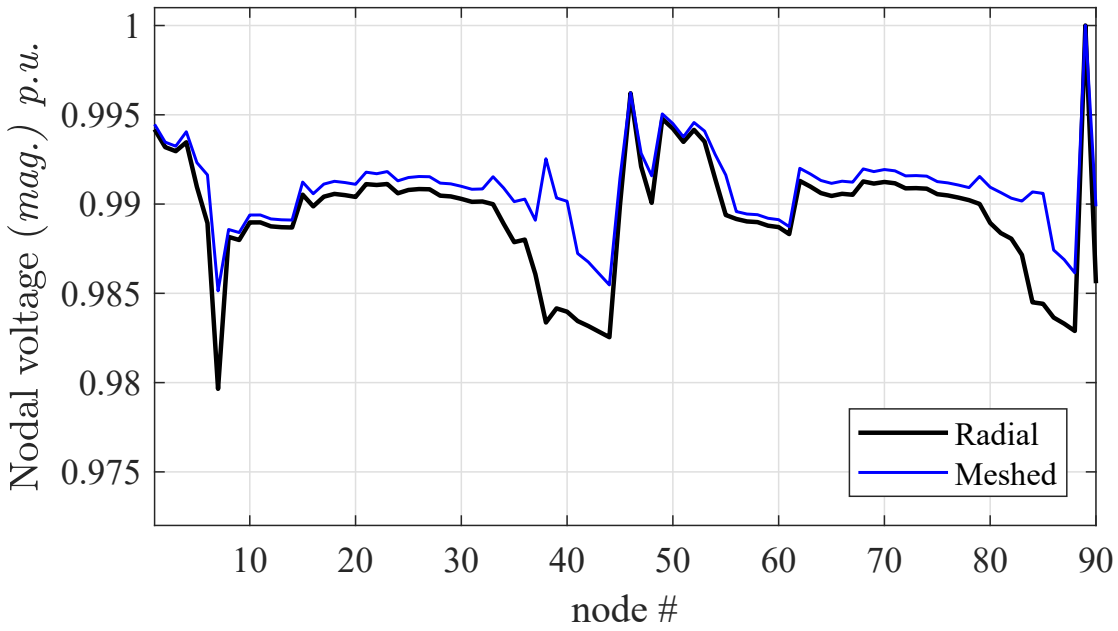

Figure 2.10: Voltage profile of the Test90 network; differences between radial and weakly meshed configuration.

Table 2.5: Voltage regulator tap positions- IEEE 37-bus Feeder

Regulator	**Bus**	**Tap Positions**
Reg.1-AB	799	7
Reg.1-BC	799	4

curves for proposesd-MNA and *Z-bus* while OpenDSS has very minimal offset due to the method of solving with Newton-Raphson. This is further validated in the next larger test networks.

2.4.4 IEEE 123-bus Feeder

This distribution test feeder operates at 4.16 kV with mix type of loads (i.e., constant current, impedance and power) [76]. This network is heavily unbalanced which features,

1. 123 three-phase buses and 6 three-phase switches, yielding to total of 378 node points
2. 1 transformer to serve LV node, connected in delta-delta, rated at 150 kVA, 4.16kV/0.48 kV line-to-line, with transformer impedance of $(1.27 + j2.72)\%$
3. 4 wye-connected SVRs, whose tap positions are given in Table 2.6

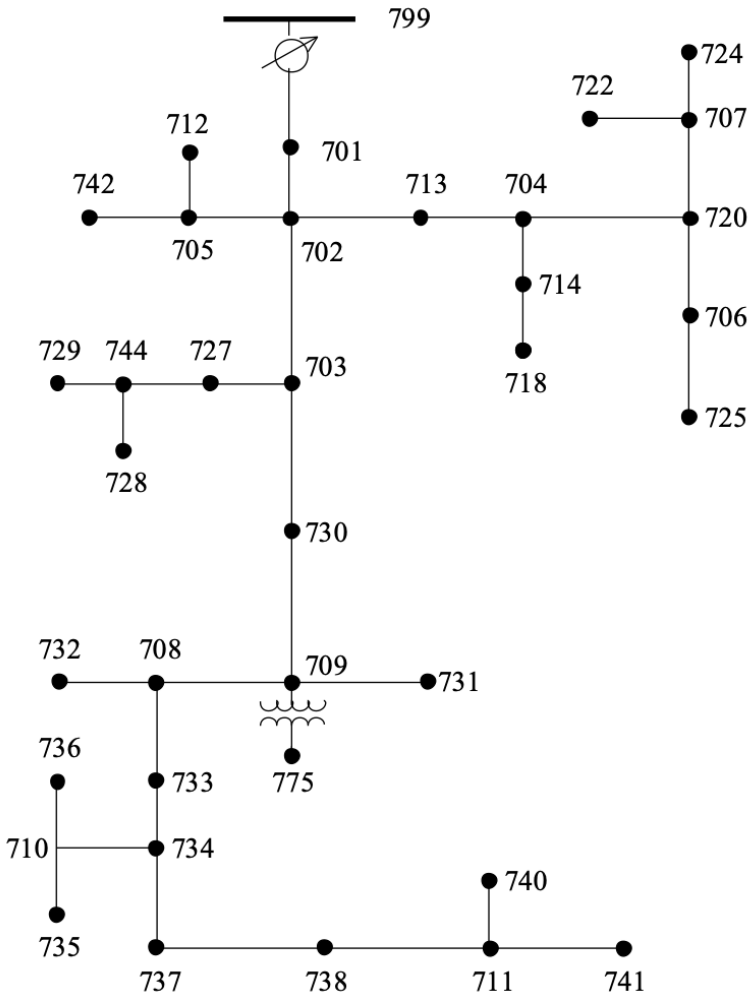

Figure 2.11: Topological structure for IEEE37-bus feeder.

4. 85 delta and star connected three-phase loads

5. 118 three-phase branch connections with three-,two-, and single-phase laterals.

6. 3 single-phase and 1 three-phase capacitor banks

The topological single-line diagram is shown in Figure 2.13. The transformers and voltage regulators are modeled as in [95, 68]. Figure 2.14 shows the network voltage magnitude and phase angles for all the three phases, solved with the proposed MNA-based solution, *Z-bus* and OpenDSS, showing overlapped curves.

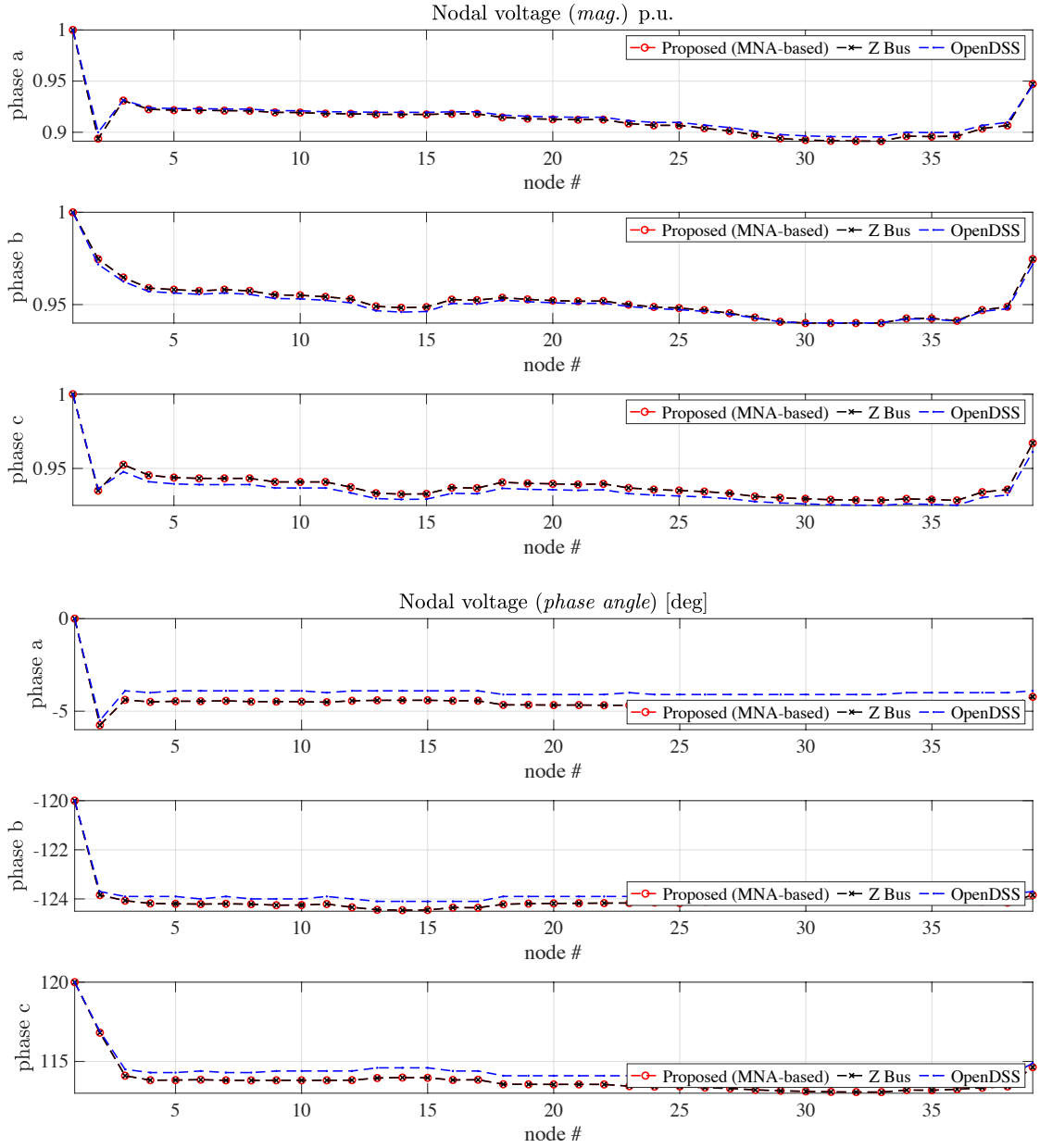

Figure 2.12: Three-phase voltage profile of the IEEE37-bus test network computed by means of the proposed MNA-based method, the *Z-bus* approach and via the OpenDSS tool. (**top**) Phase magnitudes (p.u.), (**bottom**) phase angles (degrees).

Table 2.6: Voltage regulator tap positions- IEEE 123-bus Feeder

Regulator	Bus	Tap Positions
Reg.1-A	150	7
Reg.1-B	150	7
Reg.1-C	150	7
Reg.2-A	9	-1
Reg.3-A	25	0
Reg.3-C	25	-1
Reg.4-A	160	8
Reg.4-B	160	1
Reg.4-C	160	5

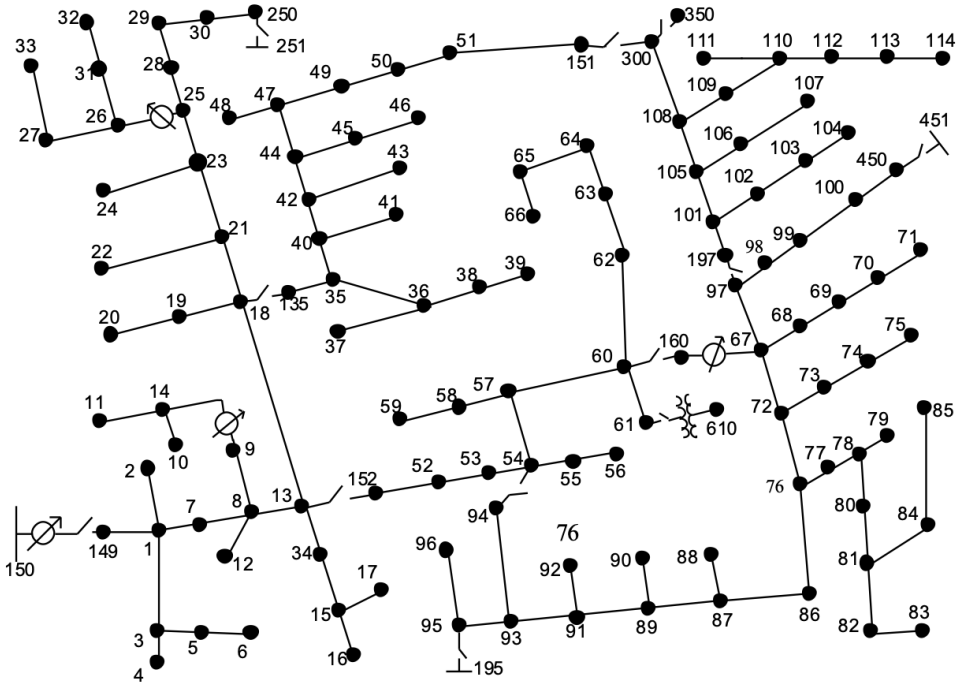

Figure 2.13: Topological structure for IEEE123-bus feeder.

2.4.5 European Low Voltage 906-Node Feeder

This three-phase test network is a typical LV feeder operating at 416 V and has a transformer at the substation point to connect it with the MV grid system. It is a radial network with 50 Hertz operating frequency and has only WYE connected loads without

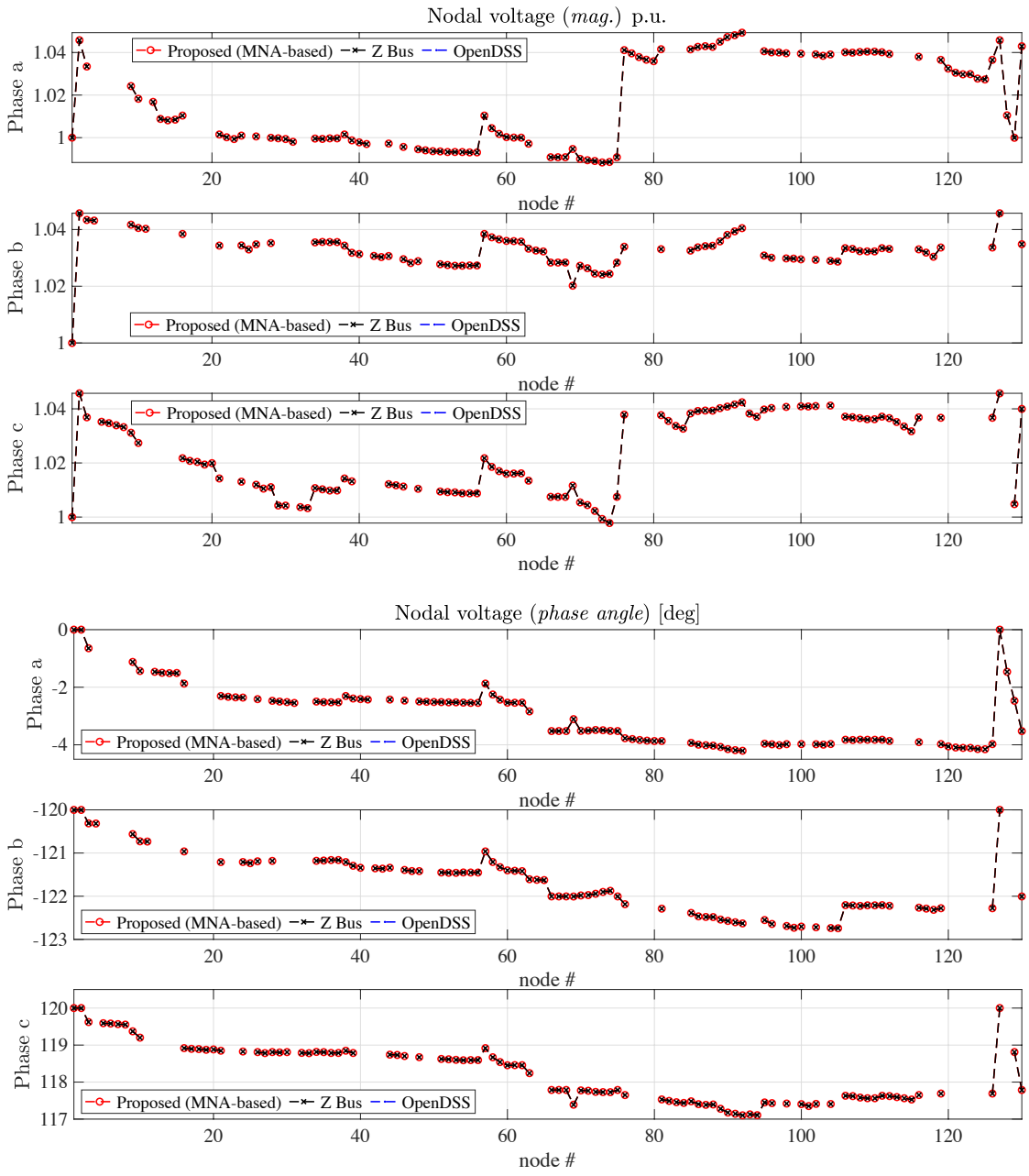

Figure 2.14: Three-phase voltage profile of the IEEE123-bus test network computed by means of the proposed MNA-based method, the *Z-bus* approach and via the OpenDSS tool. (**top**) Phase magnitudes (p.u.), (**bottom**) phase angles (degrees).

capacitors and voltage regulators [76]. Figure 2.15 shows single-line diagram of the network topology with the details listed below,

1. 906 LV three-phase buses, yielding to 2718 node-points; Bus coordinates can be found here [76]
2. operating at 416 V, which is typical in the European low voltage distribution systems
3. a substation transformer connected in delta-wye, rated at 800 kVA, 11kV/426 V line-to-line, with transformer impedance of $(0.4 + j4)\%$
4. 55 star and delta connected constant-power, constant-current and constant-impedance single-phase loads
5. 905 three-phase branch connections all with three-phase laterals

The network power-flow is solved with the proposed MNA, the *Z-bus* and OpenDSS. Figure 2.16 shows the voltage profile of the network, with magnitude and phase angles for the three phases accordingly, solved with proposed MNA and validated with both *Z-bus* and OpenDSS. This shows the feasibility of the proposed approach for comparatively larger unbalanced PDNs.

2.5 Concluding Remarks

The compact modeling of PDNs and their interpretation in terms of a non-linear circuit in the phasor domain provides an alternate and general approach. It is flexible and does not require any custom modification for a specific network being radial, weakly meshed or even heavily meshed. The interpreted circuit is described via a standard MNA formulation, where the resulting matrices are solved using fixed-point iteration. Also, the idea of splitting the network into a large linear and a non-linear portion helps solving the larger part once during the iterative process, thus speeding up the solution. The validations of the proposed approach performed with both single and three phase networks, ranging from 33-nodes to low voltage 906-node feeder, proved that the approach offers good performance in terms of both accuracy and convergence. The use of fixed-point iteration scheme also proves that it is a feasible and effective solution without use of any auxiliary matrix (for example, jacobian matrix) at each iteration of the solution. It is pertinent to highlight that similar to [18], the proposed method does not guarantee convergence, but since most of the PDNs are weakly non-linear, it is proven to work well in large application problems. The proposed approach

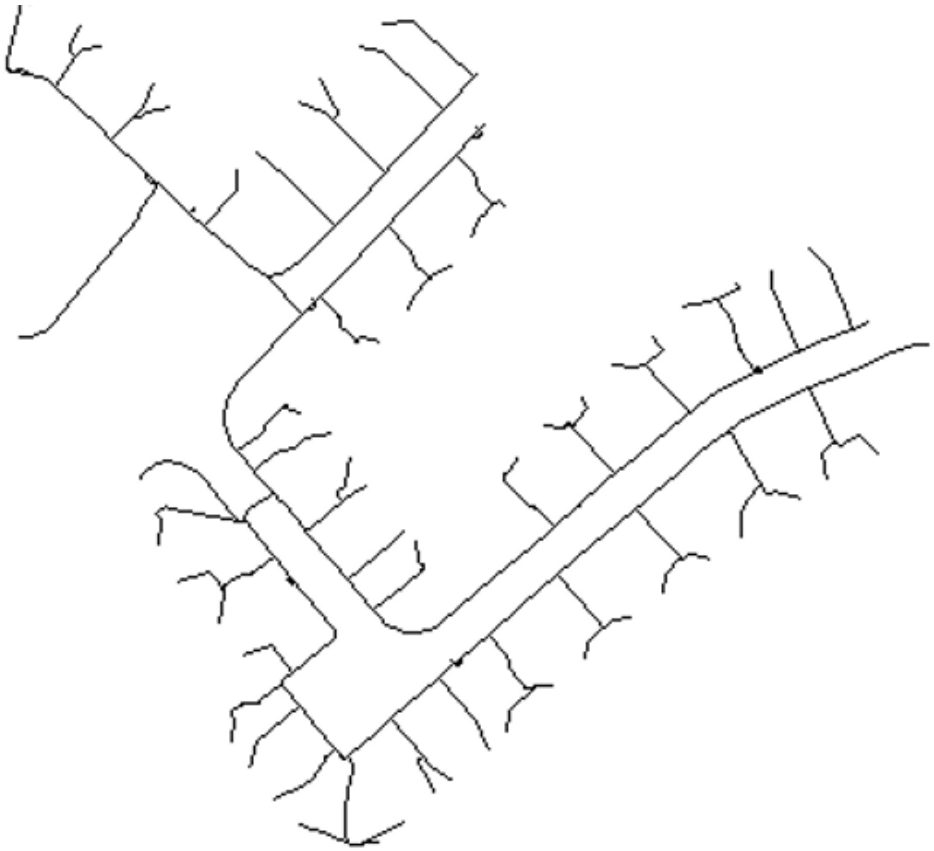

Figure 2.15: Single-line diagram of network topology for European LV 906-node feeder.

can also be used, for problematic cases, with other iterative schemes, such as Newton-Raphson. Moreover, the above interpretation of the original network allows replacing the MATLAB MNA formulation with an IDE-based circuit simulation (SPICE-based) to solve the equivalent circuit, which is explained in 2.3 and also cross validated with the state-of-the-art methods in successive section.

The effectiveness of the proposed approach for handling very large three-phase PDNs is further verified in the chapter 4. It is important to state that part of the work presented in this chapter is published in a journal paper [1].

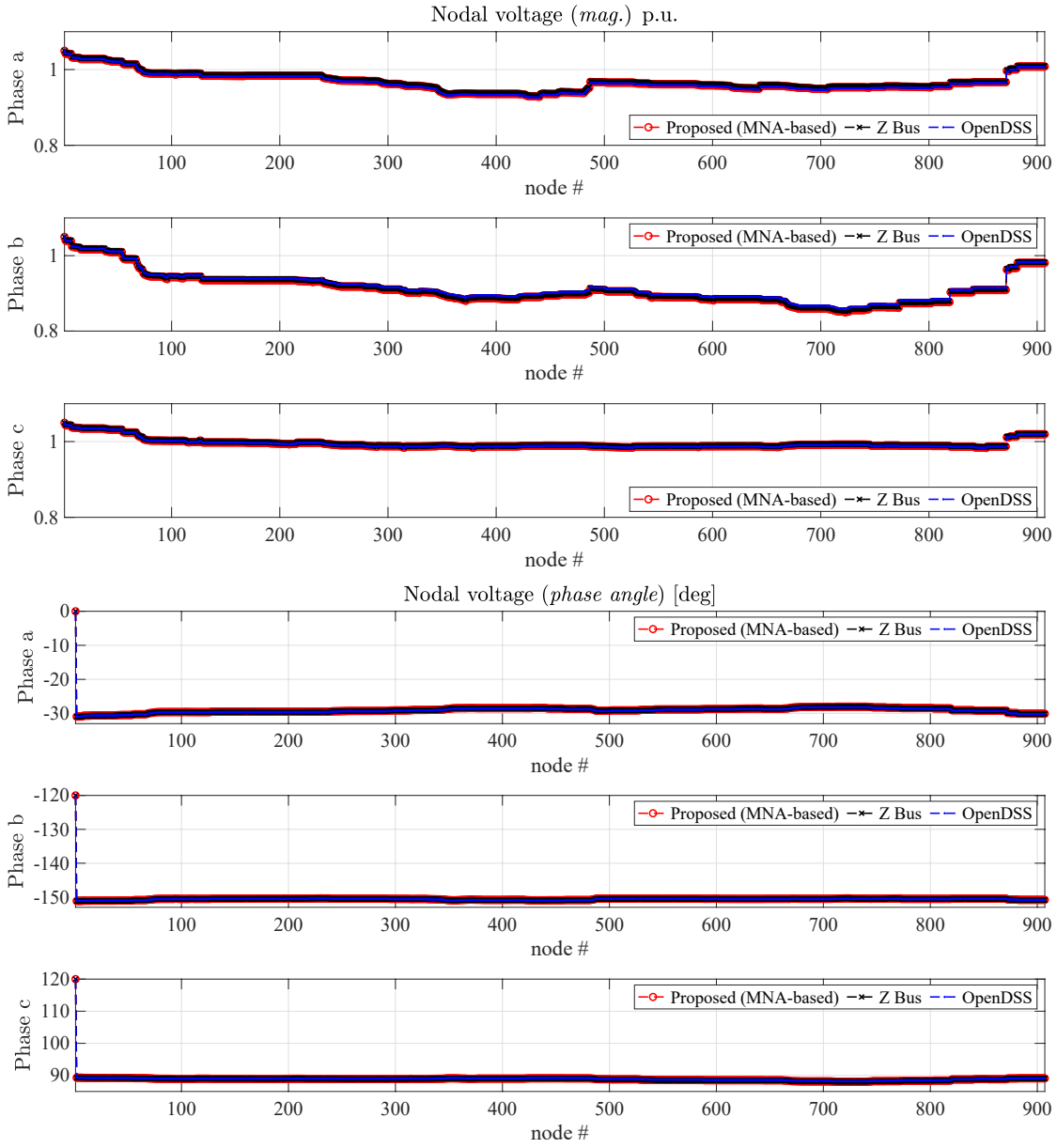

Figure 2.16: Three-phase voltage profile of the European LV 906-node feeder computed by means of the proposed MNA-based method, the *Z-bus* approach and via the OpenDSS tool. (**top**) Phase magnitudes (p.u.), (**bottom**) phase angles (degrees).

Chapter 3

Uncertainty Quantification of Power Networks

The reliability assessment of current and next generation grids must incorporate the unavoidable fluctuations of uncertain parameters in the generation, transmission and distribution networks. For the latter two, typical examples include, the number, location and strength of renewables or loads, the physical parameters of transmission lines and other equipment that might change due to aging effects or extreme weather conditions [20, 21, 22, 23]. These changes affect the functioning state of a power network and require sophisticated models for monitoring the load-flow, regulating the electricity market and assessing the network reliability. To this end, the availability of tools for UQ [24, 25, 26] is helpful to address the inherent uncertain nature of the problem at hand.

This chapter presents the UQ of power networks, with the aim of analyzing the effect of the uncertain behavior of distributed renewables and the changes in the physical medium on the network node voltages. Several techniques for the UQ are presented along the chapter, ranging from the standard MC method to the more recent approaches and techniques for the constrution of accurate and fast-to-evaluate surrogate models such as PCE and ML regressions. [2, 102].

The chapter content is organized as followed. Section 3.1 discusses the UQ performed for power networks with an MC simulation for 90-node distribution network. Section 3.2 presents the background of surrogate models used in this study. The proposed ML approach for UQ is given in Section 3.3 . Section 3.4 investigates the performance of the proposed methodology by considering the IEEE118-bus system. Summary and highlights are instead collected in Section 3.5.

3.1 UQ of Power Networks

The techniques presented in this chapter aim to quantify the impact of the uncertain parameters on magnitude of the network nodal voltages, hereafter referred to as the output vector $\mathbf{y} = [y_1, \dots, y_M]^\mathsf{T} \in \mathbb{R}^M$. The output vector is an implicit function of $\mathbf{x}$, which we denote as,

$$\mathbf{y} = \mathscr{M}(\mathbf{x}), \tag{3.1}$$

where $\mathscr{M} : \mathbb{R}^d \to \mathbb{R}^M$ generically indicates the full-computational model that is used to calculate $\mathbf{y}$ for a given configuration of $\mathbf{x}$.

The traditional method for quantifying the stochastic behavior of a system response based on uncertain parameters is MC. It is a simple technique that can be easily applied to any system without altering the system equations [103]. A large set of input configurations is used to perform a repetitive simulation. The underlying idea is to draw random samples based on PDF, which might be based on historical data, and generate the system response to each input configuration. This yields a probabilistic set that defines the system's behavior based on stochastic inputs.

Surrogate modeling can be seen as a promising alternative to the plain MC simulation. A surrogate model can be interpreted as *a model of a model*. The underlying idea is to use a set of training samples generated via the expensive computational model along with a regression.

This section focuses on a practical application of MC performed on Test90 single phase network with DGs spread along the network. Specifically 12 DGs are connected at randomly chosen nodes, for the statistical assessment of the effects of two types of DGs, the PQ and PV type (see 2.1 for DG types), in terms of location and power generation.

The uncertain parameters are the values of equivalent resistance N_r and inductance N_x of the physical medium (branch connection between two nodes) denoted by N_{branch} set of branches. Thus the total number of parameters would be

$$d = 2 * N_{branches} \tag{3.2}$$

The set of uncertain parameters is denoted by the input vector $\mathbf{x} = [x_1, \dots, x_d]^\mathsf{T} \in \mathbb{R}^d$. The output vector consists of magnitude of nodal voltages, represented $\mathbf{y} = [y_1, \dots, y_M]^\mathsf{T} \in \mathbb{R}^M$, where the output is a function of $\mathbf{x}$ (3.1).

The application is performed by first considering the network without DGs (case 1), and then with the DGs connected at different locations (case II and III), additional

details are given in Table 3.1. For the specific case III, both PQ and PV type of DGs are considered, for which the reactive power is corrected (compensated) at each iteration according to [94, 93] as stated in section 2.1.1.

Table 3.1: Description for different cases of Test90.

Case	DG Node(s)	Type	P (p.u.)	Q (p.u.)	V (p.u.)
Case I	No DGs	-	-	-	-
Case II	7	PQ	0.3	0.3	-
	20	PQ	0.1	0.1	-
	37	PQ	0.234	0.234	-
	43	PQ	0.1	0.1	-
	44	PQ	0.05	0.05	-
	58	PQ	0.19	0.19	-
	61	PQ	0.03	0.03	-
	63	PQ	0.18	0.18	-
	68	PQ	0.12	0.12	-
	81	PQ	0.05	0.05	-
	84	PQ	0.08	0.08	-
	88	PQ	0.3	0.3	-
Case III	7	PV	0.3	-	1.00
	20	PQ	0.1	0.1	-
	37	PQ	0.234	0.234	-
	43	PV	0.1	-	1.00
	44	PQ	0.05	0.05	-
	58	PQ	0.19	0.19	-
	61	PQ	0.03	0.03	-
	63	PQ	0.18	0.18	-
	68	PQ	0.12	0.12	-
	81	PQ	0.05	0.05	-
	84	PQ	0.08	0.08	-
	88	PV	0.3	-	1.00

The voltage profile of the network for the above mentioned configurations is shown in the Figure 3.1, which highlights the deterministic impact of the DGs, with their rated power and placement. The power of DGs connected to the network is assumed

to be varying, with some degree, throughout the day due to weather conditions, and this stochastic behavior of DGs is observed with a second test performed on the same network. Specifically, the variability analysis of DGs power rating is done with two tests, based on MC simulation. The DGs power is varied in the range $[-20,20]\%$ around the nominal rated capacity (the values given in Table 3.1), and in the range $[0,100]\%$, for which the simulation results are shown in Figures 3.2 and 3.3 respectively, where the vertical line represents the node with highest load connected. The later case depicts the extreme effect on the network that may arise due to unpredictable behavior of the DGs. In addition, the PDF of voltage of the node with highest load (i.e, node 7) is shown in Figure 3.4. This variability test helps to understand the network state when some DGs may fail due to weather or other factors. For example, in Figure 3.3, the band in the voltage profile is observed which shows the behavior of the distribution network lies largely on the DGs, however if all the DGs fail, the minimum range in the band can be seen and the network state is predicted. Thus the utility (service) provider can understand the effect of renewables' variability on a particular network and deduce unhealthiness behavior of the network.

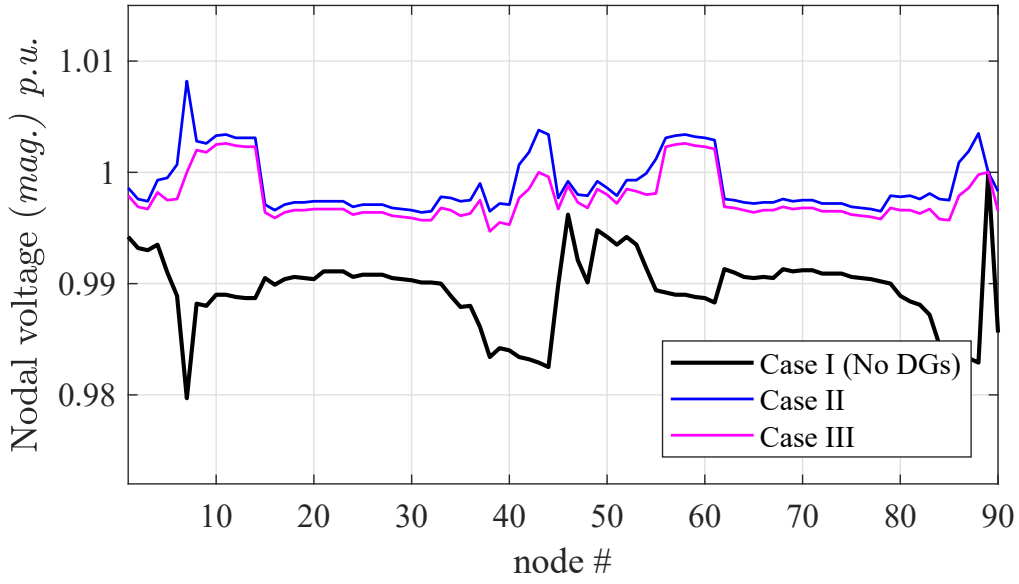

Figure 3.1: Voltage profile of the Test90 radial network; impact of generator sources (DGs) types and placement.

3.2 Surrogate Modeling

In the previous section, we observed the application of MC simulation scheme for performing UQ of power networks. Despite being simple and accurate, a naive MC

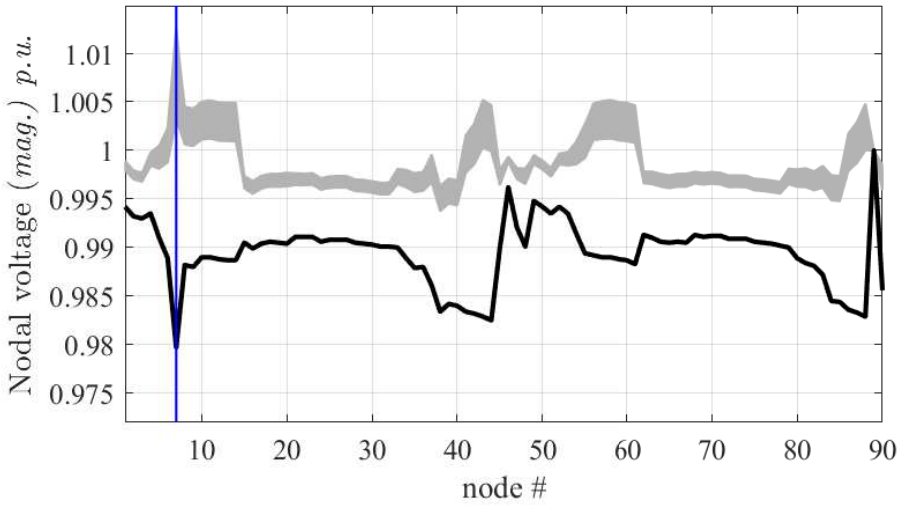

Figure 3.2: Voltage profile of the Test90 radial network. Solid line: solution without DGs, gray curves: 1000 Monte Carlo simulations where the DGs are varied in a 20% range around their nominal supply rating.

simulation turns out to be extremely expensive in terms of simulation time and it requires a huge number of samples which makes its direct application to a full-computational model unfeasible for realistic scenarios. Due to this reason, the surrogate models serve as the viable alternative which approximate the behavior of a full computational model such that:

$$\mathbf{y} = \mathscr{M}(\mathbf{x}) \approx \tilde{\mathscr{M}}(\mathbf{x}) \tag{3.3}$$

In this section, surrogate models are introduced which will be used in combination with the power-flow analysis method, explained in Section 2.1, for the UQ of power networks mentioned in Section 3.1. To avoid complexity, the discussion is based on the given system (3.1) with scalar output (i.e., $M = 1$), and it is assumed that a set of training pairs is available for reference, where $y_i = \mathscr{M}(\mathbf{x}_i) \in \mathbb{R}$, $\forall i = 1, \dots, L$. For now, it is assumed that for a multi-output system (i.e., $M > 1$), the given procedure is repeated for each output variable, while a compression strategy is proposed later in Section 3.3,

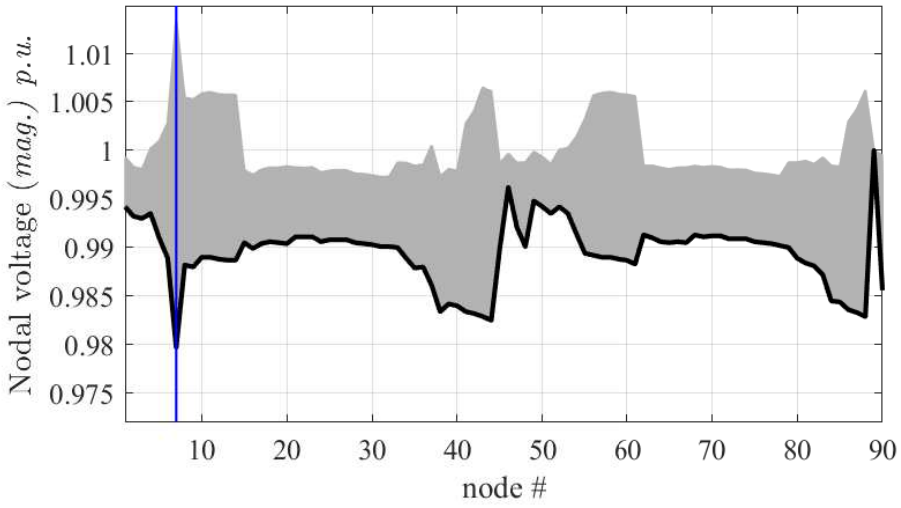

Figure 3.3: Voltage profile of the Test90 radial network. Solid line: solution without DGs, gray curves: 1000 Monte Carlo simulations where the DGs are varied in the range between disconnection and maximum supply rating.

to handle such systems more efficiently.

It is pertinent to highlight that the above analysis is used for targeting applications ranging to thousands of uncertain parameters (i.e., $d \sim 10^2$,10^3) with a similar range for output variables (i.e., $M \sim 10^3$,10^4), for which standard and advanced surrogate modeling approaches usually fail to quantify the effects.

3.2.1 Sparse PCE

This section presents the basic idea of sparse PCE approximation. As evident from its name, this formulation is based on polynomial mapping of input and output. The code for building the PCE surrogate model is available in the MATLAB toolbox UQLab [104].

A generic PCE model is given by:

$$y \approx \mathscr{M}_{PCE}(\mathbf{x}) = \sum_{k=1}^{K} c_k \varphi_k(\mathbf{x}), \tag{3.4}$$

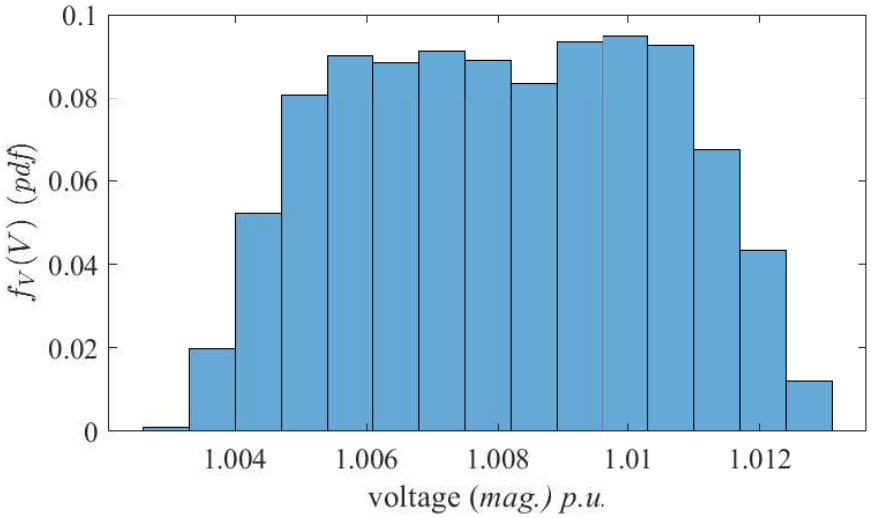

Figure 3.4: PDF of the magnitude of voltage at node #7 for the validation of Figure 3.2 (see the vertical line).

where, k is a scalar index pointing to the d-variate polynomials given by:

$$\varphi_k(\mathbf{x}) = \prod_{j=1}^{d} \phi_{k_j}(x_j). \tag{3.5}$$

where the functions $\phi_{k_j}(x_j)$ are the univariate polynomials, which satisfy the orthogonality condition as:

$$\langle \phi_{k_j}, \phi_{m_j} \rangle = \int_{\mathbb{R}} \phi_{k_j}(x_j)\phi_{m_j}(x_j)\rho(x_j)dx_j = \begin{cases} 1 & k_j = m_j \\ 0 & \text{otherwise,} \end{cases} \tag{3.6}$$

where, $\rho(x_j)$ represents the PDF of the uncertain parameter x_j.

For the quantities which show a finite second-order variance (moment), the model given in (3.4), with $K \to \infty$, fits perfectly well. However, for obvious practical reasons, the model is truncated by bounding a given u-norm of the multi-indices and order p.

Some common truncation schemes are given below by the order of popularity

- Total-degree truncation ($u = 1$), leading to $K = (p + d)!/p!d!$ terms;
- Hyperbolic truncation ($0 < u < 1$), which leads to an increasingly sparser expansion as u is decreased;
- Tensor-product truncation ($u = \infty$), which is usually avoided because of the exorbitant number of $K = (p + 1)^d$ terms.

Using one of the above predefined truncation scheme, the *sparse* PCE model is build (3.4), in which some coefficients c_k (typically many) turn out to be negligible, with a pattern which is not known prior to the solution.

For the given UQ, the PCE model (3.4) is suitable as its accuracy is defined by statistical terms, with the quadratic error given by [44],

$$\lim_{p\to\infty} \int_{\mathbb{R}^d} \left(\mathscr{M}_{PCE}(\mathbf{x}) - \mathscr{M}(\mathbf{x})\right)^2 \rho(\mathbf{x}) d\mathbf{x} = 0, \tag{3.7}$$

where, $\rho(\mathbf{x}) = \prod_{j=1}^{d} \rho(x_j)$ represents the joint PDF of the uncertain input parameters $\mathbf{x}$. As the local error is defined by the distribution of uncertain parameters, a larger error is allowed for some parameter values that are not likely to occur, without deteriorating the overall accuracy. Furthermore, the average and variance of the output y can be calculated straight from the PCE coefficients $c_{\boldsymbol{\kappa}}$ as:

$$\mathrm{E}\{y\} \approx \mathrm{E}\{\mathscr{M}_{PCE}\} = c_{\mathbf{0}} \tag{3.8}$$

$$\mathrm{Var}\{y\} \approx \mathrm{Var}\{\mathscr{M}_{PCE}\} = \sum_{\boldsymbol{\kappa}\in\mathscr{K}\setminus\mathbf{0}} c_{\boldsymbol{\kappa}}^2, \tag{3.9}$$

where, $\mathbf{0} = (0, \ldots, 0)$ is the null element of $\mathbb{N}^d$ corresponding to the zero degree polynomial (constant).

For estimating the PCE coefficients, various approaches are available. In particular, for full blown PCEs, one of the simple and common technique is the use of least-square regression [43], whose underlying idea is to minimize the norm of residuals on the training samples,

$$\text{minimize} \quad \sum_{i=1}^{L} \left(\mathscr{M}_{PCE}(\mathbf{x}_i) - \mathscr{M}(\mathbf{x}_i)\right)^2 = \sum_{i=1}^{L} \left(\sum_{k=1}^{K} c_k \varphi_k(\mathbf{x}_i) - y_i \right)^2 \tag{3.10}$$

This above optimization problem can be solved by the well-known traditional least-square solution, which is given by

$$\mathbf{c}^* = \arg\min_{\mathbf{c}} \|\Psi\mathbf{c} - \mathbf{y}\| = \Psi^+\mathbf{c} \tag{3.11}$$

where the vector $\mathbf{c} = (c_1, \dots, c_K)^\mathsf{T}$, $\Psi \in \mathbb{R}^{L\times K}$ is a matrix collecting the elements $\Psi_{ik} = \varphi_k(\mathbf{x}_i)$ while Ψ^+ is its Moore-Penrose pseudo-inverse and is defined as

$$\Psi^+ = (\Psi^\mathsf{T}\Psi)^{-1}\Psi^\mathsf{T}$$

For regression problem, the solution is generally needed to be overdetermined, i.e., $L > K$ ($L = 2K$ [43]), which means the number of training samples grows dramatically for high-dimensional problems.

On the other hand, for sparse PCEs, the non-zero coefficients, or the reduced set $\check{K}$ of the significant basis function set, are estimated during the optimization process (as explained above) using, e.g., least-square regression. This greatly reduces the number of unknowns to be calculated, hence a much smaller training set can be used for regression model.

3.2.2 LS-SVM

In this section, the fundamentals and related mathematical background of LS-SVM regression in both primal and dual space formulations for the construction of a ML surrogate model for the UQ are introduced. It is important to mention that the code for the LSSVM surrogate model construction can be found in the MATLAB toolbox LS-SVMLab, version 1.8 [105].

Primal Space Formulation

In the primal space formulation of LSSVM, the actual responses of (3.1) are approximated by the surrogate model as:

$$y \approx \mathscr{M}_{LS\text{-}SVM}(\mathbf{x}) = \sum_{n=1}^{N} w_n\phi_n(\mathbf{x}) = \langle \mathbf{w}, \boldsymbol{\phi}(\mathbf{x})\rangle + b, \tag{3.12}$$

where $\boldsymbol{\phi}(\mathbf{x}) = [\phi_1(x), \dots, \phi_1(x)]^T$ is vectorial function, i.e., $\boldsymbol{\phi}(\mathbf{x}) : \mathbb{R}^d \to \mathbb{R}^N$, which maps parameters space into the feature space, $\boldsymbol{\phi}(\mathbf{x}) = [\phi_1(\mathbf{x}), \dots, \phi_N(\mathbf{x})]^\mathsf{T}$, $\mathbf{w} = [w_1, \dots, w_N]^\mathsf{T}$ is the vector collecting corresponding coefficients, and $\langle\cdot,\cdot\rangle$ represents

the inner product in the $\mathbb{R}^N$ domain. The regression coefficients and the scalar parameter, in the above problem, are computed by the following optimization problem:

$$\begin{aligned} &\text{minimize} && \frac{1}{2}\|\mathbf{w}\|^2 + \gamma\frac{1}{2}\sum_{i=1}^{L} e_i^2 \\ &\text{subject to} && y_i = \langle \mathbf{w}, \boldsymbol{\Phi}(\mathbf{x}_i)\rangle + b + e_i, \quad \forall i = 1, \dots, L \end{aligned} \tag{3.13}$$

where, $e_i = \mathscr{M}_{LS\text{-}SVM}(\mathbf{x}_i) - \mathscr{M}(\mathbf{x}_i)$ represents the model error on the training samples and γ parameter is used for reducing overfitting [86, 47] by providing the trade off between accuracy and the flatness of the model.

It can be observed from (3.13), that this primal space formulation is equivalent to Ridge regression [45]. Also, similar to the classical least-square regressionn [43], the number of coefficients (vector $\mathbf{w}$) in the above formulation (3.12) equals to the number of basis functions, thus it scales according to the number of parameters. This means that the above implementation suffers from the curse of dimensionality, and requires an alternate solution, which is explained in the next section.

Dual Space Formulation

The dual space formulation of LSSVM is a non-parametric regression [47]. The curse of dimensionality problem is solved by the introduction of Kernel function $K(\cdot,\cdot) : \mathbb{R}^d \times \mathbb{R}^d \to \mathbb{R}$, defined as

$$K(\mathbf{x}_i, \mathbf{x}_j) = \langle \boldsymbol{\Phi}(\mathbf{x}_i), \boldsymbol{\Phi}(\mathbf{x}_j)\rangle, \tag{3.14}$$

This allows rewriting equation (3.12) as

$$y \approx \mathscr{M}_{LS\text{-}SVM}(\mathbf{x}) = \sum_{i=1}^{L} \alpha_i K(\mathbf{x}_i, \mathbf{x}) + b, \tag{3.15}$$

where, the coefficients α_i and the bias term b, are the new unknowns to be solved, which can be calculated by simply inverting the following matrix equation:

$$\begin{bmatrix} 0 & \mathbf{1}^\mathsf{T} \\ \mathbf{1} & \boldsymbol{\Omega} + \mathbf{I}/\gamma \end{bmatrix} \begin{bmatrix} b \\ \boldsymbol{\alpha} \end{bmatrix} = \begin{bmatrix} 0 \\ \mathbf{y} \end{bmatrix}, \tag{3.16}$$

where, $\mathbf{y} = [y_1, \dots, y_L]^\mathsf{T}$, $\boldsymbol{\alpha} = [\alpha_1, \dots, \alpha_L]^\mathsf{T}$, $\mathbf{1} = [1, \dots, 1]^\mathsf{T} \in \mathbb{R}^L$, $\boldsymbol{I} \in \mathbb{R}^{L \times L}$ is the identity matrix, $\in \mathbb{R}^{L \times L}$ is the kernel matrix with elements $\Omega_{ij} = K(\mathbf{x}_i, \mathbf{x}_j)$ for $i, j = 1, \dots, L$, and finally γ is the same parameter as in (3.13). For (3.14), different kernels can be used, some of which mostly used are given below as:

- linear kernel: $K(\mathbf{x}_i, \mathbf{x}) = \mathbf{x}_i^T \mathbf{x}$;
- polynomial kernel of order q: $K(\mathbf{x}_i, \mathbf{x}) = (1 + \mathbf{x}_i^T \mathbf{x})^q$;
- Gaussian radial basis function (RBF) kernel: $K(\mathbf{x}_i, \mathbf{x}) = \exp\left(-\|\mathbf{x}_i - \mathbf{x}\|^2 / 2\sigma^2\right)$, where, σ is the kernel hyperparameter, which is estimated during the model training.

It is important to highlight that the use of kernel function, the so called "kernel trick", in this non-parametric dual space formulation, the number of unknowns α_i in (3.15) are completely independent of the number of uncertain paramters or the basis functions used in the LS-SVM regression, instead it is equal to the number of training samples L used. Therefore, this dual space formulation of LS-SVM is an efficient and appealing technique for the UQ of high-dimensional problems [91].

3.3 Surrogate Modeling with multi-Output System

Until now, the surrogate modeling techniques introduced in sections 3.2.2 and 3.2.1 were focused for a single output system (i.e., $M = 1$). Where for multi-output systems ($M > 1$), the same procedure is repeated for each output component to generate the surrogate model accordingly. This seems to be a naive approach, as the computational cost and time scale almost linearly with the number of output variables which becomes impractical for systems with thousands of outputs. Although full-blown PCEs can be used for multi-output systems, in the case if same set of basis function is used for all the output components, and the optimization technique in (3.11) can be easily solved by vectorizing and stacking the training data column-wise. However, as already stated above, the full blown PCEs become impractical for high-dimensional problems.

To deal with this limitation, a comression strategy is introduced below based on PCA [106, 107]. The PCA compresses the training response set by performing singular value decomposition to find principal components of the data set. This property is employed by our proposed technique to find the principal components of the network nodal voltages to compress the large training samples, in order to build a compressed surrogate model capable of predicting the network node voltage profile, in a fast and efficient way. It is pertinent to highlight that the emphasis of this compression of

training samples is on the application of basic building blocks to increase the number of parameters up to several dozens and to speed up the generation of surrogate models, to save both execution time and computational memory.

Let us suppose again, L training pairs $\{(\mathbf{x}_i, \mathbf{y}_i)\}_{i=1}^{L}$, where now $\mathbf{y}_i = \mathscr{M}(\mathbf{x}_i) \in \mathbb{R}^M$. The training responses $\mathbf{y}_i$ are drawn column-wise into a matrix $\mathbf{Y} \in \mathbb{R}^{M \times L}$, which contains $Y_{mi} = [\mathscr{M}(\mathbf{x}_i)]_m$ elements. Moreover, the zero-mean data set $\tilde{\mathbf{Y}}$ is defined, whose elements are $\tilde{Y}_{mi} = Y_{mi} - \mu_m$, where μ_m is the column-wise mean

$$\mu_m = \frac{1}{L} \sum_{i=1}^{L} Y_{mi} \tag{3.17}$$

next, its "economy-size" singular value decomposition (SVD) is calculated as

$$\tilde{\mathbf{Y}} = \mathbf{U} \Sigma \mathbf{V}^{\mathsf{T}}, \tag{3.18}$$

where $\mathbf{U} \in \mathbb{R}^{M \times L}$ and $\Sigma, \mathbf{V} \in \mathbb{R}^{L \times L}$. Specifically, the matrix Σ is a diagonal, which collects the singular values $\{\sigma_i\}_{i=1}^{L}$, in descending order, of the data set $\tilde{\mathbf{Y}}$. The above SVD (3.18) can be approximated by a smaller set with only $\bar{n}$ most significant singular values (i.e.,the "principal components"), by setting a threshold ϵ, such that,

$$\frac{\sigma_i}{\sigma_1} < \epsilon \quad \forall i > \bar{n}, \tag{3.19}$$

The matrix $\mathbf{U}$ is therefore reduced to a compressed set, $\hat{\mathbf{U}} \in \mathbb{R}^{M \times \bar{n}}$, retaining only the principal components (first $\bar{n}$ columns of $\mathbf{U}$), which is then used to build a compressed version of the model $\mathscr{M}$ in (3.1) as followed,

$$\mathbf{z} = \mathscr{M}_{PCA}(\mathbf{x}) = \hat{\mathbf{U}}^{\mathsf{T}} \left(\mathbf{y} - \boldsymbol{\mu} \right) = \hat{\mathbf{U}}^{\mathsf{T}} \left(\mathscr{M}(\mathbf{x}) - \boldsymbol{\mu} \right), \tag{3.20}$$

where, $\mathscr{M}_{PCA} : \mathbb{R}^d \to \mathbb{R}^{\bar{n}}$ and $\boldsymbol{\mu} = (\mu_1, \ldots, \mu_M)^{\mathsf{T}}$.

Please note that the output $\mathbf{z}$ of the compressed model (3.20) contains only the $\bar{n}$ components as compared to the M output components of model (3.1). By virtue of the fact that singular values decay rather fast, it is analyzed that $\bar{n} \ll M$, normally by twice or fourth of magnitude.

It is important to point out that, any surrogate modeling approach suitable for high-dimensional problems, such as the LS-SVM or sparse PCE, can be used for building

the regression model on output components of $\mathbf{z}$, with less computational effort. Once the compressed surrogate model ($\tilde{\mathscr{M}}$) of $\mathscr{M}_{PCA}$ is build, the original output set can be recovered from (3.20) as

$$\mathbf{y} \approx \boldsymbol{\mu} + \hat{\mathbf{U}}\mathbf{z} \approx \boldsymbol{\mu} + \hat{\mathbf{U}}\tilde{\mathscr{M}}(\mathbf{x}). \tag{3.21}$$

As explained above, ML surrogate modeling is applied to the power networks to perform the UQ. The regression model for predicting the nodal voltages is generated from the limited number of training responses which are obtained from the full computational model. Figure 3.5 shows the flowchart which summarizes the main steps for building and evaluating the proposed model. For model generation (left panel), the training responses are generated using some random configuration of input uncertain parameters (3.2). The next sept involves compression of the training response set, which is achieved by truncating the SVD of the data set matrix (3.20) based on the magnitude of its singular values. The surrogate model is then trained for this reduced data. The model evaluation (right panel) involves testing the surrogate model on the new uncertain inputs (usually large number of samples). These new inputs are fed to the surrogate model to inexpensively compute the corresponding compressed output response set. Finally, the inverse transformation (3.21) is applied on this compressed data set to recover the original data.

The proposed methodology is performed on 118 nodes power network with 250 uncertain parameters, and increasing number of training samples. Two more test cases are considered in chapter 4 on the larger power network with increasing number of uncertain parameters for the accurate systemic assessment.

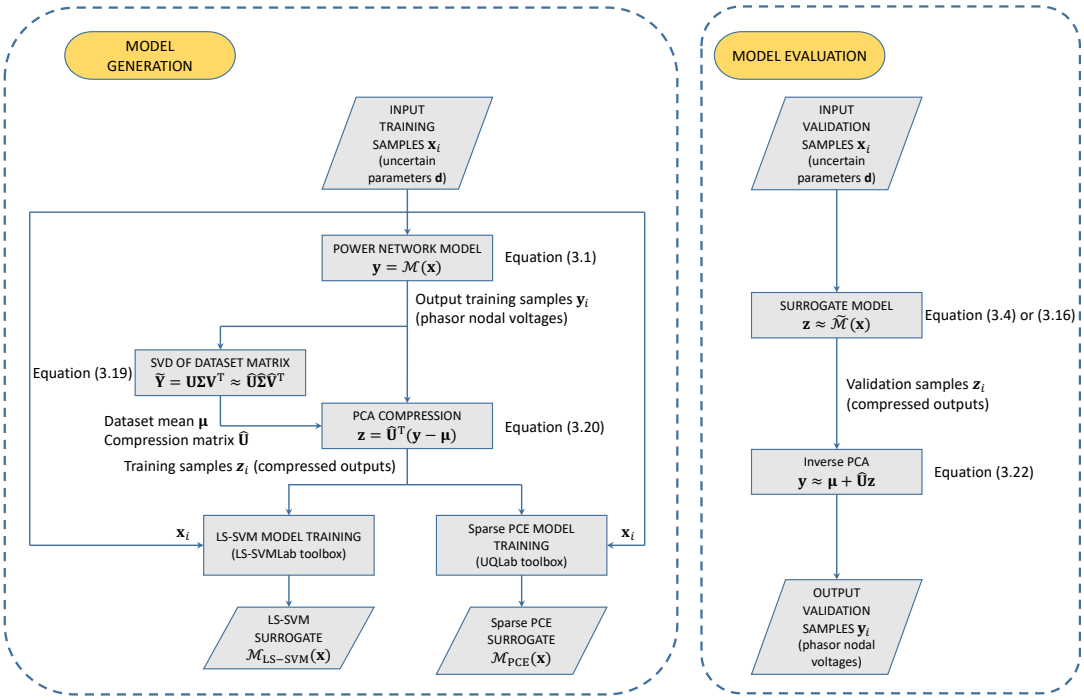

Figure 3.5: Flowchart of the proposed surrogate modeling approach.

3.4 Application Example

This section analyses the feasibility and strength of the proposed methodology in terms of accuracy and efficiency. Specifically, the sparse PCE and the LS-SVM regression are applied in conjunction with PCA to the models for the IEEE118-bus single phase power network which has $M = 118$ network nodes with 250 uncertain parameters considered. It is a single phase transmission network which includes 19 generators, 35 synchronous condensors, 9 transformers, 91 loads and 177 transmission lines [108]. The samples used to train surrogate model are generated with Latin Hypercube Sampling (LHS) scheme [109]. All the simulations have been performed with MATLAB on a PC equipped with Intel Core i7 CPU running at 3.6 GHz, and 32 GB of RAM. The uncertain parameters are the equivalent resistance and inductance of the branch transmission line. A total of 125 random branches are selected, while the network has no renewable connected, and the loads are kept constant. It means the total uncertain parameters (3.2) become $d = 2 \times 125 = 250$. These parameters are sampled with uniform distribution with a variability of 50% around the nominal values given in [108]. Since it has a total number of 118 nodes ($M = 118$), our goal is to build a compact surrogate model to

accurately predict the voltage magnitude of 118 nodes, which is computed via a power-flow analysis, as a function of 250 input uncertain parameters. In other words, we have to build a surrogate model with $M = 118$ output variables and $d = 250$ input uncertain parameters. It is important to point out that the considered test case IEEE118-bus is a transmission network, for which Matpower [110] is used as full-computational model for solving the load-flow.

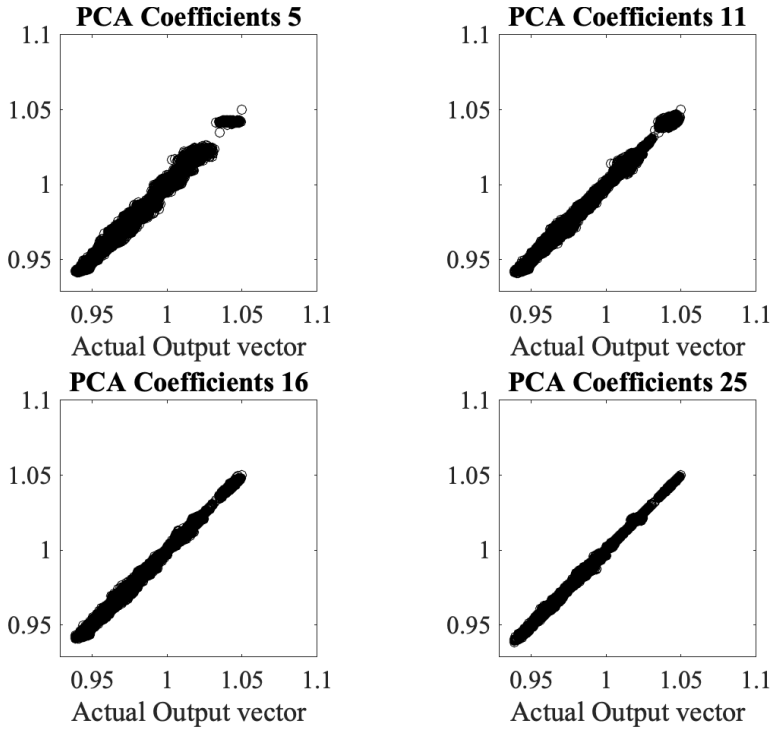

Figure 3.6: Scatter plots showing the actual training samples versus their reconstruction from PCA truncations with increasing number of components as shown in the plot headers.

For generation of the surrogate models, an increasing number of training samples is considered (i.e., $L = 50, 275$ & 500). Initially the training response set is compressed via PCA, which yields only 16 out of 118 output components (i.e., $\bar{n} = 16$), with a tolerance $\epsilon = 10^{-1}$, resulting the compression rate of 7×. For the sake of illustration, Figure 3.6 provides the performance of PCA compression of output response set with increasing number of coefficients. Specifically, the scattered plots in the mentioned figure highlight the actual training responses (horizontal axis) and the responses reconstructed from the PCA truncation (vertical axis) with an increasing number of components, with diagonal line depicting perfectly reconstruction of responses. It can be observed that using coefficients 16 and above, the PCA is relatively accurate in reproducing the training

samples, hence 16 coefficients are used for building the surrogate models. The accuracy of PCA technique is further investigated in the next chapter using comparatively larger test network.

The compressed response set is then used to train the 16 coefficient surrogate model with both LSSVM, with Radial Basis Function (RBF) kernel, and sparse PCE with a maximum polynomial order 2. The compressed surrogate models built with LSSVM and sparse PCE are then validated with 10000 MC samples estimated using full-computational model. The scatter plots in Figure 3.7, show the correlation between the nodal voltages with MC and the corresponding predictions generated by the proposed compressed models with an increasing number of training samples, where the dashed lines along diagonal indicate the perfect correlation between the pairs representing an ideal model. This shows a good comparable accuracy of both LS-SVM and sparse PCE models, however the order of PCE can hardly be increased when used for high dimensional problems, due to the computational memory constraints for estimating higher-order coefficients. This means that for high-dimensional problems, the sparse PCE would require comparatively very large memory and execution time to provide the same accuracy as of the ML surrogates. This is further investigated in the case studies carried out in the next chapter. Additionally, Figure 3.8 shows the PDF of the network nodal voltages (complete output vector) generated by MC simulation (red bars), compared with the predictions provided by the proposed LSSVM surrogate model (blue bars) and the sparse PCE surrogate model (green bars), with 500 training samples. This comparison proves that both surrogate models are capable of providing a good statistical behavior of the network voltage profile.

Lastly, Table 3.2 highlights the performance accuracy of both the models in terms of root mean-squared error (RMSE), the time required by the CPU in (i) the generation of training samples (indicated by *cost* right to the training samples), (ii) the model generation t_{model} and (iii) the model evaluation (t_{cost}) for computing the predictions for the plots in figures 3.7 and 3.8.

The above plots and statistical information summarize that the accuracy of both the models LSSVM and sparse PCE is very good in terms of RMSE and provide a dramatical improvement of execution time as compared to MC. However LS-SVM provides much greater performance in the model generation and evaluation time as compared to PCE.

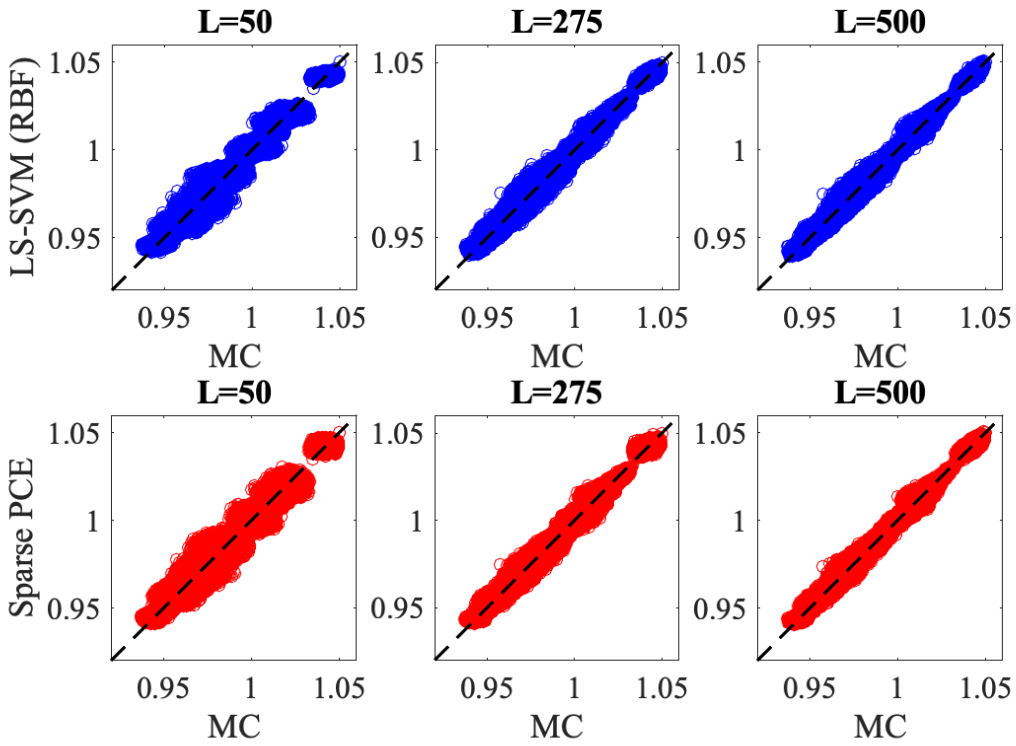

Figure 3.7: Scatter plots of the network node voltages for Case with ($d = 250$ uncertain parameters) predicted by LS-SVM regression (top three panels) and sparse PCE (bottom three panels) surrogate models trained with an increasing number of samples, versus the results of MC simulation.

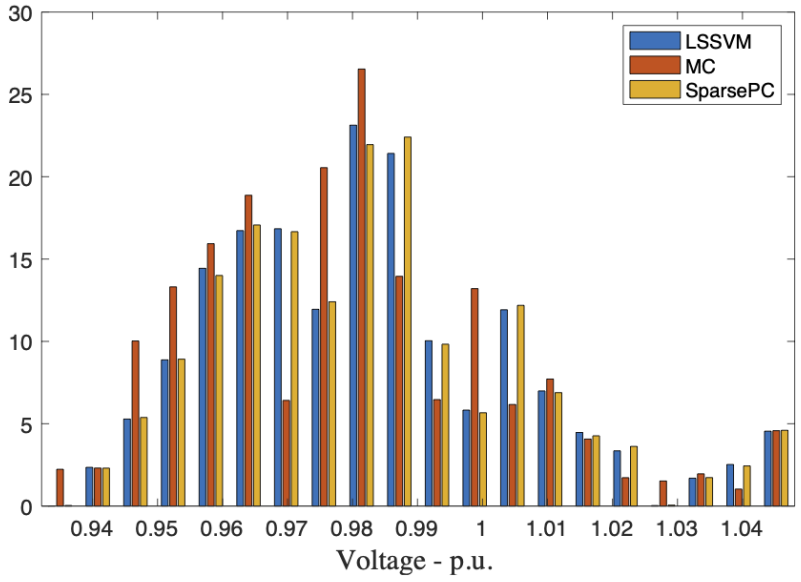

Figure 3.8: PDF of the p.u. magnitude of the nodal voltages calculated, for 250 uncertain parameters, from the MC samples and with the compressed LS-SVM and sparse PCE surrogate models.

Table 3.2: Model performance in terms of both accuracy and efficiency for an increasing number of training samples L.

d = 250	$L = 50$ (cost = 4.45 s)			$L = 275$ (cost = 12.38 s)			$L = 500$ (cost = 31.17 s)		
Method	RMS Error	t_{model}	t_{cost}	RMS Error	t_{model}	t_{cost}	RMS Error	t_{model}	t_{cost}
MC	–	–	490.7 s	–	–	490.7 s	–	–	490.7 s
LS-SVM (RBF)	$1.78 \cdot 10^{-3}$	7.48 s	0.49 s	$1.24 \cdot 10^{-3}$	14.4 s	1.6 s	$1.09 \cdot 10^{-4}$	29.1 s	2.24 s
Sparse PCE	$1.90 \cdot 10^{-3}$	21.1 s	5.88 s	$1.29 \cdot 10^{-3}$	41.4 s	7.3 s	$1.09 \cdot 10^{-4}$	76.6 s	7.9 s

3.5 Concluding remarks

This chapter proposed a solution for the UQ of power network by building a compact, accurate and fast surrogate model for predicting the effect of large uncertain parameters on the network voltage profile (of all the nodes). The uncertain parameters considered in this study involve the variation in the physical medium (transmission line). In particular, the IEEE118-bus transmission network with upto 250 uncertain parameters are considered for assessing the accuracy, feasibility and efficiency of the proposed compressed surrogate model. The uncertain parameters consist of the equivalent resistance and inductance of the physical medium (transmission line).

A two-step scheme is proposed, that involves compression of the training response set with PCA and building the surrogate models from a limited number of training samples. The PCA technique helps remove the redundant information in the output response set by truncating the singular values. The compression rate achieved through PCA is upto 7× using a threshold of $\varepsilon = 10^{-4}$.

The compressed surrogate models for LS-SVM and sparse PCE, trained with increasing number of training samples, are then evaluated with large number of samples generated by MC simulation. The case studies presented above, investigated the accuracy, efficiency, convergence and feasibility of both the surrogate models. In terms of accuracy, the LS-SVM takes the lead in almost all the case studies and training set sizes, however the convergence rate of both the surrogate models are equivalent for large training sets (e.g., $L = 500$ for 250 Uncertain Parameters). The LS-SVM is also more efficient in the model generation.

Further, Table 3.2 highlighted that the proposed compressed surrogate modeling appoach provides effective solution as compared to MC simulation method. This is due to the fact that the surrogate models provide a closed form parametric modeling rather than the blind MC approach. This study also proves that the direct application of surrogate models, without PCA compression, with 118 nodal voltage outputs would be definitely unfeasible. Please note that a similar analysis can be performed using other sensitive uncertain paramaters in a typical power network, such as a particular phase

voltage or branch power, using the same appraoch.

It is important to mention that part of the work presented in this chapter has been published in the papers [2, 102, 3].

Chapter 4

Application of the Proposed Modeling and Machine Learning Approches for Benchmark Networks

In previous chapters, power system was interpreted in terms of a circuital interpretation and the surrogate models of power networks were build for performing UQ. Particularly, chapter 2 presented the circuital interpretation of a generic PDN in which the network was suitably represented by an equivalent circuit in the phasor domain and the linear and non-linear portions of the circuit were decoupled for a simple iterative solution, and then the UQ of power system was performed in chapter 3, by building a compact surrogate model capable of accurately predicting the network nodal voltages as function of multiple number of input uncertain parameters. While multiple test networks were considered to analyse the feasibility and effectiveness of both the approaches and were proved to provide comparable efficiency and accuracy, there is still room for further validation on a large benchmark network, i.e., the three-phase IEEE 8500-node test feeder, which is used by the power research community to verify the feasibility of the techniques to handle such large realistic networks.

This chapter considers IEEE 8500-node test feeder for validating the circuital approach for power-flow analysis with the fixed-point iteration proposed in chapter 2. Validations are provided with the two state of the art methods, the *Z-bus* method and the openDSS. After that, ML algorithm LS-SVM is applied in combination with PCA to build a compact surrogate model, where large number of input uncertain parameters (i.e., the uncertain loads and photovoltaic distributed generators (PVDGs)) are considered for two case studies. The results of proposed surrogate model are validated with those of sparse PCE and MC, where the former is a polynomial regression technique while the latter is a simple traditional scheme used for variability analysis.

The chapter is organized as follows. Section 4.1 provides details of the IEEE 8500-node test feeder. Section 4.2 evaluates the proposed circuital interpretation for power-flow analyses of IEEE 8500-node network. Section 4.3 presents the ML based surrogate models for the UQ with large number of input uncertain parameters. Finally, section 4.4 summarizes the work.

4.1 IEEE 8500-Node Test Feeder

This network is considered as benchmark test network for assessing the accuracy and convergence of the proposed approach. It is a three-phase radial distribution network with both MV and LV levels, with unbalanced loads. It is a realistic network which includes most of the components in a typical North American MV Distribution Feeder [77, 76]. Figure 4.1 shows its single-line diagram with the placement of regulators and capacitors marked. The details of the components with ratings and voltage regulator tap positions are given in below.

1. 2500 MV buses, 4800 total buses including LV and loads, yielding over 8500 node-points; Bus coordinates can be found here [76]
2. a substation transformer connected in delta-wye, rated at 27.5 MVA, 115kV/12.47kV line-to-line, with transformer impedance of $(1.344 + j15.51)\%$
3. 4 Three-phase individually operated SVRs. Regulator tap positions used in this work are given in Table 4.1
4. 2354 star connected constant-power single-phase loads
5. 3703 three-phase branch connections with three-,two-, and single-phase laterals
6. 9 single-phase and 1 three-phase capacitor banks
7. 1177 load service transformers
8. Balanced and unbalanced load configurations available being latter used in this work

Table 4.1: Voltage regulator tap positions - IEEE 8500-node test Feeder

Regulator	Bus	Tap Positions
Reg.1-A	HVMV_Sub	2
Reg.1-B	HVMV_Sub	2
Reg.1-C	HVMV_Sub	1
Reg.2-A	190-8593	11
Reg.2-B	190-8593	7
Reg.2-C	190-8593	1
Reg.3-A	190-8581	16
Reg.3-B	190-8581	10
Reg.3-C	190-8581	1
Reg.4-A	190-7361	12
Reg.4-B	190-7361	12
Reg.4-C	190-7361	5

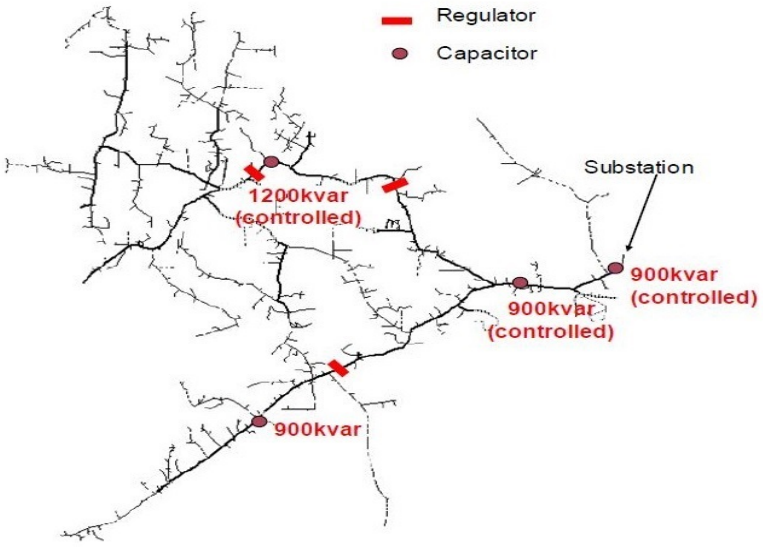

Figure 4.1: Single-line diagram of network topology for the IEEE 8500-node test feeder [77].

4.2 Power-Flow Analysis

In this section, the IEEE 8500-node PDN is solved by the scheme proposed in chapter 2 for the power-flow analysis by interpreting the given network in terms of circuital equivalents in order to verify the feasibility of the approach to handle large realistic networks. Since the network is an unbalanced three-phase, it requires the matrices, involved in the proposed solution, to be increased according the three phase lines, as explained in section 2.1. The voltage magnitude and phase angles of respective phases are calculated with the proposed MNA scheme. It is important to mention that the regulators and transformers in the network are modeled as in [95, 68], while the fixed regulator taps are considered as published in [72] (see Appendix **??**). For a fair validation, the results obtained are compared with those of *Z-bus* method [68] and the OpenDSS [98]. The simulation and plots are generated running the scripts on a PC equipped with a CPU Intel Core i7 (seventh generation) with 3.6 GHz and 32 GB ram.

Figure 4.2 shows the voltage magnitudes and angles computed by the three methods, the proposed MNA-based approach, the *Z-bus* and the OpenDSS highlighting identical results for all the three phases. Additionally, Table 4.2 provides a compact summary of performance in terms of simulation time and number of iterations. Moreover, Figure 4.3 shows, for the proposed approach, the maximum voltage difference (error) at each iteration, which highlights the typical decreasing staircase behavior of convergence for the fixed-point scheme, where the horizontal line points out the tolerance set to 10^{-4}.

From the above figures and performance table, it can be summarized that the proposed approach provides accurate results, even with a comparatively very large network, without any simulation overhead in terms of execution time. The circuital interpetation of the PDN formulated with MNA and solved with simple iterative scheme proves to handle even large networks effectively and provides a similar accuracy with the state-of-the-art approaches, without requiring custom modification for any arbitrary network.

Table 4.2: Performance of the different methods in terms of convergence for the IEEE 8500-node test feeder benchmark.

Method	**Iterations**	**CPU Time (ms)**
Proposed (MNA-based)	11	96.6
Z-bus	12	101.1
OpenDSS	10	53.4

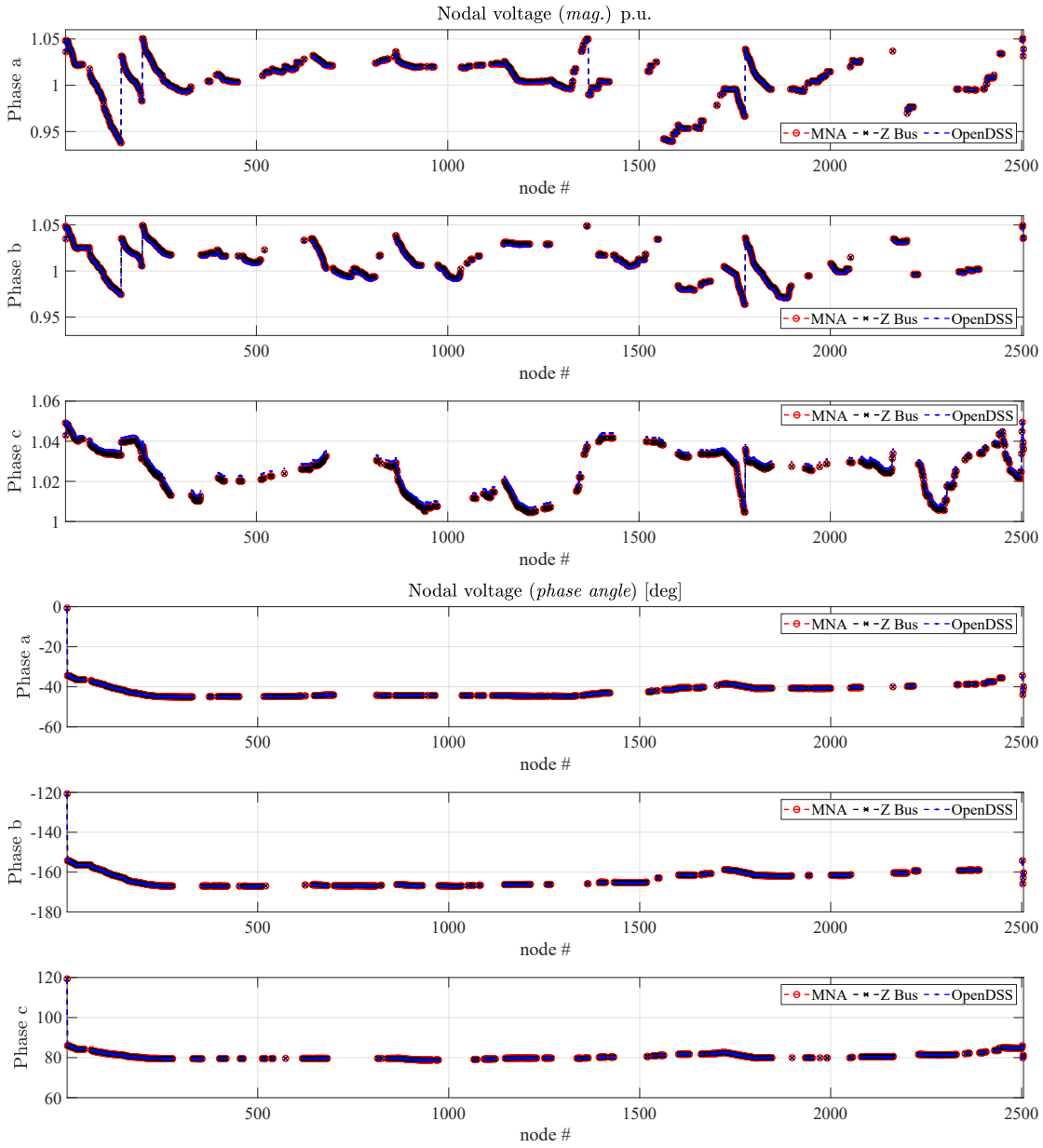

Figure 4.2: Three-phase voltage profile of the IEEE 8500-node test feeder computed by means of the proposed MNA-based method, the *Z-bus* approach and via the OpenDSS tool. (**top**) Phase magnitudes (p.u.), (**bottom**) phase angles (degrees).

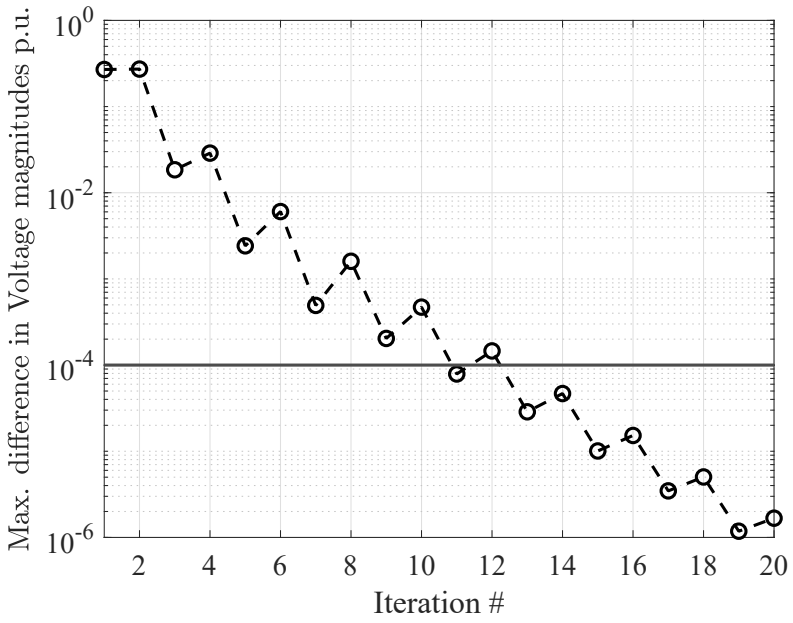

Figure 4.3: Maximum voltage difference (in magnitude) at each iteration of the proposed method.

4.3 Uncertainty Quantification of IEEE 8500-node PDN with Machine Learning

In this section, UQ of the above given IEEE 8500-node PDN is performed by building the compact surrogate model using the approach proposed in chapter 3 to further verify its feasibility and strength with a large number of uncertain parameters. The network is modified by adding 400 PVDGs at random load nodes. The surrogate model is built with both LS-SVM and sparse PCE along with the compression technique PCA to predict the nodal voltage of $M = 3798$ network nodes which are a function of input uncertain power of loads/PVDGs. The statistical properties of the network voltage profile are investigated by considering the following two cases,

1. Case 1: d = 450 parameters, i.e., $N_{load} = 250$ loads and $N_{PV} = 200$ PVDGs
2. Case 2: d = 900 parameters, i.e., $N_{load} = 500$ loads and $N_{PV} = 400$ PVDGs

4.3.1 Case 1: 450 Uncertain Parameters

In this case, the statistical properties of the voltage profile of three-phase IEEE 8500-node test feeder PDN [77] are studied by building the surrogate model considering $d = 450$ uncertain parameter including 250 loads (N_{load}), and 200 PVDG generators (N_{pv}) while

the branch connection parameters are fixed, (i.e., $d = 250 + 200 = 450$). For loads, the real power is varied with a relative standard deviation of 80% from its nominal value. The random samples are drawn following a Guassian distribution and negative samples are discarded. The reactive power is calculated according to constant power factor, which means the variability of real and reactive power is correlated. The generalization of independent real and reactive power components is straightforward and can be modified accordingly. For PVDGs, the rated power of each PVDG is 100kVA, with a penetration level of 17.5%. The real power of a PVDG generator is estimated as a function of solar radiation [111] and, according to [112], it can be described with a beta distribution. In particular, a beta distribution with parameters $\alpha = 0.90$ and $\beta = 0.85$ is considered here.

A large variability can be observed on all the phases, with the maximum variability of 20% on phase a, while some nodes have very small variability (see figure 4.4). Particularly, 283 out of 3798 nodes, of phases a,b or c, have relative variation of less than 1%. It is important to point out that the training responses are generated using the power-flow analysis explained in chapter 2 as a full-computational model, however any load-flow analysis technique could be alternatively adopted.

A reduced set of $L = 450$ responses is considered as "training samples". The normalized singular values for the corresponding zero-mean data set matrix $\tilde{\mathbf{Y}}$ is shown in Figure 4.5. The dashed horizontal lines correspond to the thresholds $\varepsilon = 10^{-i}$, for $i = 1,2,3,4,5$ and the graph shows that the singular values cross the lowest threshold at index $\bar{n} = 38$. This means that the compressed training response set retain only 38 out of the 3798 original components. Therefore with PCA, the compression rate achieved is 100×. The PCA compression on the training data set can be observed by the scatter plots shown in Figure 4.6. The plots show pairs corresponding to the actual training responses (horizontal axis) and the responses reconstructed from the PCA truncation (vertical axis) with an increasing number of components. Ideally, the pairs should form a diagonal line (perfectly matched points). The mentioned figure highlights very high accuracy in reproducing the training samples from the threshold (ε) of 10^{-4} and onwards. Hence, this threshold is used in the following analysis.

The training data sets compressed with PCA, are then used with increasing sample size L to train both sparse PCE (2nd order) and LS-SVM surrogate models. The performance of surrogate models build with the proposed methodology is evaluated by comparing the predicted responses with those of MC simulation with 10,000 samples. Figure 4.7 shows the scatter plots with the reference outputs from the MC simulation paired with the corresponding outputs predicted by the LS-SVM and sparse PCE surrogate models with increasing number of training samples. Where the best model is one with the pairs lying along the diagonal (back dashed line). From the above figure, it can be observed that for training samples $L = 900$, both the models are comparable

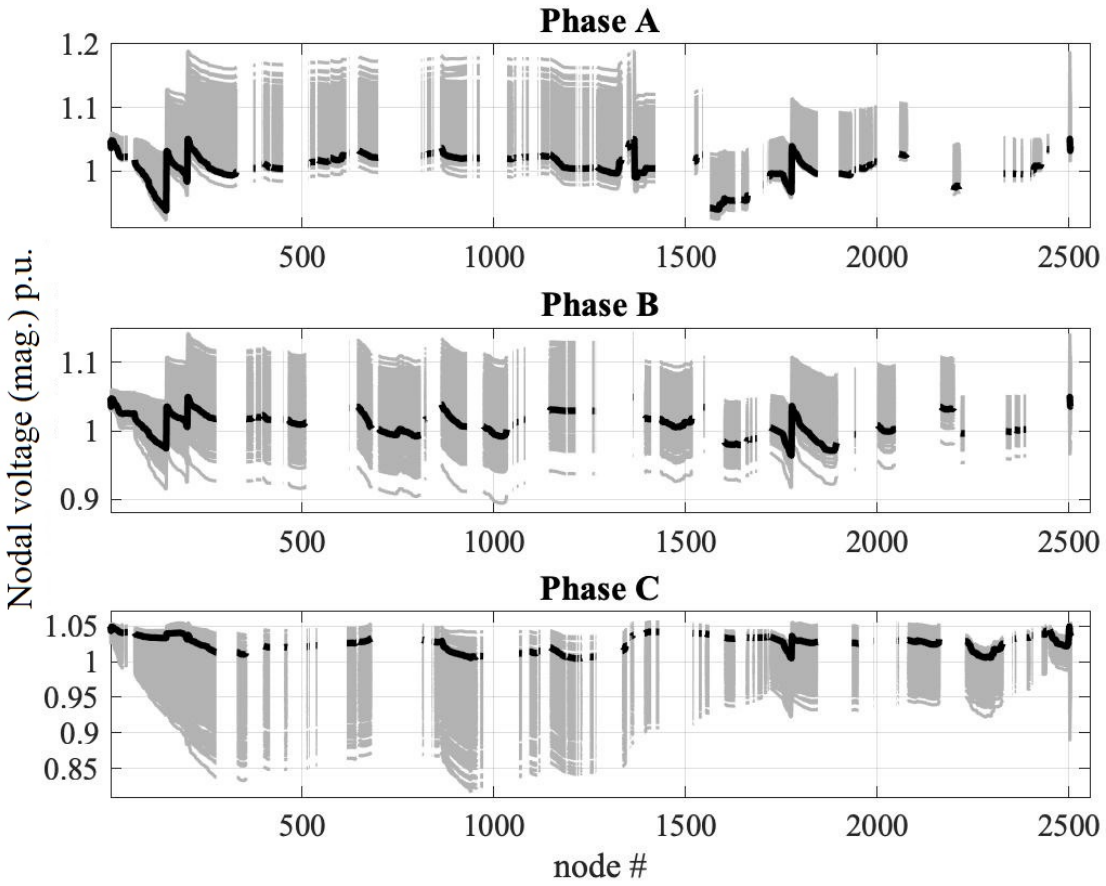

Figure 4.4: Overall voltage profile of IEEE 8500-node test feeder generated by considering a subset of MC simulations (gray curves). The solid black curves correspond to the nominal network response

and provide good efficiency. However, when using smaller training samples, larger error is observed for PCE as oppose to the LS-SVM. This can be justified by the fact that, PCE allows a large error for unlikely samples, as discussed in section 3.2.1 and therefore the application of PCE is generally not intended for parametric modeling. While here it is used only as a tool for comparison with ML-based LS-SVM surrogate modeling. Undoubtedly, scatter plots provide a deterministic assessment of the accuracy of models in reproducing the system behavior for a wide range of uncertain parameter configurations, regardless of their actual probability of occurrence.

The probabilistic analysis is shown in Figure 4.8, which highlights the PDFs of the all nodal voltages (i.e., all the entries of the output vector $\mathbf{y}$), which are obtained from 10,000 MC samples (grey bars), compared to the predictions obtained by the PCA compressed sparse PCE (dashed black curve) and LS-SVM (solid red-curve) surrogate models, and an excellent accuracy can be seen for both the models. The statistical information is

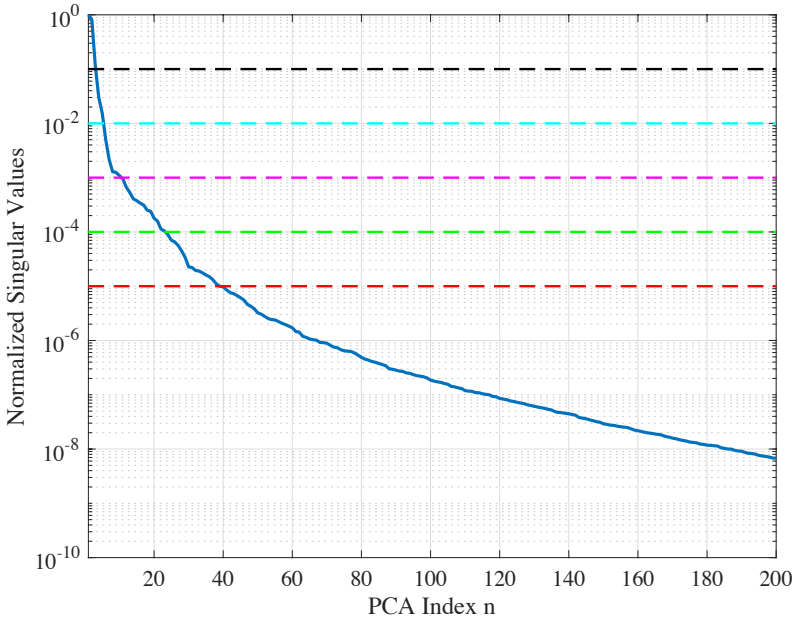

Figure 4.5: Normalized singular values of a training dataset for Case 1 with $L = 450$ (solid blue curve). The horizontal dashed lines indicate different thresholds for the PCA truncation.

helpful in observing the global picture of the possible behavior of the network, in terms of the minimum and maximum voltage profile.

4.3.2 Case 2: 900 Uncertain Parameters

In this case study, the uncertain parameters (loads and PVDGs) are twice the previous case (i.e., $d = 900$). Specifically, $N_{load} = 500$ random loads, and $N_{pv} = 400$ PVDGs randomly connected at load nodes of the same three-phase IEEE 8500-node test feeder. The real power of loads and PVDGs, variability and the samples' distribution are similar to the one used for previous with same relative standard deviation of 80%. Each PVDG is rated at 100 kVA with a penetration level of 17.5%. In this case also, an increasing training samples are considered, (i.e., $L = 450$, 900 and 1800). While, the surrogate model with 3798 outputs and 900 input uncertain parameters is required for this case. The application of PCA on the original output response vector yields $\bar{n} = 39$ principal components using a tolerance (ε) of 10^{-4}. After that, the surrogate models with sparse PCE (order 2) and LS-SVM are trained with increasing number of training samples. These compressed models are evaluated with the results of MC simulation with 10,000 samples. The scatter plots and the PDFs for the MC samples and model predictions (both sparse PCE and LS-SVM) are shown in Figures 4.9 and 4.10 respectively. Similar to

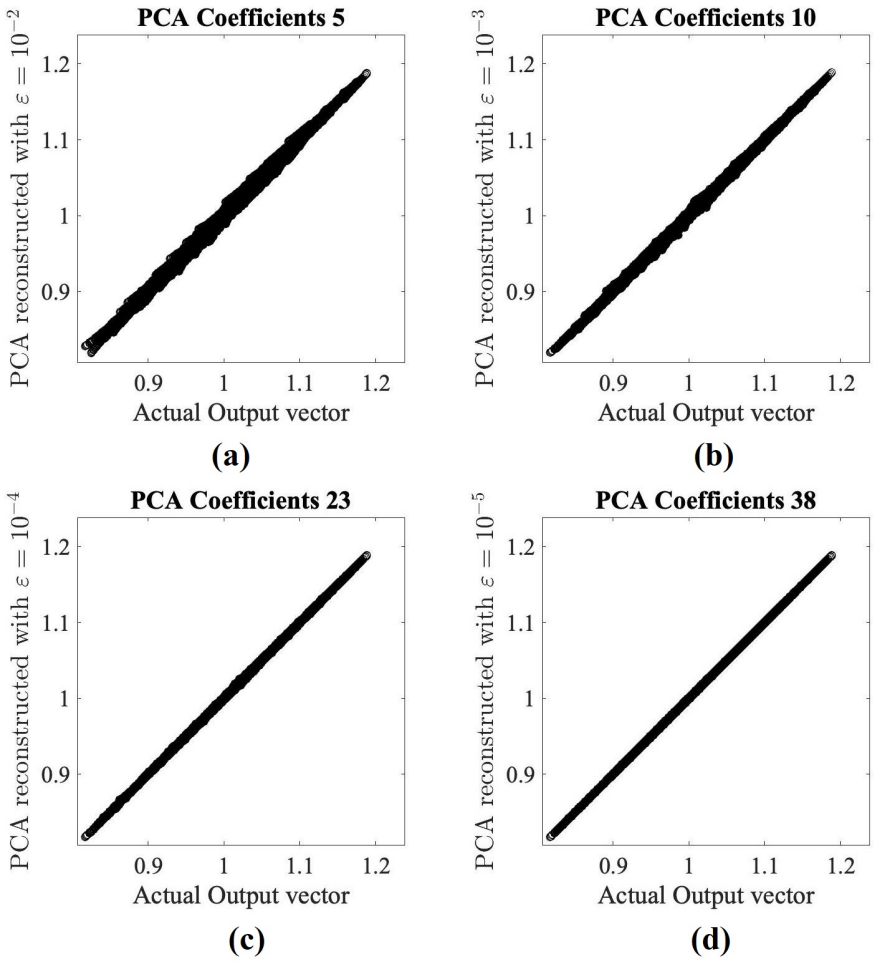

Figure 4.6: Scatter plots showing the actual training samples versus their reconstruction from PCA truncations with increasing number of components as shown in the plot headers.

the previous case study, the sparse PCE shows larger error, specially for low number of training samples, and it confirms again that the PCE is not intended for parametric modeling. However for higher training samples (i.e., L=1800), the accuracy of both sparse PCE and LS-SVM is comparable. The statistical information provided by the PDF plots, shown in Figure 4.10, highlight the capability of both the models in providing accurate information of the expected distribution of network voltage profile for such large variability introduced by loads and uncertain renewables generators (PVDGs). This increased uncertainty introduced by 900 parameters as compared to the previous case study (450 uncertain variables) is evident from the notable distribution shape.

A more detailed validation is given in Table 4.3, which collects and compares the

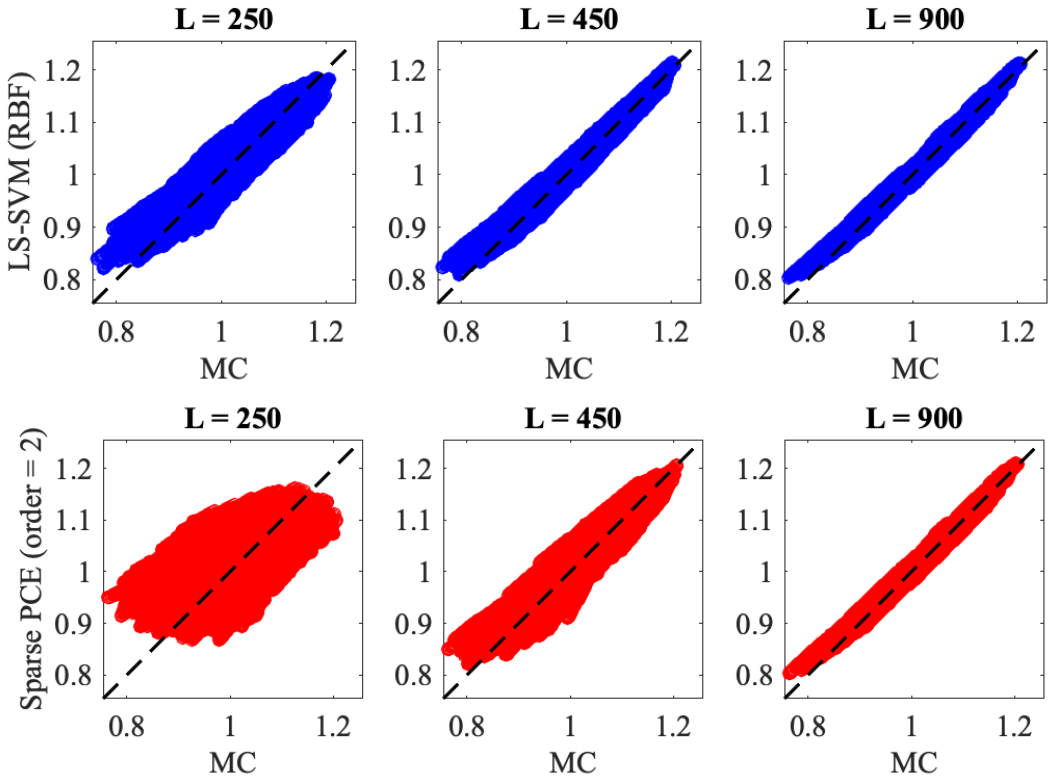

Figure 4.7: Scatter plots of the network node voltages for Case 1 ($d = 450$ uncertain parameters) predicted by LS-SVM regression (top three panels) and sparse PCE (bottom three panels) surrogate models trained with an increasing number of samples, versus the results of MC simulation.

quantitative information on the performance of the two models with both case studies (i.e., *450* and *900* uncertain parameters). Precisely, the table reports, RMSE between the MC outputs and the surrogate model predictions, the CPU time required in (i) the generation of training samples specified next to the number of training samples (L), (ii) the model generation (t_{model}) and (iii) the model evaluation (t_{cost}) for 10,000 validation samples (i.e., the time taken by surrogate models in generating the predictions). This table highlights the feasibility and efficiency of LS-SVM in terms of model generation for $L = 1800$ training samples, which is *23.8* mins as compared to *5.9* hours for sparse PCE, the difference is over one order of magnitude. Although, the overall training cost in this case is largely dominated by the generation of training samples which is *3.4* hours, while the evaluation time (t_{cost}) for both the models is almost negligible.

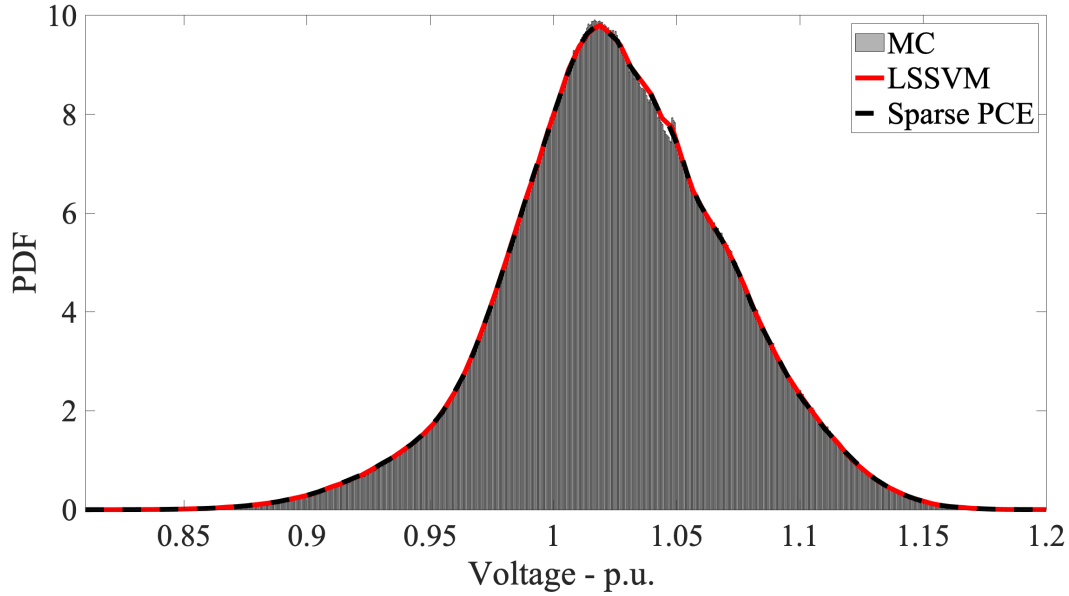

Figure 4.8: PDF of the p.u. magnitude of the nodal voltages calculated for Case 1 from the MC samples and with the compressed LS-SVM and sparse PCE surrogate models.

Table 4.3: Modeling performance in terms of accuracy and efficiency for different training set sizes.

d = 450	$L = 250$ (cost = 28.7 min)			$L = 450$ (cost = 51.6 min)			$L = 900$ (cost = 1.7 h)		
Method	RMSE	t_{model}	t_{cost}	RMSE	t_{model}	t_{cost}	RMSE	t_{model}	t_{cost}
MC	–	–	19.1 h	–	–	19.1 h	–	–	19.1 h
LS-SVM (RBF)	0.0127	18.8 s	3.3 s	0.0054	48.1 s	5.1 s	0.0028	3.6 min	8.9 s
Sparse PCE	0.0265	5.6 min	1.6 min	0.0124	8.9 min	1.6 min	0.0031	23.8 min	1.7 min
d = 900	$L = 450$ (cost = 51.6 min)			$L = 900$ (cost = 1.7 h)			$L = 1800$ (cost = 3.4 h)		
Method	RMSE	t_{model}	t_{cost}	RMSE	t_{model}	t_{cost}	RMSE	t_{model}	t_{cost}
MC	–	–	19.1 h	–	–	19.1 h	–	–	19.1 h
LS-SVM (RBF)	0.0166	55 s	7.8 s	0.0077	4 min	12.8 s	0.00401	22.7 min	22.7 s
Sparse PCE	0.0313	44.1 min	3.4 min	0.0294	1.7 h	3.5 min	0.00445	5.9 h	3.8 min

4.4 Concluding Remarks

In this chapter, the benchmark network IEEE 8500-node test feeder, which is a large realistic three-phase network, is used as a test network to analyse both the feasibility and strength of the two techniques proposed in chapters 2 and 3, for handling very large power networks.

Specifically, the circuital approach is used to interpret the mentioned test case as a circuital equivalent. The network is solved via fixed-point scheme and validated with

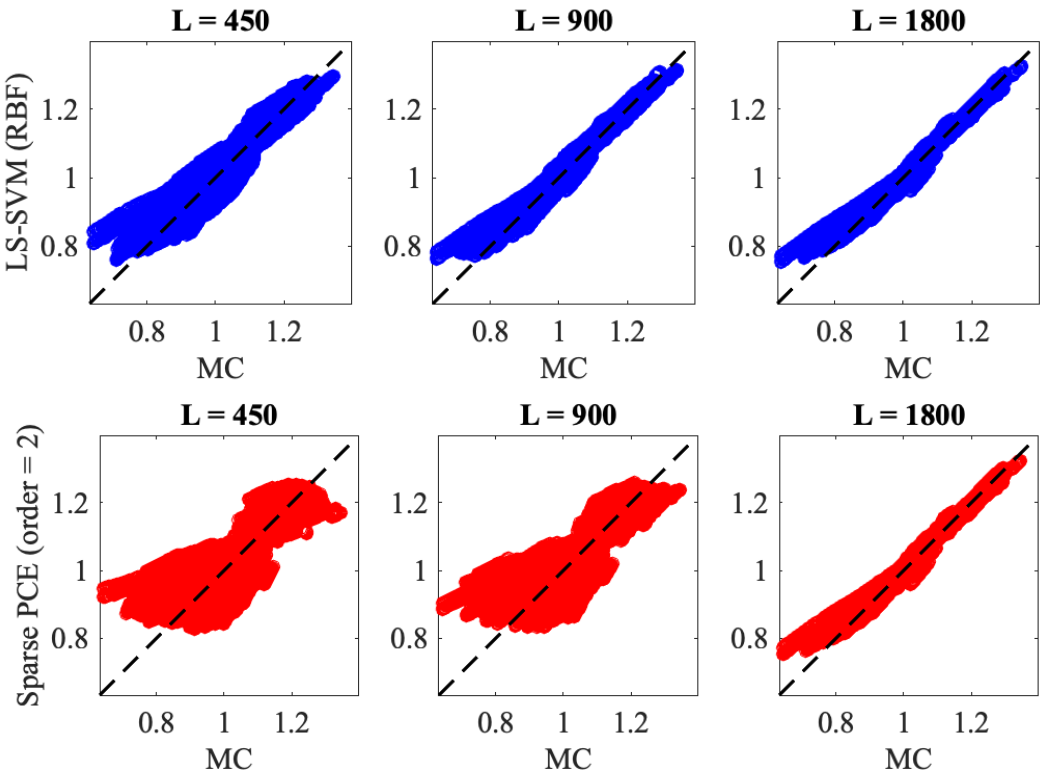

Figure 4.9: Scatter plots of the network node voltages for Case 2 ($d = 900$ uncertain parameters) predicted by LS-SVM regression (top three panels) and sparse PCE (bottom three panels) surrogate models trained with an increasing number of samples, versus the results of MC simulation.

the results performed with *Z-bus* and OpenDSS, which proves that the proposed aproach offers good performance in terms of both simulation time and accuracy and turns out to be an excellent alternative candidate to be effectively used for large networks. The results of proposed approach verify that without working on fine optimization of routines, the implementation of MNA-based formulae in MATLAB still produces the same accuracy and computational efficiency of reference commerical tools (e.g., OpenDSS) and other custom implementations of the state-of-the-art load-flow analyses (e.g., [68]).

The same network is then used to build a compact surrogate model of network nodal voltages, as function of large number of input uncertain parameters consisting of complex power of loads and renewables with the aim of highlighting the strength and feasibility of the ML class of surrogate modeling for the UQ. These surrogate models are built from a limited number of training samples via a well established two-step scheme involving the data set compression with PCA, and then training the model with LS-SVM. For the application test case, a PCA with relative truncation threshold of 10^{-4} on the

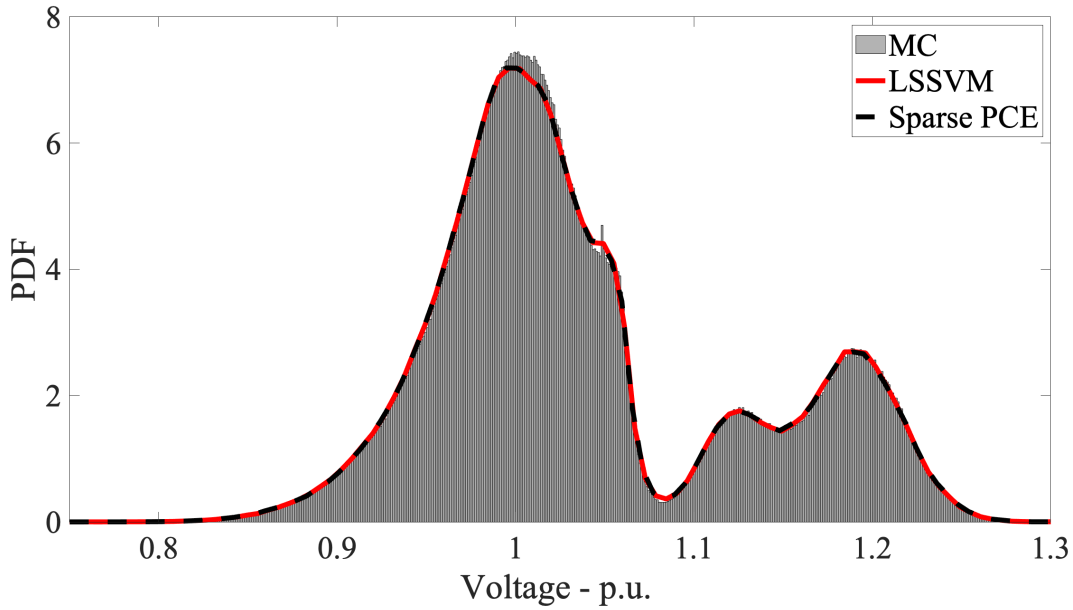

Figure 4.10: PDF of the p.u. magnitude of the nodal voltages calculated for Case 2 from the MC samples and with the compressed LS-SVM and sparse PCE surrogate models.

singular values allowed reducing the number of output variables (i.e., the nodal voltages) from 3798 to *23* and *39* for case 1 and case 2, respectively, thus achieving a compression rate of ~100x. The results provided in the above section, demonstrate that the proposed modeling methodology provides an effective alternate to MC simulations, with an overall speed-up between 2× and 4.9× (including the cost required for the generation of training samples). It is also important to highlight that the surrogate models inherently provide a closed-form parametric model, as opposed to the blind MC method. Thus, the proposed modeling strategy can be considered as a viable and robust solution for the generation of an accurate surrogate model for both the UQ and the parameteric analysis of a typical PDN with large number of node points and uncertain parameters.

In summary, the above approaches are tested on a large IEEE 8500-node test feeder and their feasibility and strengths proved well for handling large realistic networks. It is to mention that part of the work presented in this chapter has been published in the journal papers [1, 2].

Chapter 5

Conclusion

The modeling of modern PDNs requires take into account the behavior of loads, renewables and other such elements which can cause the network to fail. In this dissertation, the PDNs are modeled as circuital equivalent where the network is interpreted as a decoupled linear and non-linear sub-circuits in order to perform load-flow analysis simple and effective. The load-flow solution is performed by solving this decoupled circuit in the phasor domain using a simple iterative scheme. In the second part, the stochastic nature of above elements is taken into account by performing UQ of the power systems by building compressed surrogate model of network node voltages.

The main research work is summarized as follows:

1. LOAD FLOW ANALYSIS. A innovative simulation scheme for the power flow analysis of complex power distribution systems based on a circuital interpretation of the network has been presented. The proposed methodology has been proven to offer a comparable accuracy and efficiency with respect to other state-of-the-art techniques. Moreover, in this Thesis, emphasis has been given on the flexibility of the proposed tool, which turns out to be fully compatible and implementable in SPICE-like circuital solvers. The link between the proposed iterative solution and the so-called waveform relaxation technique, well known in the microwave and electromagnetic communities, is also provided. The solution of this circuital interpretation of PDN with MNA and fixed-point iteration does not contain any differential operator (or any auxilary matrix) which converges fast with a similar accuracy and efficiency as oppose to state-of-the-art. The linear and non-linear portions help solving linear part, which is usually very large, only once during iterative scheme, while the non-linear part is solved at each iteration. This speeds up the process. The validation of the proposed circuital approach is done using multiple single- and three-phase test networks, ranging from 33-node to a very large benchmark network, the IEEE 8500-node test feeder. The results are

compared with those of *Z-bus*, OpenDSS and PSASP and proved that it provides comparable efficiency in terms of convergence and simulation time. The MNA-based simulation can also be replaced with a SPICE-based solution, as explained in 2.3 and validated in 2.4.

2. RELIABILITY ASSESSMENT VIA MACHINE LEARNING. The effects of external parameters such as distributed renewable generators or loads on the network behavior has been modeled and analyzed by means of advanced Machine Learning techniques, combining robust nonparametric regression approaches and data compression. The proposed solution allows handling the complexity of realistic power networks with a large number of parameters (on the order of several hundreds) and nodes (thousands), generating a single compact multivariate parametric model. The UQ of power networks is performed by building a compressed surrogate model of network nodal voltages as function of input parameters consisting of uncertain power of loads/DGs and the physical parameters. The surrogate model is built with LS-SVM and PCA with a limited number of samples capable of accurately predicting the network voltage profile. The PCA yeilds ~100× compression rate. This greatly saves computational memory and execution time.

5.1 Future Work

Although the modeling of PDNs proposed in this dissertation yielded good results and proved to be effective. Following things can be considered as future work in this framework.

1. The circuital interpretation of PDNs works very well for very large network structures, and can handle all the equipment in a realistic network as proved from the results obtained in this dissertation. The technique can still improved to take into account islanded grid structures and such equipment.

2. The proposed circuital approach can be used with the co-simulation of multi-energy networks, such as gas distribution networks [19], since the same approach of steady-state operation with a compact graph description of the network can be employed.

3. The developed technique can also be aimed at modeling power transmission networks, where all sort of weather disturbances (geomegnetically induced currents) be explored for a time domain analyses.

4. The surrogate model proposed in this dissertation, for predicting network nodal voltages have been proved very effective in terms of simulation time. Further ML algorithms can also be explored in combination with PCA to predict the power generation capacity of renewables and electric vehicles' load profiles. For example, the surrogate modeling of power systems can take into account the physical parameters of PVDGs to acccurately predict the complex power to be injected into the grid for the next 24 hours. This can also help analyzing the reliability of the power networks.

5. The solution performed with SPICE-based can be extended to three-phase networks to model three-phase mutual inductances and transformers for performing three-phase power flow with SPICE in the loop.

Appendix A

LTSpice Netlist for a typical PDN

A.1 Creating Netlist for a PDN Test Case

This section briefly explains how to write a LTSpice netlist for a particular single-phase PDN test case. The technique is straightforward and can be easily extended for three-phase networks. Please note that the netlist is written and compiled through MATLAB, and all the sample variables are given for the MATLAB syntax.

A.1.1 Bus data with loads and renewables

The data available for any particular test network must be loaded to the MATLAB variables. This can be done via a simple matrix with order *mxn*, where *m* represents the number of available buses and *n* represents the parameters linking each bus, e.g., load power (real and reactive), renewable power (real and reactive), bus type, base voltage, bus voltage/phase angle, minimum/maximum operating voltage and other parameter constraints (if any). Figure A.1 details the bus data matrix with four buses.

```
%% Bus data
%     Bus_I Load_P Load_Q DG_P  DG_Q  Type  Vm  Va  basekV  Vmax    Vmin
bus=[   1   0       0       0    0     3     1  0   12.66   1.05    0.95
        2   100     60      0    0     3     1  0   12.66   1.05    0.95
        3   90      40      0    0     3     1  0   12.66   1.05    0.95
        4   120     80      0    0     3     1  0   12.66   1.05    0.95
     ];
```

Figure A.1: Bus information matrix for 4-node PDN

A.1.2 Branch connections

Similar to the above bus matrix, the branch matrix can be created to load the data for each branch and its parameters. The branch parameters consist of branch connecting buses i and j, equivalent resistance (ohms) and reactance (ohms), branch status (0=ff, 1=on), etc. Figure A.2 shows the branch matrix for a particular network with three branches.

```
 %% Line Data
%        from   to  r(ohm)  x(ohm)  Status  Ratio
branch=[ 1      2   0.0922  0.0477    1      0
         2      3   0.493   0.2511    1      0
         3      4   0.366   0.1864    1      0
        ];
```

Figure A.2: Branch connection matrix for 4-node PDN.

A.1.3 Writing netlist through MATLAB

After the test case data is loaded into the matrix variables, we need to compile the LTSpice netlist text file though MATLAB using fopen and fclose command for writing to external text files. The branch connections are represented by the equivalent resistance and inductance connecting buses i and j, as shown in Figure A.3. The equivalant inductance L can be calculated given equivalent reactance X at operating frequency f as followed,

$$L = \frac{X}{2\pi f} \tag{A.1}$$

```
%% branch between nodes N01 and N02
R1 M1 N01 {R1value}
L1 N02 M1 {L1value} Rser=0

%% load connected at node N01
I1 N01 0 AC {IL1_magvalue} {IL1_phasevalue} load
```

Figure A.3: Representing branch connection and load connected at a particular bus in generic PDN in the LTSpice netlist.

The above Figure also shows the load connected at node N01 with complex value given for load magnitude (kW) and phase angle (degrees).

After the branch connections and loads connected at all the buses are represented in the netlist, LTSpice solves the circuit via ac analysis whose directive is written in the

netlist as (*.ac lin 1 60 60*) which means the linear ac analysis is performed at frequency 60 Hz (please note this can be changed accordingly).

It is pertinent to highlight that the three-phase branch connections in the LTSpice require modeling the mutual inductances among phases which can represented by voltage controlled current source. However the SPICE-based solution of generic three-phase PDN comes under the future goal of this work. Figure A.4 shows MATLAB code for writing the LTSpice netlist for a generic 4-node power network.

```
%% defining the netlist
nl = 3; % no of branches
nb = 4; % no. of buses
netlist = ['4node.cir'];
%
fid = fopen(netlist,'w+');
fprintf(fid, '* AC Analysis - Node 4 Radial\n\n');
fprintf(fid, '.INCLUDE load_currents.cir\n\n');
fprintf(fid,['V' num2str(source_n) ' N0' num2str(source_n) ' 0 AC ' num2str(SourceV) '\r\n\n' ]);

for ii = 1:nl
    fprintf(fid,['R' num2str(ii) ' M' num2str(ii) ' N0' num2str(branch(ii,1)) ' ' num2str(R(ii)) '\r\n']);
    fprintf(fid,['L' num2str(ii) ' N0' num2str(branch(ii,2)) ' M'  num2str(ii)  ' ' num2str(L(ii)) ' Rser=0 \r\n\n']);

end

for ii = 1: size(loads,1)
    fprintf(fid,['I' num2str(ii) ' N0' num2str(ii) ' 0 AC {ILm' num2str(ii) '} {ILp' num2str(ii) '} load\r\n']);
end

fprintf(fid,['\n.ac lin 1 60 60\r\n\n']);

for ii = 1:nb
    fprintf(fid,['.probe V(N0' num2str(ii) ') \r\n']);
end

fprintf(fid,['\n.end']);

fclose(fid);
```

Figure A.4: MATLAB code for writing LTSpice netlist.

A.2 LTSpice Netlist for a simple 4-Node PDN

The LTSpice netlist given below focuses on the example network in Figure 2.1, but can be generalized for any arbitrary network.

```
* Simple 4-node Example

.PARAM R1value = [Equivalent Resistance 1 value]
.PARAM L1value = [Equivalent Inductance 1 value]
.PARAM R2value = [Equivalent Resistance 2 value]
.PARAM L2value = [Equivalent Inductance 2 value]
.PARAM R3value = [Equivalent Resistance 3 value]
.PARAM L3value = [Equivalent Inductance 3 value]


.PARAM I1_magvalue =    [Equivalent Current Injection for Load 1 Mag.]
.PARAM I1_phasevalue =  [Equivalent Current Injection for Load 1 Phase]
.PARAM I2_magvalue =    [Equivalent Current Injection for Load 2 Mag.]
.PARAM I2_phasevalue =  [Equivalent Current Injection for Load 2 Phase]


V1      N1      0       AC      1.00
R1      N1      M1      {R1value}
L1      M1      N2      {L1value}       Rser = 0
R2      N2      M2      {R2value}
L2      M2      N3      {L2value}       Rser = 0
R3      N2      M3      {R2value}
L3      M3      N4      {L2value}       Rser = 0
I3      N3      0       AC      {I1_magvalue}       {I1_phasevalue}     load
I4      N4      0       AC      {I2_magvalue}       {I2_ phasevalue}    load

.ac     lin     1       60      60

.probe          V(N1)
.probe          V(N2)
.probe          V(N3)
.proble         V(N4)

.end
```

Figure A.5: LTSpice netlist of generic PDN in Figure 2.4.

It is used to solve via a SPICE-based solver the linear part shown in the left part of the equivalent scheme of Figure 2.4. At each iteration, the values of the I_3 and I_4 behavioral sources are computed and updated before running SPICE. (see Fig. 2.5).

Nomenclature

Acronyms / Abbreviations

$CEPRI$ China Electric Power Research Institute

DGs Distributed Generators

$EPRI$ Electric Power Research Institute

IDE Integrated Development Environment

$IEEE$ Institute of Electrical and Electronics Enigneers

LHS Latin Hypercube Sampling

$LS-SVM$ Least Square Support Vector Machines

LV Low Voltage

$MANA$ Modified Augmented Nodal Analysis

MC Monte Carlo

ML Machine Learning

MNA Modified Nodal Analysis

MV Medium Voltage

$OpenDSS$ Open source Distribution System Simulator

p.u. Per Unit

PCA Principal Component Analysis

PCE Polynomial Chaos Expansion

PDF Probability Distribution Function

$PDNs$ Power Distribution Networks

PES Power and Energy Society

PPF Probablistic Power-flow

PQ Generator node with real and reactive power

$PQ(V)$ Generator node with real power and voltage dependent reactive power

$PSASP$ Power System Analysis Software Package

PV Generator node with real power and voltage magnitude

$PVDG$ Photovoltaic Distributed Generator

RBF Radial Basis Function

RES Renewable Energy Sources

$RMSE$ Root Mean Squared Error

$SPICE$ Simulation Program with Integrated Circuit Emphasis

SVD Singular Value Decomposition

SVR Step voltage regulator

UQ Uncertainty Quantification

Bibliography

[1] Zain A. Memon et al. “An iterative scheme for the power-flow analysis of distribution networks based on decoupled circuit equivalents in the phasor domain.” In: *Energies* 13.2 (2020), p. 386.

[2] Zain A. Memon et al. “Compressed machine learning models for the uncertainty quantification of power distribution Networks.” In: *Energies* 13.18 (2020), p. 4881.

[3] Zain Anwer Memon et al. “Machine Learning for the Uncertainty Quantification of Power Networks.” In: *IEEE Letters on Electromagnetic Compatibility Practice and Applications* 2.4 (2020), pp. 138–141.

[4] A. Oshnoei et al. “Direct Probabilistic Load Flow in Radial Distribution Systems Including Wind Farms: An Approach Based on Data Clustering.” In: *Energies* 11.310 (2018), pp. 504–509.

[5] B. Bockl et al. “HyFlow—A Hybrid Load Flow-Modelling Framework to Evaluate the Effects of Energy Storage and Sector Coupling on the Electrical Load Flows.” In: *Energies* 12.956 (2019), pp. 504–509.

[6] J. Yang et al. “Risk Assessment of Distribution Networks Considering the Charging-Discharging Behaviors of Electric Vehicles.” In: *Energies* 09.560 (2016), pp. 504–509.

[7] H. P. Corrêa and F. H. T. Vieira. “Load Flow Independent Method for Estimating Neutral Voltage in Three-Phase Power Systems.” In: *Energies* 12.3216 (2019), pp. 504–509.

[8] W. D. Stevenson. *Elements of Power System Analysis*. McGraw-Hill, 1982.

[9] W. F. Tinney and C. E. Hart. “Power flow solutions by Netwon’s method.” In: *IEEE Trans. on Power Apparatus and Syst.* PAS-86.11 (1967), pp. 1449–1460.

[10] B. Stott and O. Alsac. “Fast decoupled load flow.” In: *IEEE Trans. on Power Apparatus and Syst.* 93.1 (1974), pp. 859–869.

[11] H. Saadat. *Power System Analysis*. 3rd ed. McGraw-Hill, 1999.

[12] B.A. B. A. Carreras et al. "Complex dynamics of blackouts in power transmission systems." In: *Chaos* 14 (2004), pp. 643–652.

[13] H. Liao, J. Apt, and S. Talukdar. "Phase transitions in the probability of cascading failures." In: *Proceedings of Electrical Transmission in Deregulated Markets Conference*. Carnegie-Mellon Univ. 2004.

[14] D. V. Hertem et al. "Usefulness of DC Power flow for active power flow analysis with flow controlling devices." In: *Proceedings of the 8th IEE International Conference on AC and DC power Transmission*. London, UK. 2006, pp. 58–68.

[15] J. Yuan et al. "Cascading failure analysis with DC power flow model and transient stability analysis." In: *IEEE Trans. Power Syst.* 30.1 (2015), pp. 285–297.

[16] Chung Wen Ho, Albert E. Ruehli, and Pierce A. Brennan. "The modified nodal analysis." In: *IEEE Transactions on Circuits and Systems* 22.6 (1975), pp. 504–509.

[17] J.K. White and Alberto Sangiovanni-Vincentelli. *Relaxation Techniques for the simulation of VLSI Circuits*. Vol. 20. Springer Science & Business Media, 1987.

[18] Ilhan Kocar et al. "Multiphase load-flow solution for large-scale distribution systems using MANA." In: *IEEE Transactions on Power Delivery* 29.2 (2013), pp. 908–915.

[19] Enrico Vaccariello, Pierluigi Leone, and Igor S. Stievano. "Generation of synthetic models of gas distribution networks with spatial and multi-level features." In: *International Journal of Electrical Power & Energy Systems* 117 (2020), p. 105656.

[20] Kyungsung An, Kyung-Bin Song, and Kyeon Hur. "Incorporating charging/discharging strategy of electric vehicles into security-constrained optimal power flow to support high renewable penetration." In: *Energies* 10.5 (2017), p. 729.

[21] Yuttana Kongjeen and Krischonme Bhumkittipich. "Modeling of electric vehicle loads for power flow analysis based on PSAT." In: *2016 13th international conference on electrical engineering/electronics, computer, telecommunications and information technology (ECTI-CON)*. IEEE. 2016, pp. 1–6.

[22] Rong-Ceng Leou, Chun-Lien Su, and Chan-Nan Lu. "Stochastic analyses of electric vehicle charging impacts on distribution network." In: *IEEE Transactions on Power Systems* 29.3 (2013), pp. 1055–1063.

[23] Pedram Samadi et al. "Tackling the load uncertainty challenges for energy consumption scheduling in smart grid." In: *IEEE Transactions on Smart Grid* 4.2 (2013), pp. 1007–1016.

[24] AP Sakis Meliopoulos, George J Cokkinides, and Xing Yong Chao. "A new probabilistic power flow analysis method." In: *IEEE Transactions on Power Systems* 5.1 (1990), pp. 182–190.

[25] Xue Li, Yuzeng Li, and Shaohua Zhang. "Analysis of probabilistic optimal power flow taking account of the variation of load power." In: *IEEE Transactions on Power Systems* 23.3 (2008), pp. 992–999.

[26] Gan Li and Xiao-Ping Zhang. "Modeling of plug-in hybrid electric vehicle charging demand in probabilistic power flow calculations." In: *IEEE Transactions on Smart Grid* 3.1 (2012), pp. 492–499.

[27] Walid El-Khattam, YG Hegazy, and MMA Salama. "Investigating distributed generation systems performance using Monte Carlo simulation." In: *IEEE Transactions on Power Systems* 21.2 (2006), pp. 524–532.

[28] Guido Carpinelli, Pierluigi Caramia, and Pietro Varilone. "Multi-linear Monte Carlo simulation method for probabilistic load flow of distribution systems with wind and photovoltaic generation systems." In: *Renewable Energy* 76 (2015), pp. 283–295.

[29] G. E. Constante-Flores and M. S. Illindala. "Data-Driven Probabilistic Power Flow Analysis for a Distribution System With Renewable Energy Sources Using Monte Carlo Simulation." In: *IEEE Transactions on Industry Applications* 55.1 (2019), pp. 174–181.

[30] Yi Wang, Xiufen Shen, and Zemei Dai. "A probabilistic power flow calculation method considering the uncertainty of the static frequency characteristic." In: *Global Energy Interconnection* 2.1 (2019), pp. 45–53.

[31] Hui Zhang and Pu Li. "Probabilistic analysis for optimal power flow under uncertainty." In: *IET Generation, Transmission & Distribution* 4.5 (2010), pp. 553–561.

[32] Moein Moeini-Aghtaie et al. "A Decomposed Solution to Multiple-Energy Carriers Optimal Power Flow." In: *IEEE Transactions on Power Systems* 29.2 (2014), pp. 707–716. DOI: 10.1109/TPWRS.2013.2283259.

[33] Mahdi Hajian, William D Rosehart, and Hamidreza Zareipour. "Probabilistic power flow by Monte Carlo simulation with Latin supercube sampling." In: *IEEE Transactions on Power Systems* 28.2 (2013), pp. 1550–1559.

[34] Juan A Martinez-Velasco and Gerardo Guerra. "Reliability analysis of distribution systems with photovoltaic generation using a power flow simulator and a parallel Monte Carlo approach." In: *Energies* 9.7 (2016), p. 537.

[35] Morad Abdelaziz. "GPU-OpenCL accelerated probabilistic power flow analysis using Monte-Carlo simulation." In: *Electric Power Systems Research* 147 (2017), pp. 70–72.

[36] Daniel A. Maldonado, Michel Schanen, and Mihai Anitescu. "Uncertainty Propagation in Power System Dynamics with the Method of Moments." In: *2018 IEEE Power Energy Society General Meeting (PESGM)*. 2018, pp. 1–5. DOI: 10.1109/PESGM.2018.8586023.

[37] Cong Zhang et al. "A Mixed Interval Power Flow Analysis Under Rectangular and Polar Coordinate System." In: *IEEE Transactions on Power Systems* 32.2 (2017), pp. 1422–1429. DOI: 10.1109/TPWRS.2016.2583503.

[38] Yifan Zhou and Peng Zhang. "Reachable Power Flow." In: *IEEE Transactions on Power Systems* 35.4 (2020), pp. 3290–3293. DOI: 10.1109/TPWRS.2020.2974164.

[39] Riccardo Trinchero et al. "Combined parametric and worst case circuit analysis via Taylor models." In: *IEEE Transactions on Circuits and Systems I: Regular Papers* 63.7 (2016), pp. 1067–1078.

[40] Tongyu Ding et al. "How affine arithmetic helps beat uncertainties in electrical systems." In: *IEEE Circuits and Systems Magazine* 15.4 (2015), pp. 70–79.

[41] Nicola Femia and Giovanni Spagnuolo. "True worst-case circuit tolerance analysis using genetic algorithms and affine arithmetic." In: *IEEE Transactions on Circuits and Systems I: Fundamental Theory and Applications* 47.9 (2000), pp. 1285–1296.

[42] Paolo Manfredi et al. "Stochastic transmission line analysis via polynomial chaos methods: an overview." In: *IEEE Electromagnetic Compatibility Magazine* 6.3 (2017), pp. 77–84.

[43] Arun Kaintura, Tom Dhaene, and Domenico Spina. "Review of polynomial chaos-based methods for uncertainty quantification in modern integrated circuits." In: *Electronics* 7.3 (2018), p. 30.

[44] Dongbin Xiu and George Em Karniadakis. "The Wiener–Askey polynomial chaos for stochastic differential equations." In: *SIAM journal on scientific computing* 24.2 (2002), pp. 619–644.

[45] Thomas J Santner et al. *The design and analysis of computer experiments*. Vol. 1. Springer, 2003.

[46] Simon Haykin. *Neural Networks and Learning Machines, 3/E*. 2009.

[47] Joseph De Brabanter et al. *Least squares support vector machines*. World scientific: New York, NY, USA, 2002.

[48] Carl Edward Rasmussen and Christopher K.I. Williams. *Gaussian processes for machine learning*. MIT press Cambridge, MA, USA, 2006.

[49] Alejandro Garces. "A Linear Three-Phase Load Flow for Power Distribution Systems." In: *IEEE Transactions on Power Systems* 31.1 (2016), pp. 827–828. DOI: 10.1109/TPWRS.2015.2394296.

[50] F. Zhang and C. S. Cheng. "A modified newton method for radial distribution system power flow analysis." In: *IEEE Trans. Power Syst.* 12 (1997), pp. 389–397.

[51] Tao Ding et al. "Negative Reactance Impacts on the Eigenvalues of the Jacobian Matrix in Power Flow and Type-1 Low-Voltage Power-Flow Solutions." In: *IEEE Transactions on Power Systems* 32.5 (2017), pp. 3471–3481. DOI: 10.1109/TPWRS.2016.2645608.

[52] Alfredo Bonini Neto and Dilson Amancio Alves. "Singularities Analysis of the Jacobian Matrix Modified in the Continuation Power Flow: Mathematical Modeling." In: *IEEE Latin America Transactions* 14.12 (2016), pp. 4750–4756. DOI: 10.1109/TLA.2016.7817006.

[53] Jen-Hao Teng. "A modified Gauss–Seidel algorithm of three-phase power flow analysis in distribution networks." In: *International journal of electrical power & energy systems* 24.2 (2002), pp. 97–102.

[54] D. Thukaram, H. M. Wijekoon Banda, and Jovitha Jerome. "A robust three phase power flow algorithm for radial distribution systems." In: *Electric Power Systems Research* 50.3 (1999), pp. 227–236.

[55] Jen-Hao Teng. "A direct approach for distribution system load flow solutions." In: *IEEE Transactions on power delivery* 18.3 (2003), pp. 882–887.

[56] Ulas Eminoglu and M Hakan Hocaoglu. "A new power flow method for radial distribution systems including voltage dependent load models." In: *Electric power systems research* 76.1-3 (2005), pp. 106–114.

[57] Federico Bizzarri et al. "Numerical Approach to Compute the Power Flow Solution of Hybrid Generation, Transmission and Distribution Systems." In: *IEEE Transactions on Circuits and Systems II: Express Briefs* 67.5 (2020), pp. 936–940. DOI: 10.1109/TCSII.2020.2980988.

[58] S Satyanarayana et al. "An efficient load flow solution for radial distribution network including voltage dependent load models." In: *Electric Power Components and Systems* 35.5 (2007), pp. 539–551.

[59] Alejandro Garces. "A linear three-phase load flow for power distribution systems." In: *IEEE Transactions on Power Systems* 31.1 (2015), pp. 827–828.

[60] Xiao-Ping Zhang, Ping Ju, and E. Handschin. "Continuation three-phase power flow: a tool for voltage stability analysis of unbalanced three-phase power systems." In: *IEEE Transactions on Power Systems* 20.3 (2005), pp. 1320–1329. DOI: 10.1109/TPWRS.2005.851950.

[61] Yi Wang et al. "Linear three-phase power flow for unbalanced active distribution networks with PV nodes." In: *CSEE Journal of Power and Energy Systems* 3.3 (2017), pp. 321–324. DOI: 10.17775/CSEEJPES.2017.00240.

[62] Yang Liu, Kai Sun, and Jiaojiao Dong. "A Dynamized Power Flow Method Based on Differential Transformation." In: *IEEE Access* 8 (2020), pp. 182441–182450. DOI: 10.1109/ACCESS.2020.3028060.

[63] Rafael Tapia Juárez et al. "Steady-State Model of Grid-Connected Photovoltaic Generation for Power Flow Analysis." In: *IEEE Transactions on Power Systems* 33.5 (2018), pp. 5727–5737. DOI: 10.1109/TPWRS.2018.2817585.

[64] Daisuke Iioka et al. "Voltage reduction due to reverse power flow in distribution feeder with photovoltaic system." In: *International Journal of Electrical Power & Energy Systems* 113 (2019), pp. 411–418.

[65] Gibran Agundis-Tinajero et al. "Power flow modeling of islanded AC microgrids with hierarchical control." In: *International Journal of Electrical Power & Energy Systems* 105 (2019), pp. 28–36.

[66] Hassan Nikkhajoei and Reza Iravani. "Steady-State Model and Power Flow Analysis of Electronically-Coupled Distributed Resource Units." In: *IEEE Transactions on Power Delivery* 22.1 (2007), pp. 721–728. DOI: 10.1109/TPWRD.2006.881604.

[67] Morad Mohamed Abdelmageed Abdelaziz. "Effect of Detailed Reactive Power Limit Modeling on Islanded Microgrid Power Flow Analysis." In: *IEEE Transactions on Power Systems* 31.2 (2016), pp. 1665–1666. DOI: 10.1109/TPWRS.2015.2412690.

[68] Mohammadhafez Bazrafshan and Nikolaos Gatsis. "Comprehensive modeling of three-phase distribution systems via the bus admittance matrix." In: *IEEE Transactions on Power Systems* 33.2 (2018), pp. 2015–2029.

[69] Gengwu Zhang et al. "On the convergence of the implicit Z-Bus power flow method for distribution systems." In: *Electric Power Systems Research* 171 (2019), pp. 74–84.

[70] Amr Adel Mohamed and Bala Venkatesh. "Line-Wise Power Flow and Voltage Collapse." In: *IEEE Transactions on Power Systems* 33.4 (2018), pp. 3768–3778. DOI: 10.1109/TPWRS.2017.2787752.

[71] Amritanshu Pandey et al. "Robust power flow and three-phase power flow analyses." In: *IEEE Transactions on Power Systems* 34.1 (2018), pp. 616–626.

[72] Baki Cetindag et al. "Modeling of Step Voltage Regulators in Multiphase Load Flow Solution of Distribution Systems Using Newton's Method and Augmented Nodal Analysis." In: *Electric Power Components and Systems* 45.15 (2017), pp. 1667–1677.

[73] Baljinnyam Sereeter, Cornelis Vuik, and Cees Witteveen. "On a comparison of Newton–Raphson solvers for power flow problems." In: *Journal of Computational and Applied Mathematics* 360 (2019), pp. 157–169.

[74] Ujjal Sur and Gautam Sarkar. "Existence of Explicit and Unique Necessary Conditions for Power Flow Insolvability in Power Distribution Systems." In: *IEEE Systems Journal* 13.1 (2019), pp. 702–709. DOI: 10.1109/JSYST.2018.2870178.

[75] Cong Wang et al. "Existence and Uniqueness of Load-Flow Solutions in Three-Phase Distribution Networks." In: *IEEE Transactions on Power Systems* 32.4 (2017), pp. 3319–3320. DOI: 10.1109/TPWRS.2016.2623979.

[76] *IEEE PES distribution system analysis subcommittee's Distribution Test Feeders*. URL: http://sites.ieee.org/pes-testfeeders/resources/ (visited on 05/07/2019).

[77] R. F. Arritt and R. C. Dugan. "The IEEE 8500-node test feeder." In: *Proceedings of the IEEE PES T&D*. 2010, pp. 1–6.

[78] Yijun Xu et al. "Propagating Uncertainty in Power System Dynamic Simulations Using Polynomial Chaos." In: *IEEE Transactions on Power Systems* 34.1 (2019), pp. 338–348. DOI: 10.1109/TPWRS.2018.2865548.

[79] Sándor Bilicz et al. "Uncertainty quantification of wireless power transfer systems." In: *2016 IEEE Wireless Power Transfer Conference (WPTC)*. 2016, pp. 1–3. DOI: 10.1109/WPT.2016.7498861.

[80] Géraud Blatman and Bruno Sudret. "An adaptive algorithm to build up sparse polynomial chaos expansions for stochastic finite element analysis." In: *Probabilistic Engineering Mechanics* 25.2 (2010), pp. 183–197.

[81] Géraud Blatman and Bruno Sudret. "Adaptive sparse polynomial chaos expansion based on least angle regression." In: *Journal of computational Physics* 230.6 (2011), pp. 2345–2367.

[82] Zheng Zhang, Tsui-Wei Weng, and Luca Daniel. "Big-data tensor recovery for high-dimensional uncertainty quantification of process variations." In: *IEEE Transactions on Components, Packaging and Manufacturing Technology* 7.5 (2017), pp. 687–697.

[83] Mourad Larbi et al. "Variability impact of many design parameters: The case of a realistic electronic link." In: *IEEE Transactions on Electromagnetic Compatibility* 60.1 (2018), pp. 34–41.

[84] Hakki Mert Torun et al. "A spectral convolutional net for co-optimization of integrated voltage regulators and embedded inductors." In: *2019 IEEE/ACM International Conference on Computer-Aided Design (ICCAD)*. IEEE. 2019, pp. 1–8.

[85] Huan Yu et al. "Behavioral modeling of tunable I/O drivers with preemphasis including power supply noise." In: *IEEE Transactions on Very Large Scale Integration (VLSI) Systems* 28.1 (2020), pp. 233–242.

[86] V. N. Vapnik. *The Nature of Statistical Learning Theory*. Springer: NY, USA, 2000.

[87] V. N. Vapnik. *Statistical Learning Theory*. Wiley: New York, NY, USA, 1998.

[88] Riccardo Trinchero et al. "Machine learning for the performance assessment of high-speed links." In: *IEEE Transactions on Electromagnetic Compatibility* 60.6 (2018), pp. 1627–1634.

[89] R Trinchero et al. "Design of high-speed links via a machine learning surrogate model for the inverse problem." In: *2019 Electrical Design of Advanced Packaging and Systems (EDAPS)*. IEEE. 2019, pp. 1–3.

[90] Riccardo Trinchero and Flavio G. Canavero. "Combining LS-SVM and GP regression for the uncertainty quantification of the EMI of power converters affected by several uncertain parameters." In: *IEEE Transactions on Electromagnetic Compatibility* (2020).

[91] Riccardo Trinchero et al. "Machine learning and uncertainty quantification for surrogate models of integrated devices with a large number of parameters." In: *IEEE Access* 7 (2018), pp. 4056–4066.

[92] L. Philipson. "Distributed and dispersed generation: addressing the spectrum of consumer needs." In: *2000 Power Engineering Society Summer Meeting (Cat. No.00CH37134)*. Vol. 3. 2000, 1663–1665 vol. 3.

[93] Chao Cheng et al. "Calculation method and analysis of power flow for distribution network with distributed generation." In: *2015 5th International Conference on Electric Utility Deregulation and Restructuring and Power Technologies (DRPT)*. IEEE. 2015, pp. 2020–2024.

[94] J-H Teng. "Modelling distributed generations in three-phase distribution load flow." In: *IET generation, transmission & distribution* 2.3 (2008), pp. 330–340.

[95] Baljinnyam Sereeter, Kees Vuik, and Cees Witteveen. "Newton power flow methods for unbalanced three-phase distribution networks." In: *Energies* 10.10 (2017), p. 1658.

[96] Paul Wagner. *Fast Import of Compressed Binary .RAW Files Created with LTspice Circuit Simulator*. URL: https://www.mathworks.com/matlabcentral/fileexchange/23394-fast-import-of-compressed-binary-raw-files-created-with-ltspice-circuit-simulator (visited on 12/17/2019).

[97] Paul W Tuinenga. *SPICE: a guide to circuit simulation and analysis using PSpice*. Prentice Hall PTR, 1995.

[98] *OpenDSS Program*. URL: http://sourceforge.net/projects/electricdss (visited on 12/02/2019).

[99] Baofeng Tang and Hui Fan. *Method for calculating primary time constant of power grid*. US Patent 8,805,666. Aug. 2014.

[100] C. Cheng et al. "Calculation method and analysis of power flow for distribution network with distributed generation." In: *2015 5th International Conference on Electric Utility Deregulation and Restructuring and Power Technologies (DRPT)*. 2015, pp. 2020–2024.

[101] SK Goswami and SK Basu. "Direct solution of distribution systems." In: *IEE proceedings C generation, transmission and distribution*. Vol. 138. 1. IET. 1991, pp. 78–88.

[102] Zain A. Memon et al. "Machine learning models for the uncertainty quantification of power distribution Networks." In: *6th IEEE Global Electromagnetic Compatibility Conference (GEMCCON2020)*. IEEE, 2020, pp. 1–4.

[103] Kurt Binder and Dieter W Heermann. *Monte Carlo Simulation in Statistical Physics: An Introduction*. Springer Science & Business Media, 2010.

[104] Stefano Marelli and Bruno Sudret. "UQLab: A framework for uncertainty quantification in Matlab." In: *2nd International Conference on Vulnerability Risk Analysis and Management*. 2014, pp. 2554–2563.

[105] Belgium Department of Electrical Engineering (ESAT) Katholieke Universiteit Leuven: Leuven. *LS-SVMlab, version 1.8*. URL: http://www.esat.kuleuven.be/sista/lssvmlab/ (visited on 02/03/2020).

[106] Vahid Yaghoubi et al. "Sparse polynomial chaos expansions of frequency response functions using stochastic frequency transformation." In: *Probabilistic engineering mechanics* 48 (2017), pp. 39–58.

[107] Paolo Manfredi and Riccardo Trinchero. "A Data Compression Strategy for the Efficient Uncertainty Quantification of Time-Domain Circuit Responses." In: *IEEE Access* (2020).

[108] *Power System Tests Case Archive*. URL: http://www.ee.washington.edu/research/pstca/pf118/pg%5C_tca118bus.htm (visited on 06/27/2020).

[109] Michael D McKay, Richard J Beckman, and William J Conover. "A comparison of three methods for selecting values of input variables in the analysis of output from a computer code." In: *Technometrics* 42.1 (2000), pp. 55–61.

[110] Ray Daniel Zimmerman, Carlos Edmundo Murillo-Sánchez, and Robert John Thomas. "MATPOWER: Steady-state operations, planning, and analysis tools for power systems research and education." In: *IEEE Transactions on power systems* 26.1 (2011), pp. 12–19.

[111] Hao Sheng and Xiaozhe Wang. "Probabilistic power flow calculation using non-intrusive low-rank approximation method." In: *IEEE Transactions on Power Systems* 34.4 (2019), pp. 3014–3025.

[112] SH Karaki, RB Chedid, and R Ramadan. "Probabilistic performance assessment of autonomous solar-wind energy conversion systems." In: *IEEE Transactions on energy conversion* 14.3 (1999), pp. 766–772.